Physical Layer Security in Integrated Sensing and Communication Systems

Nanchi Su

A dissertation submitted in partial fulfillment

of the requirements for the degree of

Doctor of Philosophy

of

University College London.

Department of Electronic and Electrical Engineering

University College London

April 25, 2023

I, Nanchi Su, confirm that the work presented in this thesis is my own. Where information has been derived from other sources, I confirm that this has been indicated in the work.

Abstract

The development of integrated sensing and communication (ISAC) systems has been spurred by the growing congestion of the wireless spectrum. The ISAC system detects targets and communicates with downlink cellular users simultaneously. Uniquely for such scenarios, radar targets are regarded as potential eavesdroppers which might surveil the information sent from the base station (BS) to communication users (CUs) via the radar probing signal. To address this issue, we propose security solutions for ISAC systems to prevent confidential information from being intercepted by radar targets.

In this thesis, we firstly present a beamformer design algorithm assisted by artificial noise (AN), which aims to minimize the signal-to-noise ratio (SNR) at the target while ensuring the quality of service (QoS) of legitimate receivers. Furthermore, to reduce the power consumed by AN, we apply the directional modulation (DM) approach to exploit constructive interference (CI). In this case, the optimization problem is designed to maximize the SINR of the target reflected echoes with CI constraints for each CU, while constraining the received symbols at the target in the destructive region.

Apart from the separate functionalities of radar and communication systems above, we investigate sensing-aided physical layer security (PLS), where the ISAC BS first emits an omnidirectional waveform to search for and estimate target directions. Then, we formulate a weighted optimization problem to simultaneously maximize the secrecy rate and minimize the Cramér-Rao bound (CRB) with the aid of the AN, designing a beampattern with a wide main beam covering all possible angles of targets. The main beam width of the next iteration depends on the optimal

CRB. In this way, the sensing and security functionalities provide mutual benefits, resulting in the improvement of mutual performances with every iteration of the optimization, until convergence.

Overall, numerical results show the effectiveness of the ISAC security designs through the deployment of AN-aided secrecy rate maximization and CI techniques. The sensing-assisted PLS scheme offers a new approach for obtaining channel information of eavesdroppers, which is treated as a limitation of conventional PLS studies. This design gains mutual benefits in both single and multi-target scenarios.

Impact Statement

Integrating the sensing functionality into the wireless communication system is a crucial feature of the forthcoming sixth-generation (6G) Radio Access Network (RAN), enabling the use of dense cell infrastructures to create a perceptive network. Integrated sensing and communication (ISAC) systems can detect targets and communicate with users simultaneously, providing enhanced capabilities for a range of applications such as intelligent transportation, remote healthcare, and industrial automation. The attractive advantages of ISAC have drawn great attention from both academia and industry. The benefits of integrated sensing in upcoming 6G networks have been stressed by Ericsson and Nokia in their white papers in 2021, indicating that the inclusion of sensing capabilities in a communication network enhances the network performance itself by providing optimized input for rapid beam steering.

In the ISAC paradigm, the emitted dual-functional waveform carries confidential information, thus one of the key challenges of ISAC systems is preventing the communication data from being recovered by malicious targets to be detected. In 2021, Ericsson launched the Hexa-X as one of the essential projects of 6G. It is reported that ”for high security, the next generation should assure data privacy, the integrity of communications, confidentially, and operational resilience”, which highlighted the critical role of security studies for transmitted data, as well as extensions of research on information privacy at each end user. As per above, it motivates the security concerns for ISAC systems in this Thesis.

Moreover, opportunities regarding privacy, security, and trust have been implicated as the 6G flagship on localization and sensing have been presented by NXP and the University of Oulu. Therefore, it is crucial to be concerned about the security

of confidential information when evolving the sensing functionality toward future networks. However, there are several challenges to ensuring the security of ISAC systems: i) useful information is commonly embedded in probing signals for target detection, which possibly results in information leakage; ii) the use of Rician channels in mmWave frequencies, which contain a line of sight (LoS) component, results in an inescapable correlation with the sensing channel; iii) a unique and interesting conflict arises from the radar functionality side, the power is expected to be focused towards targets of interest to improve the detectability, while the useful signal information has to be protected from being intercepted by the targets (a.k.a. potential eavesdroppers). The research in this thesis bridges the gap to tackle these challenges and provides pioneer optimization results from the perspective of academia. The capability of decoding can be deteriorated at each target by designing the artificial noise (AN) at the transmitter side, while maintaining the power pointing to targets of interest. Additionally, it is illustrated that the confidential data intended for users can be efficiently protected even when the communication channel correlates with the sensing channel in mmWave frequencies.

The research in this thesis also provides theoretical support for the characterization and development of the PLS in ISAC schemes in the industry. The advanced approaches regarding the PLS in ISAC studied in this thesis are promising to be utilized in B5G and 6G networks. Additionally, threats and enablers for security and trust in the 6G era have been exploited in the white paper of Nokia in 2021, which stressed that 6G security research will be a key prerequisite to ensure the trustworthiness of communications in the year 2030.

Acknowledgements

Undertaking the Ph.D. has been an incredible experience and it would not have been possible without the support and guidance of many people.

First and foremost, I would like to express my sincere gratitude to my Ph.D. supervisor, Prof. Christos Masouros, for his invaluable support in pursuing my Ph.D. degree at UCL. He always inspires me to explore research both broadly and deeply, giving me the maximum freedom to pursue my research interests. I appreciate his generous support and encouragement in each paper we have produced together. The inestimable advice he gave to me has exerted an imperceptible influence and will continue to benefit me for the rest of my life. Academically and personally, working with him has truly been a joy. I also would like to acknowledge Prof. Christos Masouros, UCL, and the China Scholarship Council for the financial support during my Ph.D. study.

Then, I would like to thank my co-authors, including Dr. Fan Liu, Dr. Zhongxiang Wei, Dr. Ya-Feng Liu, Prof. Tharmalingam Ratnarajah, and Prof. Athina Petropulu, for their valuable and insightful remarks in the paper we worked together. In particular, I would like to give my special thanks to Dr. Fan Liu, whose unstinting support from the very beginning of my Ph.D. has been of great help in my academics.

I would like to further express my appreciation to Prof. Kai-kit Wong and Dr. Matt Ritchie for attending my MPhil to Ph.D. transfer and providing helpful advice on my presentation skills and research topics. I am also grateful to Prof. Miguel Rodrigues and Dr. Yansha Deng for being examiners of my Ph.D. viva, and for their insightful comments that highly improved the quality of this thesis.

Moreover, I am also thankful to my UCL colleagues, including but not limited

to: Dr. Ang Li, Dr. Xiaoyan Hu, Dr. Jianjun Zhang, Dr. Abdelhamid Albaraesi, Dr. Aryan Kaushik, Dr. Mohammad Abdullahi, Dr. Murat Temiz, Dr. Tongyang Xu, Dr. Yin Bi, Dr. Nithin Babu, Mr. Jingsong Sun, Miss. Xiaoye Jing, Mr. Iman Valiulahi, Miss Jiaqi Zou, Mr. Jiaming Hu, Miss Victoria Cao, and Mr. Zhiyuan Chu.

Finally, I would like to express my deepest and most sincere gratitude to my parents, who always support me and love me unconditionally. I am profoundly grateful for their understanding, encouragement, and support in me to pursue my Ph.D. at UCL.

Contents

List of Abbreviations

5G	Fifth Generation
AML	Approximate Maximum Likelihood
AN	Artificial Noise
AOD	Angle of Departure
AP	Access Point
AWGN	Additive White Gaussian Noise
B5G	Beyond Fifth Generation
BPSK	Binary Phase-Shift Keying
BS	Base Station
CAESAR	Multi-Carrier AgilE phaSed Array Radar
CAML	Capon and Approximate Maximum Likelihood
CC	Communication-Centric
CE	Constant Envelope
CI	Constructive Interference
CM	Constant Modulus
CRB	Cramér-Rao bound
CSI	Channel State Information
CSIT	Channel-Side Information at the Transmitter

CU	Communication User
DoF	Degree of Freedom
DAC	Digital-to-Analog Converter
DFRC	Dual-Functional Radar Communication
DI	Destructive Interference
DM	Directional Modulation
DOA	Direction of Arrival
DOD	Direction of Departure
DPC	Dirty Paper Coding
FFT	Fast Fourier Transform
FH	Frequency Hopping
FIM	Fisher Information Matrix
FP	Fractional Programming
IM	Index Modulation
IPM	Interior Point Method
ISAC	Integrated Sensing and Communication
LFM	Linear Frequency Modulation
LMI	Linear Matrix Inequality
LoS	Line of Sight
LS	Least-Squares
MF	Matched Filter
MI	Mutual Information
MIMO	Multi-Input Multi-Output
MMSE	Minimum Mean Square Error

MRT	Maximum Ratio Transmission
MSE	Mean Square Error
NOMA	Non-Orthogonal Multiple Access
MUI	Multi-User Interference
MU-MISO	Multi-User Multiple-Input Single-Output
MVDR	Minimum Variance Distortionless Response
NFDAM	Near-Field Direct Antenna Modulation
OFDM	Orthogonal Frequency-Division Multiplexing
PAPR	Peak-to-Average Power Ratio
PDF	Probability Density Function
PLS	Physical Layer Security
PLSR	Peak to Sidelobe Ratio
PS	Phase Shifter
QCQP	Quadratically Constrained Quadratic Program
QoS	Quality of Service
QPSK	Quadrature-Phase-Shift Keying
R&C	Radar and Communication
RadCom	Radar-Communication System
RF	Radio Frequency
RC	Radar-Centric
RMSE	Root Mean Square Error
RR	Radar Receiver
RZF	Regularised Zero-Forcing
S&C	Sensing and Communication

SCA	Successive Convex Approximation
SDP	Semidefinite Programming
SDR	Semi-Definite Relaxation
SER	Symbol Error Rate
SLP	Symbol Level Precoding
SNR	Signal-to-Noise Ratio
SINR	Signal-to-Interference-plus-Noise Ratio
SOA	Sequential Optimization Algorithm
SOC	Second-Order Cone
SQ	Successive Quadratically Constrained Quadratic Program
SVD	Singular Value Decomposition
THP	Tomlinson-Harashima Precoding
ULA	Uniform Linear Array
ZF	Zero-Forcing

List of Notations

a	Scalar
$\mathbf{a}$	Vector
$\mathbf{A}$	Matrix
j	Imaginary unit
$\mathcal{O}(\cdot)$	Order of numerical operations
$\mathbb{C}^{m\times n}$	A $m\times n$ matrix in the complex set
$\mathbb{CN}(\alpha,\beta)$	Complex normal distribution
$\mathbb{R}$	Set of real numbers
$\mathbb{E}\{\cdot\}$	Expectation of a random variable
$(\cdot)^T$	Transpose
$(\cdot)^*$	Conjugate
$(\cdot)^H$	Conjugate transpose
$(\cdot)^{-1}$	Inverse of a square matrix
$(\cdot)^\dagger$	Moore-Penrose inverse
$\mathrm{tr}\{\cdot\}$	Trace of a matrix
$\det(\cdot)$	The determinant of a square matrix
$\mathrm{diag}(\mathbf{a})$	Transformation of the vector $\mathbf{a}$ into a diagonal matrix
$\mathrm{vec}(\cdot)$	Vectorisation operation
$\mathrm{vecd}(\cdot)$	Diagonal extraction operator

$\mathrm{card}(\cdot)$	Cardinality of $(\cdot)$
$\mathrm{var}(\cdot)$	Variance of random variables
$\min(\cdot)$	Minimum entry of a vector
$\max(\cdot)$	Maximum entry of a vector
∞	Infinity
$\in$	$\mathrm{X} \in \mathrm{Y}$ indicates that X takes values from the set Y
$\forall$	For all
$\sim$	Indicates "distributed as"
$\lvert\cdot\rvert$	Absolute value or modulus
$\lVert\cdot\rVert$	Standard norm
$\lVert\cdot\rVert_2$	Euclidian form
$\lVert\cdot\rVert_F$	Frobenius norm
$[\mathbf{A}]_{m,n}$	The element in the m-th row and n-th column of $\mathbf{A}$
$[\mathbf{a}]_m$	The m-th entry in the vector $\mathbf{a}$

List of Figures

List of Tables

Chapter 1

Introduction

1.1 Background and Motivation

1.1.1 Background

As the 5G wireless networks are being rolled-out worldwide, emerging applications, such as connected cars, smart factories, and digital twins, have intensified the need to extend the capabilities of existing network infrastructures [6]. These applications demand both increasingly high-quality communication as well as high accuracy and robustness of sensing, and it is well-recognized that the cooperation and co-design between communication and radar systems will play a significant role in the upcoming beyond 5G (B5G) and 6G eras.

At the early stage of the radar-communication (RadCom) system studies, the two systems were conceived to spectrally coexist with each other, thus easing the severe competition over the scarce spectrum resources [7, 8]. In the forthcoming B5G/6G eras, radio sensing and communications (S&C) are both evolving towards higher frequency bands and large-scale antenna arrays, which leads to striking similarities between S&C systems in terms of hardware architecture, channel characteristics, and information processing pipeline [9]. In light of this, the research on the coexistence of radar and communication systems has evolved into dual-functional radar communication (DFRC) systems. The joint design of the S&C operations, in the form of Integrated Sensing and Communications (ISAC), have been initially proposed in [10]. ISAC systems are expected to achieve higher spectral and energy efficiencies,

but most importantly, promote a new paradigm of integration for attaining mutual benefits from a co-design perspective, wherein the S&C functionalities can mutually assist each other. Benefiting from these two advantages, applications of ISAC have been extended to numerous emerging areas, including smart manufacturing, environmental monitoring, vehicular networks, as well as indoor services such as human activity recognition.

In the ISAC system, radar and communication functionalities are realized by a well-designed probing waveform that also carries communication signaling and data. Evidently, this operation implicates security concerns, which are largely overlooked in the relevant ISAC literature. This is because the probing signal conveys information intended for communication users, while the radar beam is designed to point towards targets, thus it opens the possibility for malicious targets to eavesdrop on confidential information.

With the increasingly deep integration of the communication and sensing functionalities, it has arisen wide concerns about the PLS in the practical implementations of ISAC. For instance, in smart grids, a secure and reliable communication infrastructure is essential for the smooth functioning of smart grids. PLS techniques can protect sensitive data, such as energy consumption patterns and grid control commands, from eavesdropping and tampering. This will improve the overall security and stability of the smart grid system. Besides, the ISAC systems in autonomous vehicles are critical for their safe operation. By implementing PLS techniques, these vehicles can maintain secure communication channels, preventing potential attackers from intercepting or manipulating data, which could lead to accidents or compromise the privacy of passengers. Moreover, the Internet of Things (IoT) and Industry 4.0 rely heavily on interconnected devices and sensors to optimize operations and automate industrial processes. PLS methods can safeguard these systems from unauthorized access and cyberattacks, ensuring the privacy of data and the reliability of communication between devices.

In light of the above, this Thesis focuses on interesting open-ended related to exploiting the PLS in ISAC systems.

1.1.2 Motivations

The PLS techniques have been widely studied in existing literature for communication-only scenarios. With the evolution of ISAC, increasing security risks emerge and should be taken into consideration, which presents a significant number of open questions. Opportunities regarding privacy, security, and trust have been implicated as the 6G flagship on localization and sensing. Therefore, it is crucial to be concerned about the security of confidential information when evolving the sensing functionality toward future networks. However, there are several challenges to ensuring the security of ISAC systems: i) useful information is commonly embedded in probing signals for target detection, which possibly results in information leakage; ii) the use of Rician channels in mmWave frequencies, which contain a line of sight (LoS) component, results in an inescapable correlation with the sensing channel; iii) a unique and interesting conflict arises from the radar functionality side, the power is expected to be focused towards targets of interest to improve the detectability, while the useful signal information has to be protected from being intercepted by the targets (a.k.a. potential eavesdroppers).

It is known that typical radar requires focusing the transmit power towards the directions of interest to estimate targets accurately. Nevertheless, in the case of ISAC transmission, critical information embedded in the probing waveform could be leaked to the radar targets, which might be potential eavesdroppers at the adversary's side. To this end, it is essential to take information security into consideration for the ISAC design. To secure confidential information in ISAC systems, existing approaches can be generally divided into the following categories, i.e., 1) Cryptography and 2) Physical layer security (PLS). Conventionally, the security of communication systems is regarded as an independent feature and addressed at the upper layers of the protocol stack by deploying cryptographic technologies. The studies of cryptography commonly assume that the physical layer provides an error-free link [11], while the wireless links are vulnerable to attacks in practice, which would result in a high risk of information leakage. It is worth pointing out that 5G has already been a large-scale heterogeneous network with multiple levels and weakly-structured architectures,

which makes it difficult to distribute and manage secret keys [12]. Also, complicated encryption/decryption algorithms cannot be straightforwardly applied considering the power consumption in 5G networks. Furthermore, even if the data is encrypted, the detection of a wireless link from a potential eavesdropper can reveal critical information. In contrast to complex cryptographic approaches, signal processing operations of PLS are usually simple with little additional overheads.

In the communication literature, PLS has been widely investigated, where the eavesdroppers' reception can be crippled by exploiting transmit degrees of freedom (DoFs) [13]. For instance, a meaningful technique for enabling physical layer secrecy was presented in [13, 14], namely, artificial noise (AN) aided transmission. Besides, the AN generation algorithm studied in [14, 15] was with the premise of publicly known channel state information (CSI) in a fading environment, where AN lies in the null-space of the transmission channel. However, these techniques are conceived to address the PLS for communication-only scenarios such that they are unable to be straightforwardly applied to secure ISAC transmission. Methods applying the AN to secure the ISAC systems will be explored in Chapter 3 of this Thesis.

Moreover, in conventional beamforming designs, AN indeed degrades SINR at both communication users (CUs) and eavesdroppers, which requires a higher power budget to ensure the quality of service (QoS). In view of the redundant power consumption caused by AN, directional modulation (DM) has attracted growing research attention as an emerging hardware-efficient approach to secure wireless communication systems in recent years [16–18]. The DM transmitter sends confidential information to the CUs such that the malicious eavesdroppers cannot intercept the transmitted messages [19]. Unlike the secrecy rate-based methods, DM technique adjusts the amplitude and phase of the symbols at the users of interest directly while scrambling the symbols in other undesired directions, which implies that the modulation happens at the antenna level instead of at the baseband level. As a result, a low symbol error rate (SER) can be endorsed at the CUs, while the received symbols of the eavesdropper are randomized in the signal constellation. Since the expensive and power-consuming radio frequency (RF) chains and digital-to-analog

converter (DAC) deployed in conventional beamforming design are not required, the DM-based scheme is efficient in aspects of both cost and energy. The DM approach is based on the principles of exploiting constructive interference (CI) [2, 20–22], where the received signal is not necessary to be aligned with the intended symbols, but is pushed away from the detection thresholds of the signal constellation. One step further, the CI-based method will be presented in Chapter 4 of this Thesis.

Finally, we note that existing works on secure ISAC transmission, the radar and communication systems work individually over separate end goals rather than cooperating with each other. A major limitation of PLS is the need to obtain some information for the potential Eves. This ranges from full CSI, to an SNR estimate of the eavesdropper's link, or the eavesdropper's direction as a minimum. This difficult-to-obtain information often renders PLS impractical. Benefiting from the ISAC framework naturally, the sensing functionality of ISAC offers an enabling role here, by estimating the directions of potential Eves to inform PLS. To this end, a sensing-aided algorithm to ensure communication data security in ISAC systems will be presented in Chapter 5 of this Thesis.

1.2 Main Contributions

This Thesis aims at protecting the confidential information from the transmitter to CUs in ISAC systems by introducing and analyzing various techniques regarding PLS and implementing the algorithms in the ISAC systems. The main contributions of this Thesis can be highlighted and summarized in the following list:

- Joint design of the beamformer and AN is presented in order to ensure the information transmission security of the ISAC system, where a MIMO dual-functional BS serves multiple legitimate users while detecting a target. The designed strategy takes possible robustness into consideration, including the knowledge of imperfect target location and the partial CSI. The results show the feasibility of the algorithms with the existence of instantaneous and statistical CSI errors. In addition, the secrecy rate of secure ISAC systems grows with the increasing angular interval of location uncertainty. (Chapter 3)

- Security solutions are studied for ISAC systems by exploiting known interference, where the directional modulation approach is applied to exploit the CI. Transmit waveform and receive beamforming are jointly designed to maximize the SINR of the radar under security and power budget constraints. Then, destructive interference (DI) was utilized by pushing the received symbols at the target towards the destructive region of the signal to further deteriorate the eavesdropping signal at the radar target. Simulation results verify the effectiveness of the proposed design showing a secure transmission with enhanced performance. (Chapter 4)

- Rather than the radar and communication units working individually in most existing studies, approaches of the sensing-aided PLS towards ISAC systems are studied. A well-known limitation of PLS is the need to have information about potential eavesdroppers. The sensing functionality of ISAC offers an enabling role here, by estimating the directions of potential Eves to inform PLS. A weighted optimization problem is formulated to simultaneously maximize the secrecy rate and minimize the Cramér-Rao Bound (CRB) with the aid of the AN, and minimize the CRB of targets'/Eves' estimation. Numerical results avail of these mutual benefits and reveal the usefulness of sensing as an enabler for practical PLS. (Chapter 5)

1.3 Thesis Organization

Sequential to this chapter of introduction, the rest of this thesis is organized as follows. Chapter 2 introduces some fundamental concepts and preliminaries of the related works. Chapter 3 and Chapter 4 introduce efficient approaches to ensuring the PLS in ISAC systems, including AN-aided algorithm and CI-based symbol level precoding (SLP). Furthermore, Chapter 5 studies a sensing-assisted PLS approach, which promotes deeper integration between communication and sensing functionalities. Finally, the conclusions and future works based on this thesis are presented in Chapter 6. Fig. 1.1 shows the architecture of the thesis organization. The content and contributions of the chapters following the Introduction are summarized as follows.

Chapter 2: Fundamental Concepts and Related Works. This chapter provides a thorough review of the fundamental concepts related to this thesis, and a comprehensive literature review is also given to demonstrate the relevant state-of-the-art work. In particular, this chapter focuses on the precoding schemes in communication and waveform designs in radar, followed by an overview of the ISAC systems and approaches to ensuring the PLS. At the end of this chapter, fundamental metrics for secure ISAC systems are introduced.

Chapter 3: Artificial Noise Aided Physical Layer Security in ISAC Systems. In this chapter, we study the security issue in ISAC systems with the assistance of AN. The DFRC base station (BS) emits dual-functional waveforms to communicate with CUs and sense targets simultaneously. To avoid information leakage, AN is added at the transmitter side. We jointly design the beamforming matrix and the AN covariance matrix to ensure the transmission rate difference between the CUs and the target, in order to maximize the secrecy rate accordingly. To be practical, the robustness of the target location known to the BS and imperfect CSI are further taken into account.

Chapter 4: Secure ISAC Systems Deploying the Constructive Interference Technique. In this chapter, we deploy the SLP to secure the ISAC system. Inspired by the concept of CI, the known multi-user interference (MUI) is exploited to contribute to the SNR at CUs, which pushes the received symbols into the constructive region by designing the waveform and the receive beamforming matrix jointly. Due to the nature of the CI technique, symbols received at eavesdroppers are randomly distributed. To further deteriorate the decoding capability of the eavesdropper, DI is applied to limit the received symbols at the target within the destructive region. Considering the target location is commonly estimated imprecisely, the robustness of the target angle is considered in the problem formulations.

Chapter 5: Sensing-assisted PLS in ISAC Systems. In this chapter, we present a sensing-assisted PLS technique, which integrates the functionalities deeply. To start with, the DFRC access point (AP) emits an omnidirectional beampattern for target search and angle estimation. Note that the CRB of the deployed estimation

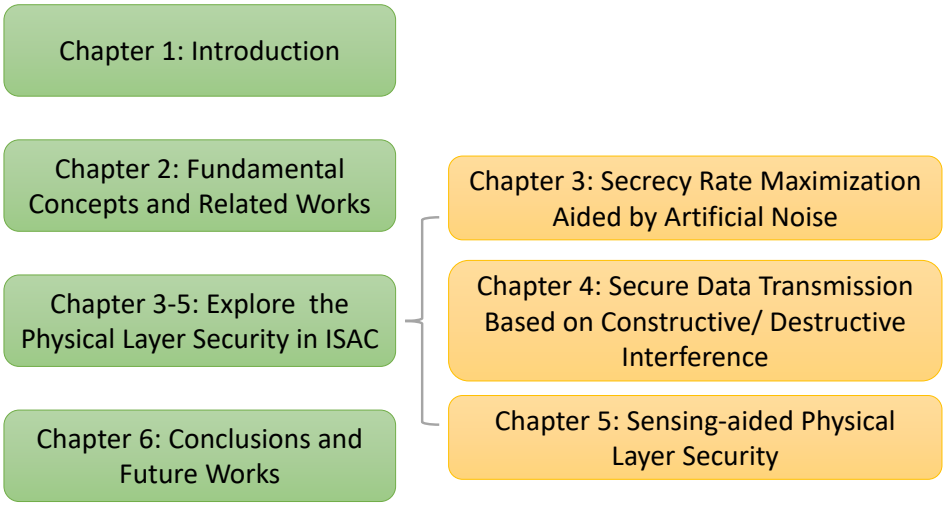

Figure 1.1: Thesis Organisation.

method can be derived. With the initially estimated target direction and estimating accuracy at hand, a weighted optimization problem is designed to maximize the secrecy rate and minimize the CRB, while generating a beampattern with a wide main beam, where the main beam covers all possible angles of targets. Then, the beam width is narrowed by the optimal CRB. The weighted optimization problem can be reformulated by updating the main beam width. In this way, the security metric and the estimation accuracy can be jointly optimized by solving the optimization problem iteratively.

Chapter 6: Conclusions and Future Work. This chapter concludes this Thesis with a summary of all the contributions presented in the previous chapters, and future research work within the framework of this Thesis is also discussed.

1.4 List of Publications

The above-mentioned contributions in this Thesis have resulted in the following publications.

1.4.1 Journal Papers

[J1] **N. Su**, F. Liu and C. Masouros, "Secure Radar-Communication Systems With Malicious Targets: Integrating Radar, Communications and Jamming Functionalities," in IEEE Transactions on Wireless Communications, vol. 20,

no. 1, pp. 83-95, Jan. 2021, doi: 10.1109/TWC.2020.3023164.

[J2] **N. Su**, F. Liu, Z. Wei, Y. -F. Liu and C. Masouros, "Secure Dual-Functional Radar-Communication Transmission: Exploiting Interference for Resilience Against Target Eavesdropping," in IEEE Transactions on Wireless Communications, vol. 21, no. 9, pp. 7238-7252, Sept. 2022, doi: 10.1109/TWC.2022.3156893.

[J3] **N. Su**, F. Liu, and C. Masouros, "Sensing-Assisted Eavesdropper Estimation: An ISAC Breakthrough in Physical Layer Security". arXiv preprint arXiv:2210.08286, 2022. *(submitted to TWC, under review)*

1.4.2 Conference Papers

[C1] **N. Su**, F. Liu and C. Masouros, "Enhancing the Physical Layer Security of Dual-Functional Radar Communication Systems," 2019 IEEE Global Communications Conference (GLOBECOM), 2019, pp. 1-6, doi: 10.1109/GLOBECOM38437.2019.9013227.

[C2] **N. Su**, Z. Wei and C. Masouros, "Secure Dual-Functional Radar-Communication System via Exploiting Known Interference in the Presence of Clutter," 2021 IEEE 22nd International Workshop on Signal Processing Advances in Wireless Communications (SPAWC), 2021, pp. 451-455, doi: 10.1109/SPAWC51858.2021.9593096. *(Invited Paper)*

[C3] **N. Su**, F. Liu, C. Masouros, T. Ratnarajah and A. Petropulu, "Secure Dual-functional Radar-Communication Transmission: Hardware-Efficient Design," 2021 55th Asilomar Conference on Signals, Systems, and Computers, 2021, pp. 629-633, doi: 10.1109/IEEECONF53345.2021.9723251. *(Invited Paper)*

[C4] **N. Su**, F. Liu, and C. Masouros, "Sensing-Assisted Physical Layer Security". *(submitted to WSA&SCC 2023, invited paper)*

1.4.3 Book Chapter

[B1] **N. Su**, F. Liu, C. Masouros, and A. Petropulu, Security and Privacy in ISAC, *Integrated Sensing and Communications (ISAC)*. *(under review)*

1.4.4 Contributions during Ph.D. that are not included in this thesis: Magazine Paper

[E1] Z. Wei, F. Liu, C. Masouros, **N. Su** and A. P. Petropulu, "Toward Multi-Functional 6G Wireless Networks: Integrating Sensing, Communication, and Security," in IEEE Communications Magazine, vol. 60, no. 4, pp. 65-71, April 2022, doi: 10.1109/MCOM.002.2100972.

Chapter 2

Fundamental Concepts and Related Works

2.1 Precoding Methods for Communications

2.1.1 Preliminaries on Precoding

In multi-antenna wireless communication, precoding is the generalization of beamforming to support multiple streams of data, which exploits the channel-side information at the transmitter (CSIT) by operating on the signal before transmission [23, 24]. Linear precoder is optimal from an information-theoretic viewpoint with the knowledge of partial CSIT [25], serving as a multi-mode beamformer via matching the input signal optimally to the channel. This is achieved by splitting the transmit signal into orthogonal spatial eigenbeams, with stronger channels assigned higher power, and weak channels with lower or no power. Precoding design varies depending on the type of CSIT and the performance criteria [24, 26, 27].

We firstly introduce how precoding works in the downlink transmission of a multi-antenna system as preliminaries, where the precoding techniques can be classified into two categories: linear precoding and nonlinear precoding. Since users are usually separate and do not cooperate in the downlink transmission, in order to manage the potential MUI, the BS needs to perform some signal processing techniques on the data symbols prior to transmission based on the CSI, and this is where the term 'precoding' comes from.

We consider a multi-user multiple-input single-output (MU-MISO) system in the downlink, where the BS is equipped with N_t to transmit antennas communicating with K users. The channel is assumed to be baseband discrete memoryless. The received signal at the k-th user can be expressed as

$$y_k = \mathbf{h}_k^T \mathbf{x} + z_k, \tag{2.1}$$

where $\mathbf{x} \in \mathbb{C}^{N_t \times 1}$ is the precoded signal vector, $\mathbf{h}_k \in \mathbb{C}^{N_t \times 1}$ is the channel vector corresponding to the k-th user, and z_k is a complex scalar representing the AWGN at the k-th receiver with zero mean and variance σ_C^2. Particularly, the output signal at the transmitter is given as

$$\mathbf{x} = \sum_{k=1}^{K} \mathbf{w}_k s_k = \mathbf{W}\mathbf{s}, \tag{2.2}$$

where $\mathbf{W} = [\mathbf{w}_1, \cdots, \mathbf{w}_K] \in \mathbb{C}^{N_t \times 1}$ denotes the precoding matrix with each column being the precoder for the k-th user and $\mathbf{s} \in \mathbb{C}^{K \times 1}$ is the data symbol vector.

The signal model can be equivalently recast in a vector form as follows

$$\mathbf{y} = \mathbf{H}\mathbf{x} + \mathbf{z}, \tag{2.3}$$

where $\mathbf{H} = [\mathbf{h}_1, \cdots, \mathbf{h}_K]^T \in \mathbb{C}^{N_t \times K}$ represents the channel matrix, $\mathbf{y} \in \mathbb{C}^{K \times 1}$ is the received signal vector, and $\mathbf{z}$ is the noise vector. Assume that each block contains L symbols and the channel matrix remains constant in each block.

Precoding methods can be classified on two major axes, i.e., group size and switching rate, as shown in Fig. 2.1. In this section, we overview the existing precoding schemes based on different switching rates.

2.1.2 Block-level Precoding

The block-level precoding matrix is applied across a block of symbols, indicating that the beamformer designs at a block level by utilizing the knowledge of the channel information. It is updated with the channel and fixed over a block of information symbols. Block-level precoding approaches have been widely studied in existing work, including linear closed-form precoding schemes such as maximum

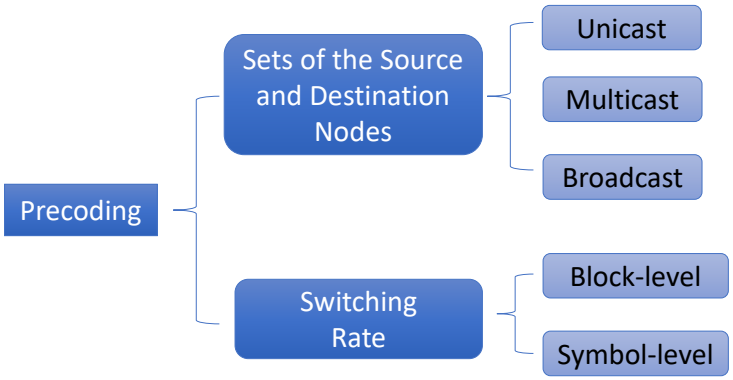

Figure 2.1: Precoding categories.

ratio transmission (MRT), zero-forcing (ZF), regularised zero-forcing (RZF) [24, 28–30], non-linear precoding schemes such as Dirty Paper Coding (DPC), Tomlinson-Harashima Precoding (THP), [31, 32], and optimization-based precoding approaches [33–35].

2.1.2.1 Linear Precoding

Maximum Ratio Transmission (MRT): The MRT precoding algorithm is known as a counterpart of the Matched Filter (MF) precoding, which is the simplest precoding method. MRT aims to maximize the received SNR but ignores the MUI, thus the precoding matrix is written as [36–38]

$$\mathbf{W}_{\text{MRT}} = \frac{1}{f_{\text{MRT}}} \cdot \mathbf{H}^H = \frac{\mathbf{H}^H}{\sqrt{\text{tr}\{\mathbf{H}\mathbf{H}^H\}}}. \tag{2.4}$$

where f_{MRT} is the normalization factor that maintains the power of the transmit signal after precoding, which is known as the noise amplification factor. It can be noted from (2.4) that the MRT/MF precoding creates MUI, however, the residual MUI is minimized because channels corresponding to each user tend to be quasi-orthogonal when the number of antennas of the BS is sufficiently large.

Zero-Forcing (ZF): ZF precoding is also widely applied as a simple linear precoding in existing studies [39–41]. The precoding matrix is given by the Moore-

Penrose inverse of the channel as

$$\mathbf{W}_{\mathrm{ZF}} = \frac{1}{f_{\mathrm{ZF}}} \cdot \mathbf{H}^{\dagger} = \frac{1}{f_{\mathrm{ZF}}} \cdot \mathbf{H}^{H}\left(\mathbf{H}\mathbf{H}^{H}\right)^{-1}, \tag{2.5}$$

where $f_{\mathrm{ZF}} = \sqrt{\mathrm{tr}\left\{(\mathbf{H}\mathbf{H}^{H})^{-1}\right\}}$ denotes the normalization factor. ZF precoding is designed to eliminate the MUI by pointing the signal beam towards the intended user, while nulling the rest directions of other users. However, it meanwhile raises the pre-detection noise at the receiver which is negligible in practice. Thus, the ZF algorithm achieves accurate results at high SNR [32, 42].

Regularised Zero-Forcing (RZF): RZF is also referred to as the MMSE precoder, which is considered as the state-of-the-art linear precoder for MIMO wireless communication systems to balance the trade-off of the advantages with respect to MF and ZF precoders [30]. According to [43, 44], the RZF precoding matrix is given as

$$\begin{aligned} \mathbf{W}_{\mathrm{RZF}} &= \frac{1}{f_{\mathrm{RZF}}} \cdot \mathbf{H}^{H}\left(\mathbf{H}\mathbf{H}^{H} + \vartheta \cdot \mathbf{I}\right)^{-1} \\ &= \frac{\mathbf{H}^{H}\left(\mathbf{H}\mathbf{H}^{H} + \vartheta \cdot \mathbf{I}\right)^{-1}}{\sqrt{\mathrm{tr}\left\{(\mathbf{H}\mathbf{H}^{H} + \vartheta \cdot \mathbf{I})^{-1}\mathbf{H}\mathbf{H}^{H}(\mathbf{H}\mathbf{H}^{H} + \vartheta \cdot \mathbf{I})^{-1}\right\}}}, \end{aligned} \tag{2.6}$$

where ϑ the scalar to regularize $\mathbf{H}^{H}\mathbf{H}$. Specifically, it performs as ZF precoding when $\vartheta \to 0$ and as the MF precoding when $\vartheta \to \infty$ [43]. Unlike ZFB, multi-user interference cannot be canceled by RZF and thus needs to be limited by optimizing the regularization parameter, i.e., minimizing the mean square error (MSE) between the transmitted and received symbols. Thus, it is termed as minimum MSE (MMSE) precoder [45–47]. For clarity, the main complexity of linear precoding techniques is summarized in table 2.1.

Linear Precoding			
Name	Closed-form Expression	Complexity	Performance
MF	$\mathbf{W}_{\mathrm{MF}} = \frac{1}{f_{\mathrm{MF}}} \cdot \mathbf{H}^{H}$	$\mathcal{O}\left(K^3\right)$	Lowest
ZF	$\mathbf{W}_{\mathrm{ZF}} = \frac{1}{f_{ZF}} \cdot \mathbf{H}^{H}\left(\mathbf{H}\mathbf{H}^{H}\right)^{-1}$	$\mathcal{O}\left(K^3\right)$	Better than MF
RZF	$\mathbf{W}_{\mathrm{RZF}} = \frac{1}{f_{RZF}} \cdot \mathbf{H}^{H}\left(\mathbf{H}\mathbf{H}^{H} + \vartheta \cdot \mathbf{I}\right)^{-1}$	$\mathcal{O}\left(K^3\right)$	Balance benefits from MF and ZF

Table 2.1: Summary of linear precoding methods

2.1.2.2 Non-linear Precoding

The linear block-level precoding algorithms given above are characterized by lower complexity and are widely applied in practical implementations. However, it is at the expense of performance loss, especially when the number of users K is close to the number of transmit antennas N_t. In order to enhance the flexibility of the transmitter, non-linear precoding methods are developed, including DPC, THP algorithms [31,32,48,49]. Besides, a number of optimization-based precoding techniques have also been developed, which generally aim to optimize the transmitted average sum power, whilst ensuring the quality of service (QoS). In what follows, formulations of optimization-based precoding algorithms will be elaborated.

The transmit power can be expressed as $P_t = \sum_{k=1}^{K} \|\mathbf{w}_k\|^2$ in the block-level precoding. To this end, the power minimization problem with constraints on communication QoS can be generally formulated as follows [50, 51]

$$\begin{aligned} \mathbf{W}(\mathbf{H}, \boldsymbol{\gamma}) = &\arg \min_{\mathbf{W}} \sum_{k=1}^{K} \|\mathbf{w}_k\|^2 \\ &\text{s.t.} \ \frac{\left|\mathbf{h}_k^T \mathbf{w}_k\right|^2}{\sum_{i=1, i\neq k}^{K} \left|\mathbf{h}_k^T \mathbf{w}_i\right|^2 + \sigma_C^2} \geq \gamma_k, \forall k, \end{aligned} \tag{2.7}$$

where $\mathbf{W}$ is the precoding matrix to be designed, which is regarded as a function of $\mathbf{H}$ and $\boldsymbol{\gamma}$, and $\boldsymbol{\gamma}$ represents a vector with elements of each user's SINR threshold.

Moreover, another optimization-based precoder design is to maximize the minimum SINR of communication users, while ensuring the transmit power is lower than a given threshold [52, 53]. It is known as the max-min fair optimization problem and formulates as

$$\begin{aligned} \mathbf{W}(\mathbf{H}, P_0) = &\arg \max_{\mathbf{W}} \min_{k} \frac{\left|\mathbf{h}_k^T \mathbf{w}_k\right|^2}{\sum_{i=1, i\neq k}^{K} \left|\mathbf{h}_k^T \mathbf{w}_i\right|^2 + \sigma_C^2} \\ &\text{s.t.} \sum_{k=1}^{K} \|\mathbf{w}_k\|^2 \leq P_0, \end{aligned} \tag{2.8}$$

where P_0 denotes the given power budget. Note that the optimization problems above can be tackled by adopting semi-definite relaxation (SDR) technique. Typically, a multi-antenna BS has individual power amplifiers in its analog front-end, and each amplifier's linearity limits each antenna individually [54, 55]. The optimization problem can be further extended to the per-antenna power constraints by replacing the one regarding the power budget with $\sum_{k=1}^{K}\left[\mathbf{w}_k\mathbf{w}_k^H\right]_{nn} \leq \tilde{P}_0$.

As given above, block-level precoding approaches can be classified into linear precoding and nonlinear precoding, which are deployed to mitigate the interference among the users' data streams. Moreover, with the knowledge of transmitting data and channel information, the precoding can be performed at the symbol level. In what follows, the SLP techniques will be introduced in detail.

2.1.3 Symbol-level Precoding

Differing from the block-level precoding, the SLP scheme indicates that the data and channel information can be used to perform SLP at the transmitter [56]. The SLP paradigm is proposed in this subsection in two different research directions, including DM through analog SLP derived from antennas and propagation, as well as digital SLP for CI, developed in signal processing.

The main difference between DM and digital SLP for CI is that DM technique uses array weights in the analog domain to adjust the amplitude and phase of the signals received on the receiving antennas, while the latter uses SLP as part of the digital signal design at the transmitter in order to create CI at the receiver [57]. For clarity, the architectures of the conventional transmitter, the analog SLP/DM, and the digital SLP/CI are given in Fig. 2.2, Fig. 2.3, and Fig. 2.4, respectively. In the following, a detailed description of DM and digital SLP (CI) is presented to show the differences and similarities between both schemes.

2.1.3.1 Analog Symbol-level Precoding for DM

The DM transceiver consists of only one RF chain fed by a local RF oscillator, which is illustrated in Fig. 2.3. In DM, the CSI and transmit symbols are utilized to design the phase and amplitude of each antenna in a symbol level, such that the MUI can be

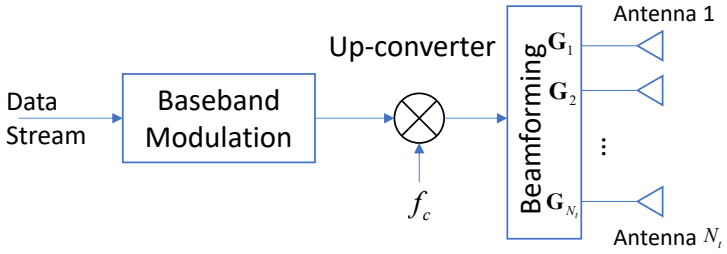

Figure 2.2: Conventional transmitter array architecture [1].

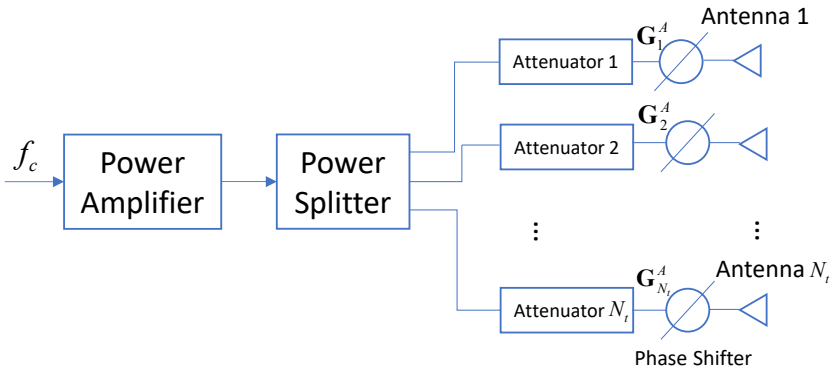

Figure 2.3: Generic analog SLP/DM transmitter architecture [1].

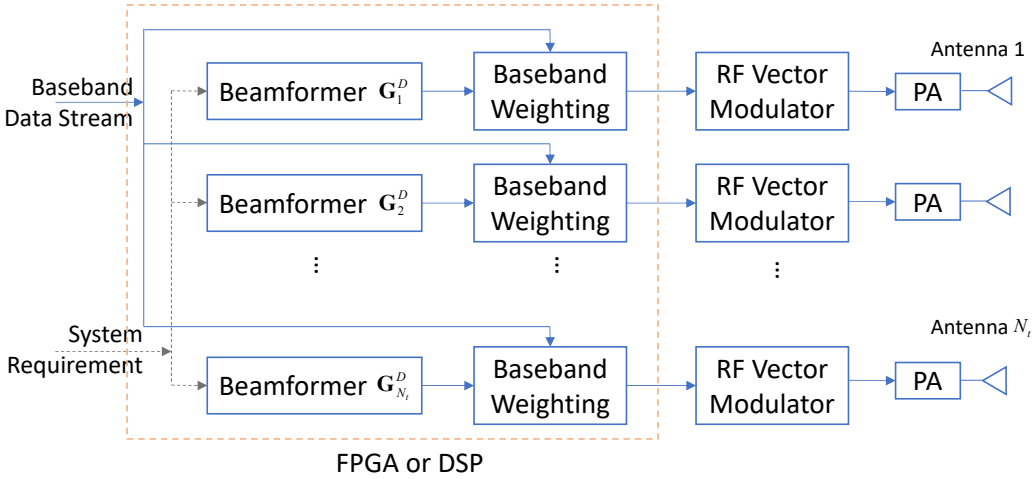

Figure 2.4: Generic digital SLP/CI transmitter architecture [1].

degraded or even eliminated in the communication cellular network. By adjusting the antennas, we can obtain the array weight vector, which modulates the emitted RF signals from the transmitting antenna array. To this end, symbols are well-designed for the desired phase and amplitude at the receiver side instead of generating the symbols at the transmitter and sending them. It implies that the receivers' antennas can directly recover the symbols without channel equalization [16, 18, 58, 59].

Early DM research employed parasitic antennas to produce the desired amplitude and phase in the far field via near field interactions between driven antenna elements and multiple reflectors [60–63]. In [63], the authors introduced a near-field direct antenna modulation (NFDAM) technique, which forms a DM signal by both a transmit beam and a reflected beam. To be specific, transistor switches or varactor diodes can be deployed to change the reflector length or its capacitive load, respectively, deploying LoS channels [60]. Furthermore, the authors in [61] concluded that the coverage area of the parasitic antenna is a planar convex region.

Unlike the research above using a single driven element in a parasitic array, symbol-level array switching techniques were presented in [18, 64–66], which aimed to transmit information only in a specified direction. Particularly, a reconfigurable array with a specific fixed delay in each RF chain was proposed to create the desired symbols by properly switching the antennas, which allows information to be sent over a narrower beamwidth and provides more selectivity in the possible transmit angles [64]. Moreover, as studied in [65], BPSK constellations were directionally modulated by switching the array elements.

2.1.3.2 Digital Symbol-level Precoding for CI

Despite the simplicity of RF chain transceivers and the low power consumption, there are several limitations relating to implementation difficulties and a lack of an algorithmic framework that needs to be studied further in the field of directional modulation. In digital SLP for CI, the transmit signal is precoded at the transmitter to create CI at the receiver. According to the criteria of digital precoding, the SLP happens before transmitting the signal to the antenna array. Differing from the analog symbol-level precoding in DM, the SLP developed in signal processing and wireless

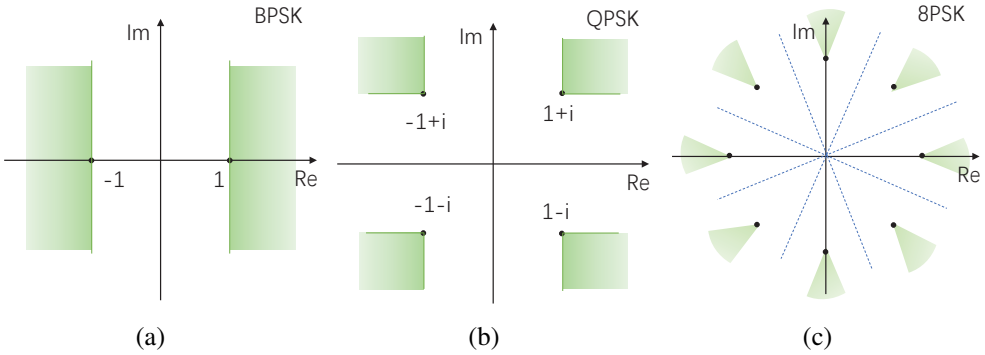

Figure 2.5: Constructive interference sectors for (a) BPSK, (b) QPSK, (c) 8PSK.

communications focused on algorithmic studies.

In block-level designs, the MUI is considered harmful which should be mitigated [67–69]. However, in CI studies, the instantaneous interference for PSK symbols can be classified as constructive and destructive according to concepts of PSK modulation [2, 70, 71]. As shown in Fig. 2.5, the CI sectors for BPSK, QPSK, and 8PSK modulations are denoted by green shadows. In practical designs regarding the CI method, the knowledge of the downlink channel and all user data is assumed to be known to the transmitter. For clarity, the optimization regions of conventional optimization and CI optimization are given in Fig. 2.6, where we take the QPSk modulated symbol as an example.

In conventional optimizations, the signal power is minimized subject to QoS constraints. Especially in the multi-user scenario, this is equivalent to constraining the MUI corresponding to each user, such that the received symbol is contained within a circle (or a hyper-sphere for multidimensional optimizations) around the nominal constellation point [2, 71–74], which is shown as Fig. 2.6 (a). In contrast to conventional designs, the CI scheme allows a relaxation of α_I and α_R for all transmit symbols, under the condition that the interference falls into the constructive region and contributes to the SNR of intended users. It is clear that the CI region in Fig. 2.6 (b) is only constrained along the vicinity of the decision thresholds. Therefore, the decision region extends infinitely towards the directions away from the decision bounds and hence provides a more relaxed optimization compared with the conventional region in Fig. 2.6 (a) [2, 56, 71, 75].

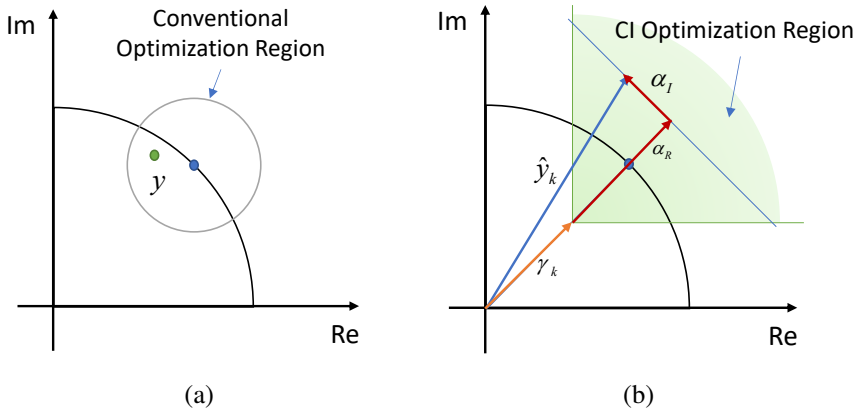

Figure 2.6: Optimization regions for QPSK symbols (a) conventional precoding and (b) precoding for CI technique [2].

CI-based optimal designs have been widely studied, which typically minimized the power consumption, while ensuring the QoS [22, 75–78]. We here briefly introduce the power minimization problem design with the constraints of the CI technique. Consider a Gaussian broadcast channel serving K users, the received signal at the i-th user is

$$y_i = \mathbf{h}_i^T \sum_{k=1}^{K} \mathbf{t}_k d_k + n_i = \mathbf{h}_i^T \sum_{k=1}^{K} \mathbf{t}_k e^{j(\phi_k - \phi_i)} d_i + n_i, \tag{2.9}$$

where $\mathbf{t}_i$ denotes the precoding vector, $\mathbf{h}_i$ denotes the channel of the i-th used, $n_i \sim \left(0, \sigma_0^2\right)$ denotes the AWGN of the i-th user, and $d_i = de^{j\phi_i}$ is the transmit data. Note that $d = 1$ for $d_i, \forall\ i$ due to the concept of PSK modulation. Thereby, the instantaneous transmit power for a signal is

$$P_t = \left\| \sum_{k=1}^{K} \mathbf{t_k} e^{j(\phi_k - \phi_1)} \right\|^2. \tag{2.10}$$

Given the CI criteria above, the MUI contributes to the useful power at the intended receivers, the SNR of which is given as

$$\gamma_i = \frac{\left| \mathbf{h}_i^T \sum_{k=1}^{K} \mathbf{t}_k d_k \right|^2}{\sigma_0^2}. \tag{2.11}$$

By observing Fig. 2.6, we note that the region of correct detection lies in $\vartheta_i \in \left[\angle d_i - \frac{\pi}{M}, \angle d_i + \frac{\pi}{M}\right]$ for any M-PSK modulated symbol, where ϑ_i is the angle of the detected symbols at the i-th receiver. We also have the following definitions $\alpha_I = \mathrm{Im}\left(\mathbf{h}_i^T \sum_{k=1}^{K} \mathbf{t}_k e^{j(\phi_k - \phi_i)}\right)$ and $\alpha_R = \mathrm{Re}\left(\mathbf{h}_i^T \sum_{k=1}^{K} \mathbf{t}_k e^{j(\phi_k - \phi_i)}\right)$, denoting the imaginary and real component of the noise-free receive symbol $\hat{y}_i \triangleq \mathbf{h}_i^T \sum_{k=1}^{K} \mathbf{t}_k e^{j(\phi_k - \phi_i)}$, and the SNR threshold is defined as $\bar{\gamma} = \sqrt{\omega_i \sigma_0^2}$. Accordingly, the power minimization problem can be formulated as

$$\begin{aligned} &\min_{\mathbf{t}_i} \ P_t(\mathbf{t}_i) \\ &\text{s.t.} \ \left| \angle\left(\mathbf{h}_i^T \sum_{k=1}^{K} \mathbf{t}_k d_k\right) - \angle d_i \right| \leq \beta, \forall i \\ &\quad \mathrm{Re}\left(\mathbf{h}_i^T \sum_{k=1}^{K} \mathbf{t}_k e^{j(\phi_k - \phi_i)}\right) \geq \sqrt{\omega_i \sigma_0^2}, \forall i. \end{aligned} \tag{2.12}$$

and for β, it is defined as

$$\tan\beta = \tan\tilde{\beta}\left(1 - \frac{\sqrt{\omega_i \sigma_0^2}}{\mathrm{Re}\left(\mathbf{h}_i^T \sum_{k=1}^{K} \mathbf{t}_k e^{j(\phi_k - \phi_i)}\right)}\right). \tag{2.13}$$

The optimization above is solvable and detailed in [2].

As mentioned above, the CI designs require knowledge of the downlink channel and all user data. However, the perfect CSI acquisition is still a key limitation in practice. Some literature regarding symbol-level schemes has studied the robustness of communication systems, which will be reviewed as follows. In [79], interference was decomposed into predictable and unpredictable interference, which were manipulated constructively by a BS and caused by the quantization error, respectively. The upper bound of the unpredictable interference was derived to reduce performance loss. To exploit the interference, the BS aligns the predictable interference so that its power is much greater than the derived upper bound. During this process, to intensify the received signal power, the BS simultaneously aligns the predictable interference

Precoding	Related applications	Reference
Block-level Precoding	Interference Mitigation	[85–88], [52], [89–92], [55] [39], [93–95]
	Energy Efficiency	[96–98], [86], [87], [91] [54]
	Max-min Fairness	[86], [52], [55], [99], [100], [101]
	Robust CSI	[102–116]
	Capacity	[117], [118]
	PLS	[113, 119–125]
	Hybrid Precoding	[34], [126–130], [98]
Symbol-level Precoding	Energy Efficiency	[78, 131–135]
	Max-min Fairness	[75, 78, 135, 136]
	PLS	[137–142]
	Constant Envelope	[143–150]
	Interference Exploitation	[2, 70, 76, 79, 136, 151–154] [78, 81, 131–134, 144, 155]
	Robust CSI	[2, 79, 81, 83, 156]

Table 2.2: Literature review of block-level precoding and symbol-level precoding with related applications.

so that it is constructively superimposed with the desired signal. Also, the authors in [80] designed CI-based hybrid precoders that require minimum transmit power to guarantee a certain QoS to the users in the presence of phase errors in the PSs. Algorithms for exploiting the robustness of the SLP schemes are proposed in [81–84]. In these approaches, errors in CSI are assumed to be bounded, such that precoding designs account for worst-case scenarios.

In addition, the DM and CI techniques enable PLS due to their natural criteria of data distortions at unintended receivers. One way to further deteriorate the decoding capability of the eavesdropper is to cooperate with the AN scheme. All of the above regarding PLS designs will be elaborated on in Section 2.4. For clarity, the literature review for block-level precoding and symbol-level precoding is summarized in Table 2.2.

2.2 Radar Waveform

Typically, radar systems work by sending a specific electromagnetic signal into a region and detecting the echo returned by reflecting targets, involving information

about the target, such as range, radial velocity, angular direction, size, shape, etc. As mentioned above, the radar waveform plays a vital role in the accuracy, resolution, and ambiguity of radar. For years, radar waveforms have been studied intensively in order to improve the performance of detecting targets and extracting information. In this section, typical examples of radar waveform designs will be summarized as follows.

2.2.1 Radar Waveform Designs

2.2.1.1 Mutual Information Maximization

MI is a typical metric to measure the received information with respect to the knowledge of the channels. The signal model over a frame of L time slots can be written as

$$\textbf{Radar signal: } \mathbf{Y}_R = \mathbf{H}_R(\boldsymbol{\eta})\mathbf{X} + \mathbf{Z}_R. \tag{2.14a}$$

In sensing systems, MI is defined as the entropy between the sensing channels and the received signals. Thus, the MI between the sensing channel matrix $\mathbf{H}_R$ and reflected signals $\mathbf{Y}_R$ given the knowledge of $\mathbf{X}$ can be used to measure the sensing performance. The MI is accordingly given as [157]

$$I_R(\mathbf{H}_R; \mathbf{Y}_R|\mathbf{X}) = N_r \log\left(\det\left(\mathbf{I} + \frac{\mathbf{X}^H \boldsymbol{\Sigma}_{H_R} \mathbf{X}}{\sigma_r^2}\right)\right), \tag{2.15}$$

where $\boldsymbol{\Sigma}_{H_R} = \mathbb{E}\left\{\mathbf{H}_R \mathbf{H}_R^H\right\}$, N_r denotes the number of receive antennas.

Given the expression above, the MI maximization problem can be written as [158]

$$\begin{aligned} &\max_{\mathbf{X}} \ \ I_R(\mathbf{H}_R; \mathbf{Y}_R|\mathbf{X}) \\ &\text{s.t. } \ \mathbf{X} \in \mathcal{P}. \end{aligned} \tag{2.16}$$

2.2.1.2 Waveform Similarity Design

The waveform similarity design is also widely studied in the existing literature. The optimization problem aims to design the transmit waveforms to be close to the desired beampattern by optimizing the covariance matrix of the signal $\mathbf{X}$, under

constraints of communication performance, which is given as [159]

$$\begin{aligned} &\min_{\mu,\mathbf{R}_d} \sum_{m=1}^{M} \left|\mu P_d(\theta_m) - \mathbf{a}^H(\theta_m)\mathbf{R}_d\mathbf{a}(\theta_m)\right|^2 \\ &\text{s.t.} \quad \mathbf{R}_d \succeq 0, \mu \geq 0, \mathbf{R}_d \in \mathcal{P}. \end{aligned} \tag{2.17}$$

where μ is a scaling factor, θ_m denotes an angular grid covering the detection angular range, $P_d(\theta_m)$ is the desired ideal beampattern gain at θ_m, and $\mathbf{R}_d$ represents the desired waveform covariance matrix. The optimal $\mathbf{R}_d$ is regarded as a well-designed benchmark covariance matrix that constraints the $\mathbf{R}_x \triangleq \mathbb{E}\left\{\mathbf{X}\mathbf{X}^H\right\}$ for further optimization of the communication performance.

2.2.2 Wide Main Beam Design

The 3 dB main-beam width of an antenna is a measurement of the angle over which the antenna is able to transmit or receive significant power. It is defined as the angle between the two points on the antenna's radiation pattern where the power drops to one-half, or 3 dB, of the maximum power. This is a commonly used measurement of the beamwidth of an antenna because the 3 dB points on the radiation pattern are considered to represent the "half-power" points, where the antenna's performance is half as effective as it is at its peak. As a result, the 3 dB beamwidth provides a good indication of the overall directivity and focus of the antenna's radiation pattern.

The 3 dB main-beam width design has been applied in many studies. Let $\mathbf{x}$ denote the emitted waveform, we accordingly have the covariance matrix expression as follows

$$\mathbf{R}_x = \mathbb{E}\left[\mathbf{x}\mathbf{x}^H\right]. \tag{2.18}$$

The beampattern is expressed $P(\theta) = \mathbf{a}^H(\theta)\mathbf{R}_x\mathbf{a}(\theta)$. Therefore, the optimization problem can be designed to minimize the sidelobe power in a prescribed region and

achieve a 3 dB main-beam width, which is given as [160, 161]

$$\begin{aligned}
&\min_{t,\mathbf{R}_x} \ -t \\
&\text{s.t. } \mathbf{a}^H(\theta_0)\mathbf{R}_x\mathbf{a}(\theta_0) - \mathbf{a}^H(\alpha_l)\mathbf{R}_x\mathbf{a}(\alpha_l) \geq t, \forall\ \alpha_l \in \Omega \\
&\quad \mathbf{a}^H(\theta_1)\mathbf{R}_x\mathbf{a}(\theta_1) = 0.5\mathbf{a}^H(\theta_0)\mathbf{R}_x\mathbf{a}(\theta_0) \\
&\quad \mathbf{a}^H(\theta_2)\mathbf{R}_x\mathbf{a}(\theta_2) = 0.5\mathbf{a}^H(\theta_0)\mathbf{R}_x\mathbf{a}(\theta_0) \\
&\quad \mathbf{R}_x \succeq \mathbf{0}, \mathbf{R}_x \in \mathcal{F},
\end{aligned} \tag{2.19}$$

where Ω is the sidelobe region of interest, $[\theta_1, \theta_2]$ is the predefined region of the 3 dB main-beam width. Note that this beampattern sidelobe minimization problem can be efficiently solved in polynomial time by the SDP technique.

2.3 Integrated Sensing and Communication Systems

The increasing spectrum congestion leads to the development of the competitive coexistence of radar and communication (R&C) systems, which was straightforwardly implemented by the opportunistic spectrum sharing between the rotating radar and the cellular networks as proposed in [162, 163]. As the demand for space and spectral resources continues to explode, R&C systems are enabled to operate in higher frequency bands, providing sufficient radio resources for high-resolution imaging and facilitating high-rate data exchange. Meanwhile, the R&C coexistence in multiple frequency bands results in either inevitable mutual interference or resource efficiency degradation. In order to enable the co-design of the communication and radar functionalities, and explore the mutual benefits from each other, ISAC is reckoned as a promising key technology in next-generation networks. The four-level vision describing the evolution path of ISAC technologies is introduced in [3], including the R&C spectral coexistence, hardware platform sharing, joint waveform design and signal processing for R&C, and the share of network structure. All of the state-of-the-art approaches imply ISAC to be the critical enabler in the foreseeing applications of future networks, which is capable of high-quality S&C functionalities. For clarity, the technological vision of ISAC is given in Fig. 2.7.

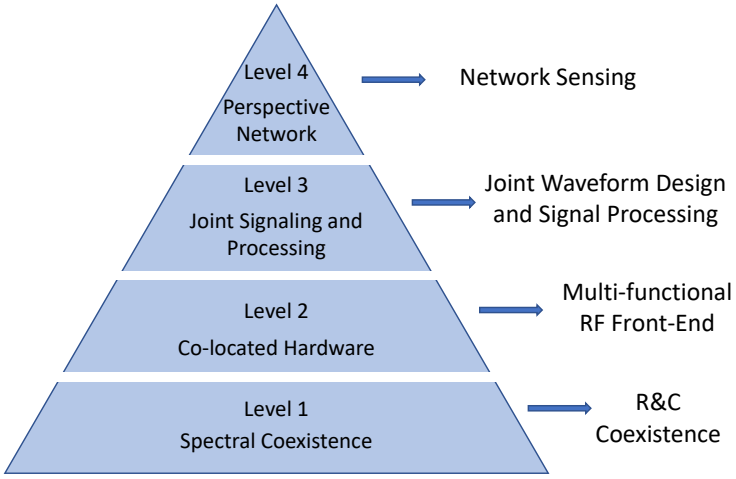

Figure 2.7: Evolution path for ISAC technologies [3].

The existing designs of the ISAC can be classified into three categories, including communication-centric design, radar-centric design, and joint optimizing design, which will be elaborated in this section.

2.3.1 Linear Gaussian Signal Models

By taking the additive white Gaussian noise (AWGN) into account, we have the generic linear signal models for the radar and communication receiver in ISAC can be respectively given as [3]

$$\textbf{Radar signal: } \mathbf{y}_r = \mathbf{H}_r(\boldsymbol{\eta})\mathbf{x} + \mathbf{z}_r \tag{2.20a}$$

$$\textbf{Comm signal: } \mathbf{y}_c = \mathbf{H}_c\mathbf{x} + \mathbf{z}_c, \tag{2.20b}$$

where $\mathbf{x}$ denotes the ISAC waveform, employed for both R&C, $\mathbf{H}_c$ is the communication channel, which can be estimated *a priori* via pilots. The radar channel $\mathbf{H}_r$ is modeled as a function of the physical parameters $\boldsymbol{\eta}$, which commonly includes the angle, Doppler, and range. $\mathbf{z}_r$ and $\mathbf{z}_c$ denote the AWGN with zero mean and variance σ_r^2 and σ_c^2, respectively. From the perspective of radar, one wishes to extract and estimate the parameters $\boldsymbol{\eta}$ by observing the received signal $\mathbf{y}_r$. While the communication receiver aims to decode and recover the transmit signal $\mathbf{x}$ according to the observed signal $\mathbf{y}_c$. Note that (2.20) is a variety of R&C signal models. Related to this Thesis, the reflected target echo received by a multi-input multi-output (MIMO)

radar is detailed as

$$\mathbf{H}_r = \sum_{l=1}^{L} \alpha_l \mathbf{b}(\theta_l)\mathbf{a}^T(\vartheta_l), \tag{2.21}$$

where α_l, θ_l, and ϑ_l denote the channel coefficient, direction of arrival (DOA), and direction of departure (DOD) of the l-th path. L is the number of resolvable targets. $\mathbf{a}(\vartheta_l)$ and $\mathbf{b}(\theta_l)$ are the transmit and the receive steering vectors, where the steering vector of the uniform linear array (ULA) equipped with N antennas, with spacing d and wavelength λ is written as

$$\mathbf{a}(\theta) = \left[1, e^{-j2\pi\frac{d}{\lambda}\sin(\theta)}, \cdots, e^{-j2\pi(N-1)\frac{d}{\lambda}\sin(\theta)}\right]. \tag{2.22}$$

Additionally, in light of the channel models above, we specify the single-target scenario in two cases: 1) point-like target; 2) extended target. [164]

- Point-like target case: In this case, the target response matrix is equivalent to the expression given in (2.21) when we let $L = 1$. It is accordingly written as

$$\mathbf{H}_r = \alpha \mathbf{b}(\theta)\mathbf{a}^T(\vartheta). \tag{2.23}$$

  Note that the DOA θ is the same as DOD ϑ with the monostatic radar setting.

- Extended target case: The extended target is typically modeled as a surface with a large number of distributed point-like scatterers, such as a vehicle or a pedestrian moving on the road [165]. To this end, the target response matrix is expressed as

$$\mathbf{H}_r = \sum_{n=1}^{N_s} \alpha_n \mathbf{b}(\theta_n)\mathbf{a}^T(\vartheta_n), \tag{2.24}$$

  where N_s denotes the number of scatters, and α_n denotes the reflection coefficient of the n-th scatterer.

2.3.2 Communication-centric Design

In communication-centric (CC) designs, the related radar functionalities are integrated to an existing or even commercialized communication waveform as a secondary function. As demonstrated in [166], systems can be classified into two types,

which are realizing sensing 1) in point-to-point communication systems; 2) in large networks such as mobile networks. They deploy the orthogonal frequency-division multiplexing (OFDM)-based ISAC signaling, which directly exploits the OFDM communication waveform to simultaneously accomplish R&C tasks [3, 167].

Note that the Doppler estimation and compensation is critical for combating time-varying mmWave channels in communication-centric ISAC systems. With a typical configuration, the sensing receiver and DFRC transmitter are co-located. Let us assume that the ISAC transmitter emits the OFDM signal to communicate with a user, while sensing a point target with delay τ and Doppler υ. The radar receiver samples the reflected echo at each OFDM symbol, followed by block-wise FFT processing. In the resultant discrete signal matrix, the (n,m)-th entry corresponds to the n-th symbol on the m-th subcarrier, which is

$$y_{n,m} = \alpha_{n,m} x_{n,m} e^{-j2\pi(m-1)\Delta f \tau} e^{j2\pi(n-1)\upsilon T_c} + z_{n,m}, \tag{2.25}$$

where $\alpha_{n,m}$ is the channel coefficient and $z_{n,m}$ denotes the noise. It is worthwhile to note that the interference resulting from the random communication data $x_{n,m}$ can be simply mitigated by element-wise division

$$\tilde{y}_{n,m} = \frac{y_{n,m}}{x_{n,m}} = \alpha_{n,m} e^{-j2\pi(m-1)\Delta f \tau} e^{j2\pi(n-1)\upsilon T_c} + \frac{z_{n,m}}{x_{n,m}}. \tag{2.26}$$

Afterward, in order to get the delay-Doppler profile of the target, we can then apply a 2D-fast Fourier transform (FFT) to (2.24). For clarity, we summarize the related reference for the CC ISAC system in Table 2.3.

2.3.3 Radar-centric Design

In contrast to the CC designs, radar-centric (RC) designs aim to implement communication data transmission over existing radar infrastructures. The emitted waveform in radar-only systems conventionally contains no information, while research on RC ISAC systems mainly focused on embedding the information in the waveform to be transmitted. As radar is capable of realizing long-range propagation, the embedded communication data is expected to be transmitted in a long-range with lower latency,

Categories	Typical Network	Signal	Reference
Point-to-point Communiaction	IEEE 802.11 DFRC for Vehicular Networks	Spread Spectrum	[167, 168]
		Waveform design based on OFDM	[169–172]
		Single carrier (OFDM preamble)	[173–177]
Large Networks	Perspective Mobile Networks	Multiuser-MIMO OFDM	[178–181]

Table 2.3: Summary of Reference for CC ISAC Systems.

while the achievable transmission rate is limited in such designs [182–188].

Since communication data embedded radar systems rely on pulsed or continuous-wave radar signals, eliminating the induced interference to radar functionality is a fundamental challenge. This has been widely investigated in the existing literature and is summarized in Table 2.4. Early RC designs have mainly focused on exploiting the linear frequency modulation (LFM) signal as an information carrier [189–191]. This approach enables a low probability of intercept/detection communications, administrative communications, or auxiliary functions such as navigation for a combined radar-navigation signal at the expense of data rates [189, 190]. To ensure the performance of radar, index modulation (IM) is one of the techniques of interest. It was first proposed in [192] for MIMO radar transmitting orthogonal waveforms, where the communication information was conveyed by shuffling the waveforms across multiple antennas, which does not break the orthogonality. It is also further studied in [193–195] for MIMO-OFDM, multi-Carrier AgilE phaSed Array Radar (CAESAR) and frequency hopping (FH)-MIMO radar. In these cases, frequency combination randomly selects different sets of frequencies, and antenna permutation allocates the selected frequencies to different antennas, which again keeps the orthogonality unaffected.

2.3.4 Optimization-based Joint Design

In the CC and RC designs above, both schemes aim to ensure the performance of a specific system, i.e., communication and radar, respectively, which lack flexibility in exploring tradeoff between the two functionalities. The joint design schemes are

Modulations		Methods	Reference
Modified Waveforms	Time Frequency Embedding	Apply a combination of amplitude, phase, and/or frequency shift keying to radar chirp signals.	[182], [196], [197], [190]
		Map data to multiple chirp subcarriers via the use of fractional Fourier Transform	[198]
	Code Domain Embedding	Modulate binary/poly-phased codes in radar signals using direct spread spectrum sequences.	[199]
	Spatial Embedding	Modulate information bits and embed in the sidelobes of the radar beampattern.	[182], [196]
Index Modulation		Embed information bits through indices of certain parameters involved in the transmission (antennas, frequencies, and/or codes for signals).	[187], [200] [193], [194] [192], [195]

Table 2.4: Summary of Information Embedding Approaches in RC ISAC Systems.

conceived through convex optimization techniques, which take performance metrics of both communication and radar systems into account, enabling the balance of the requirements for R&C. An typical example of this will be briefly presented.

We here consider a MIMO DFRC BS equipped with N_t antennas, serving K single-antenna users, while simultaneously detecting a point-like target located at the direction θ. The optimization problem aims to minimize the CRB of angle estimation under constraints of the CUs' sum rate and the power budget is formulated as

$$\begin{aligned} &\min_{\mathbf{X}} \ \ \mathrm{CRB}\,(\theta) \\ &\text{s.t.} \ \ \|\mathbf{X}\|_F^2 \le P_t, \sum_{k=1}^{K} R_k \ge R_0, \forall\, k, \end{aligned} \tag{2.27}$$

where $\mathbf{X}$ is the ISAC signal, R_k is the achievable rate of the k-th user, R_0 is the threshold of sum rate, and P_t is the power budget. The Pareto frontier between R&C can be obtained by increasing R_0, which leads to the increased objective CRB [3]. Moreover, the precoder optimization design plays an important role in joint R&C systems. This may involve interference mitigation between the radar and communication signals, and maximizing the SNR of the transmitted signals.

As per above, we have introduced the basic concept of ISAC systems, containing the RC R&C and the CC R&C designs. To be more specific to this Thesis, existing approaches for PLS are further elaborated in the following section.

2.4 Physical Layer Security

Information security has been a critical issue from the very beginning of research in wireless networks, dating back to the 1970s with a mathematical description of a wiretap channel [201, 202]. By exploiting the properties of wireless channels, including fading, noise, and interference, the PLS has been widely studied as an efficient approach to enhance wireless security alongside high-layer encryption. Nevertheless, with the development of the wireless network, conventional cryptographic techniques may be insufficient or even unsuitable, as private key exchange must take place over a secure channel. Thereby, PLS enables secure communication by solely relying on the characteristics of wireless channels, avoiding the extra utilization of spectral resources and reducing communication overhead [203]. As illustrated in Fig. 2.8, a typical network employing PLS comprises three nodes: a transmitter (Alice), a legitimate receiver (Bob), and an eavesdropper (Eve). With this setup, the transmitter sends confidential information to the legitimate receiver, while preventing it from being intercepted by the eavesdropper [204].

In this section, the optimization and design in PLS employing the AN-aided and DM/CI-based algorithms will be summarized. In addition, a further discussion will be provided regarding the impacts of CSI on PLS designs, as wiretap CSI acquisition is still a limiting factor for PLS algorithms.

2.4.1 Secure Beamforming with AN

As elaborated in Section 2.1, in signal processing, the beamforming technique is to transmit signals towards intended directions by maximizing the SINR in the directions of desired users, while suppressing the SINR in the directions of undesired receivers [205, 206]. As a result, the energy is transmitted or focused in specific directions instead of being dispersed in a diffuse manner, which significantly increases the energy efficiency of the system.

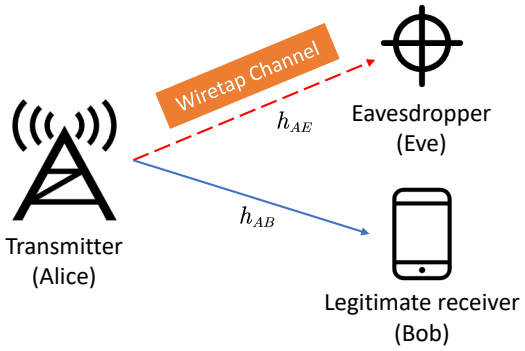

Figure 2.8: A three-node point-to-point secure communication model consists of a transmitter, a legitimate node, and an eavesdropper.

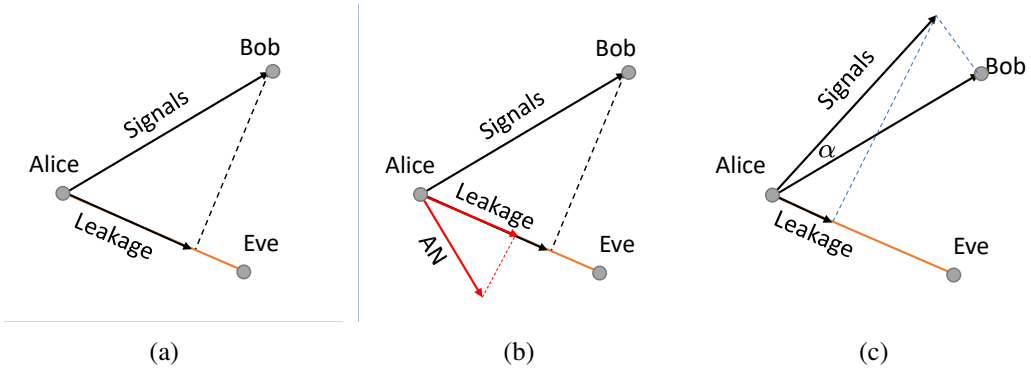

Figure 2.9: Secure techniques, (a) Beamforming (b) AN-aided approach, and (c) Optimization-based beamforming [4].

AN-aided PLS technique is an efficient way to utilize the channel quality advantages in the transmission link, which is designed to inject the well-designed artificial signal at the transmitter side such that only the wiretap channel degrades while the main channel is kept intact [207, 208]. The secure signal transmission with AN and optimization-based beamforming designs are illustrated in Fig. 2.9, which are representative techniques to ensure the PLS. In what follows, we review the fundamental works that utilize the AN to improve PLS performance.

AN-assisted secure transmission was firstly presented in [15], which indicated that the key of AN design is to avoid interference leakage to legitimate users while impairing the AN at the eavesdropper. To this end, AN is adopted in conjunction with multiple-antenna techniques or with the help of relays, where the AN and the transmit signals are jointly designed to maximize the secrecy rate [119, 209–213]. Intuitively, the security performance depends on the accuracy of the CSI known at

the transmitter in most studies. However, the CSI of the eavesdropper's channel is impractical to be known perfectly at the transmitter, which promotes further studies on the robustness of wiretap CSI for PLS techniques [22,214–216]. In [105,217,218], a robust beamforming method was proposed to maximize the worst-case secrecy rate via semidefinite programming (SDP) optimization problem. For further relaxing the assumption of CSI, the case that the wiretap CSI is statistically known to the transmitter was studied in [214, 219, 220]. Moreover, when no wiretap CSI is available at the transmitter, the artificially generated noise is designed to be orthogonal to the channels towards legitimate users, thus the AN only deteriorates the wiretap channel [14, 221–225].

Apart from concerns about the robustness of wiretap CSI, the CSI of the legitimate receiver is sometimes partially known to the transmitter in practice. If the transmitter receives limited feedback from the legitimate receiver, the AN that was originally intended to jam the eavesdropper may now strongly interfere with the main channel, resulting in a significant secrecy rate loss [203, 226]. In [222], Lin et al. investigated the scenario where only quantized channel direction information of the legitimate receiver's channel is available at the transmitter. For a given transmission power and a fixed number of feedback bits, a power allocation scheme for information signal power and the AN power was proposed to maximize the secrecy rate [222]. Furthermore, the secrecy performance with limited CSI feedback is further improved by optimizing the number of feedbacks and transmit power jointly in [227]. Additionally, the delay of feedback leads to a CSI mismatch, which leads to noise leakage at the legitimate receiver as well as a loss in the achievable secrecy rate. The beamforming and power allocation algorithms were proposed to minimize the performance loss in [228].

2.4.2 DM/CI Based PLS Designs

DM is considered as an efficient method to ensure the PLS in wireless communication networks, the paradigm of which is illustrated in Fig. 2.10. It shows that DM ensures the PLS by adjusting the amplitude and phase of the transmit signal along a specific direction, while scrambling the symbols in other undesired directions. The

fundamental concept of the DM technique implies that the modulation happens at the antenna level, rather than the baseband. By doing so, low bit error rate (BER) achieves at the intended receiver for a specific modulation, while the constellation will be distorted in other undesired directions, resulting in a high BER.

The scheme presented in [18] was to produce a directional frequency/phase-modulated signal by hopping antennas. This technique was then extended to modulate at both baseband and antenna levels for PLS in communication networks, including a dual-beam scheme to create a modulated signal with two distinct radiation patterns [229] and switching antennas according to a chipping sequence [66]. The DM scheme in [63] was designed to modulate the phase and amplitude by changing the antenna characteristics (its near- and far-field) at the symbol rate in order to properly modulate the signal, As a result, it is able to transmit different signals independently to the desired and the undesired directions. In [230], a phased array was deployed at the transmitter and the genetic algorithm was deployed to derive the phase values of a phased array in order to create symbols in a specific direction. Furthermore, to jointly exploit DM with new array techniques, a hybrid MIMO phased array time-modulated DM scheme was proposed in [141] for safeguarding the mmWave wireless communication system.

The DM implementation can be extended to the scenario of transmitting confidential information to more than one destination. The singular value decomposition (SVD) is deployed to directionally modulate symbols towards the receiver with two separately located receive antennas for MIMO systems [231]. The algorithm in [232] studied a multi-beam DM scheme, which was to create two orthogonal far-field patterns to modulate two independent data streams towards two different directions, and the least-norm solution was proposed for the array weights derivation and symbol modulation [233].

For further security improvement, the symbol-level precoder in [57] was proposed by using the concept of CI in directional modulation aiming at improving energy efficiency. Emerging studies combine the DM technique with the help of AN, such as [225, 231, 234–238]. Particularly, [225, 236, 238] utilized an orthogonal

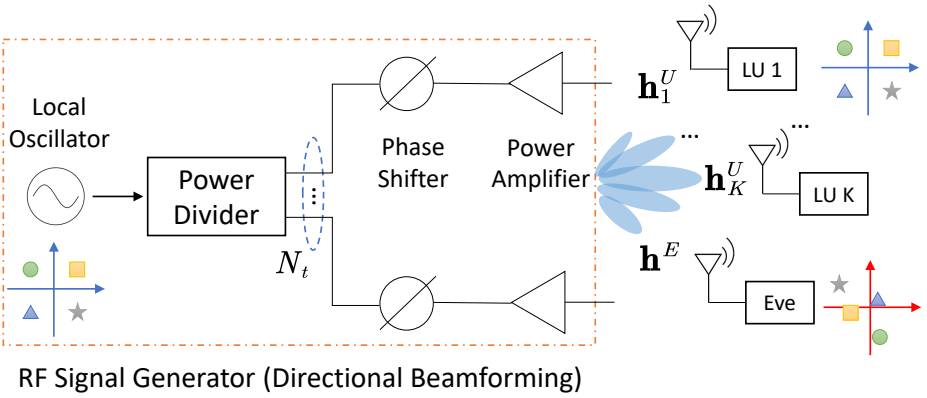

Figure 2.10: Architecture of DM (QPSK modulation).

vector scheme to design the array weights in order to directionally modulate the data and inject the AN in the direction of the eavesdropper. In [235], the DM synthesis method was achieved with a closed-form expression by projecting the AN into the null space of the steering vector along the desired direction. Besides, authors in [239] redesigned AN signals in the form of CI to the intended receiver while keeping AN disruptive to potential eavesdroppers.

In general, the DM may achieve a high-performance gain along the desired directions via beamforming and provide a secure transmission by injecting AN to deteriorate the data transmission towards the undesired directions [57, 240].

2.4.3 The Impacts of CSI on PLS Designs

As discussed above, it can be found that the impact of CSI is non-negligible in PLS designs, which determines the choice secrecy metric and the design of the secrecy scheme [241, 242]. In practice, the CSI of both the legitimate user channel and the wiretap channel may be imperfectly known to the transmitter, or even unknown to the transmitter. In one sense, the CSI of legitimate channels can be estimated through training and feedback, whereas obtaining a precise CSI is difficult due to errors in estimation and feedback delays. On the other hand, the eavesdropper is typically considered malicious and uncooperative, resulting in difficulties in estimating the CSI. In what follows, we will examine cases where information on the wiretap channel is perfectly known, partially known, and unknown to the transmitter.

2.4.3.1 Perfect CSI for Legitimate and Wiretap Channels

In the existing literature on PLS, perfect CSI of both legitimate and wiretap channels is assumed to be known at the transmitter, such as [14, 223, 242–250]. Particularly, in [249,251], all the nodes are active and can be monitored. These nodes play double roles in multicast communication, that is, each node is legitimate with respect to some specific data streams, while being malicious to other streams. As a result, friendly and legitimate nodes are able to feed back the CSI perfectly, which in turn allows the transmitter to know the CSI of both channels perfectly [252].

2.4.3.2 Partial CSI of the Wiretap Channel is Knowledgeable

CSI of legitimate channels is easily obtained, while CSI of wiretap channels is difficult or impossible to obtain in many situations. In the cases where the perfect CSI of the wiretap channel is unknown, imperfect CSI of the wiretap channel can be estimated based on the past channel observation or prior knowledge of the propagation environment [253, 254]. Note that the CSI of the wiretap channel can be characterized following

- The CSI can be estimated according to a specific probability distribution that the channel follows, such as the Gaussian distribution, Rayleigh distribution, Rician distribution, etc. By adopting this method, only the statistical information, including the mean and covariance of the probability distribution, is required.

- The deterministic uncertainty model proposed in [105, 209, 255, 256] can be deployed to characterize the uncertainties of eavesdroppers' channels, where the unknown wiretap channels are assumed to fall in a sphere or a set [257]. To this end, the uncertainty region of the eavesdropper's channel is modeled as

$$\Im = \left\{ \mathbf{h}_E \middle\| \mathbf{h}_E - \hat{\mathbf{h}}_E \right\|^2 \leq \varepsilon \Big\} = \left\{ \hat{\mathbf{h}}_E + \mathbf{e}_E \| \mathbf{e}_E \|^2 \leq \varepsilon \right\}, \tag{2.28}$$

  where $\Im$ denotes the sphere region with the estimated channel vector $\hat{\mathbf{h}}_E$ being the center and the channel mismatch $\sqrt{\varepsilon}$ being the radius, and $\mathbf{e}_E$ is the estimation error vector.

- The channel can also be modeled as

$$\mathbf{h}_E = \sqrt{\upsilon}\hat{\mathbf{h}}_E + \sqrt{1-\upsilon}\mathbf{e}_E \tag{2.29}$$

where $\upsilon \in [0,1]$ is a scalar for indicating the degree of channel knowledge, and $\upsilon = 0$ means that the eavesdropper's CSI is perfect, $\upsilon = 1$ corresponds to a perfect channel estimation. $\hat{\mathbf{h}}_E$ and $\mathbf{e}_E$ denote the estimated channel and estimation error with *i.i.d*. entries.

2.4.3.3 Unknown CSI of Wiretap Channels

Considering eavesdroppers' concealment and hostility, we further discuss the practical assumption that the wiretap CSI is unknown to the transmitter [258–260]. In the absence of the wiretap CSI, the instantaneous secrecy rate cannot be expressed. To this end, secrecy rate optimization cannot be performed in this case. As shown in [256], a transmission antenna selection strategy to enhance the secrecy performance of MIMO wiretap channels without eavesdroppers' CSI is proposed based on three key metrics, namely, the probability of non-zero secrecy capacity, the probability of secrecy outages, and the probability of ϵ-outage secrecy [261, 262]. Additionally, authors in [258] proposed a QoS-based secure strategy to enhance the security of a cooperative relay network without the knowledge of the wiretap CSI. Likewise, the secrecy sum rate maximization problem subjecting to the legitimate users' QoS requirements for the non-orthogonal multiple access (NOMA) system was presented in [259].

In light of the above, when the eavesdropper's CSI is unknown or imperfect, exploiting AN or jamming signals has proven to be effective in improving secrecy performance [263–265].

In the following section, several fundamental metrics in the study of PLS for ISAC systems are given from the perspective of radar communication, respectively.

2.5 Performance Metrics

In this section, we present the performance metrics for secure ISAC in this section, including the estimation-theoretic metrics for sensing functionality and information-theoretic metrics for communication functionality. To be more specific to the topic of this Thesis, the secrecy rate is further proposed as a metric of communication information security.

2.5.1 Estimation-theoretic Metrics for Sensing

Recall the signal model given in (2.20), where $\boldsymbol{\eta}$ is the parameters to be extracted by observing $\mathbf{Y}_r$, we Let the $\hat{\boldsymbol{\eta}}$ denote the estimated vector. To measure the accuracy of the estimation, the MSE is given as $\varepsilon = \mathbb{E}\|\boldsymbol{\eta} - \hat{\boldsymbol{\eta}}\|^2$. Moreover, the MSE can also be defined as the trace of the following matrix

$$\mathrm{MSE}_{\boldsymbol{\eta}} = \mathbb{E}\left[(\boldsymbol{\eta} - \hat{\boldsymbol{\eta}})(\boldsymbol{\eta} - \hat{\boldsymbol{\eta}})^H\right], \tag{2.30}$$

with the diagonal elements denoting the individual MSE for parameters $\eta_1, \ldots, \eta_K$, where K is the number of elements to be estimated. It is practical to minimize the MSE in order to find the optimal estimator.

Additionally, if the parameter is deterministic, the Cramér-Rao bound (CRB) lower-bounds the variance of unbiased estimators in estimation theory and statistics, defined as the inverse of the Fisher Information Matrix (FIM) $\mathbf{J}(\boldsymbol{\eta})$ [266, 267], which is given as follows

$$\mathbb{E}\left[(\boldsymbol{\eta} - \hat{\boldsymbol{\eta}})(\boldsymbol{\eta} - \hat{\boldsymbol{\eta}})^H\right] \geq \mathbf{J}^{-1}(\boldsymbol{\eta}), \tag{2.31}$$

where $\mathbf{J}(\boldsymbol{\eta}) = \mathbb{E}\left[\frac{\partial \ln p(\mathbf{Y}_r;\boldsymbol{\eta})}{\partial \boldsymbol{\eta}^2}\right]$, and $p(\mathbf{Y}_r;\boldsymbol{\eta})$ is the probability density function (PDF) of $\mathbf{Y}_r$ associated with estimating the deterministic parameter vector $\boldsymbol{\eta}$. Note that $\left.\frac{\partial \ln p(\mathbf{Y}_r;\boldsymbol{\eta})}{\partial \boldsymbol{\eta}^2}\right|_{\boldsymbol{\eta}=\hat{\boldsymbol{\eta}}} = 0$ if the MSE of an unbiased estimator achieves the CRB.

Apart from the metrics given above, there are some more sensing performance criteria that are commonly considered in related works, which are listed as follows:

- Radar range resolution is defined as the capability of the radar to distinguish

or resolve nearby adjacent targets in the range, which is expressed as

$$\Delta R = \frac{c}{2B}, \tag{2.32}$$

where c is the speed of light and B is the bandwidth [268].

- The ambiguity function (AF) represents the time response of a filter matched to a given finite energy signal when the signal is received with a propagation delay τ and a Doppler frequency f relative to the nominal values (zeros) expected by the filter [269]. For a given complex baseband pulse $s(t)$, the narrowband ambiguity function is expressed as

$$\chi(\tau, f) = \int_{-\infty}^{\infty} s(t)\, s^*(t-\tau) e^{j2\pi f t} dt. \tag{2.33}$$

- Besides, the probability of detection and false alarm are also critical performance metrics for target detection, where the former denotes the correct detection of existing targets and the latter corresponds to the probability of detecting a target when a target does not exist [270].

2.5.2 Information-theoretic Metrics for Communication

From the perspective of communication, the information is expected to be transmitted as reliably as possible [271]. Information theory, developed by Claude E. Shannon in 1948 [272, 273], defines the notion of channel capacity as the tight upper bound on the rate at which communication information can be reliably transmitted over a channel of a specific bandwidth in the presence of noise, known as the Shannon-Hartley theorem. The capacity of any discrete memoryless channel is defined as the maximum mutual information $I(X;Y)$ with input X and output Y can be written as

$$C = \max_{p(X)} I(X;Y). \tag{2.34}$$

Given a power constraint P over the input X, the channel capacity of a Gaussian channel with AWGN is written as the well-known Shannon's formula, i.e., $C_{\text{Gau}} =$

$\log_2\left(1+\frac{P}{\sigma^2}\right)$, where σ^2 is the noise variance,

To be more specific to the theme of this Thesis, we introduce a fundamental secrecy metric for the measurement of communication security based on the channel capacity given above. In PLS studies, secrecy capacity is commonly given as a key evaluation metric, which is led by Wyner's original work [201] and expressed as

$$C_s = \max_{p(X)} \{I(X;Y) - I(X;Z)\}, \tag{2.35}$$

where X is the input, Y and Z are the output at the intended receiver and the eavesdropper, respectively. To evaluate the secrecy more conveniently and computation affordably, the secrecy rate is applied in PLS studies as well. Assume that the inputs are Gaussian distribution, thus the achievable secrecy rate can be expressed as

$$R_s = [R_c - R_e]^+, \tag{2.36}$$

where $[\cdot]^+ \triangleq \max\{\cdot, 0\}$ The secrecy rate is to assess the transmit effectiveness of PLS strategies, where R_m denotes the data rate of the legitimate user and R_e denotes the wiretap channel. Note that the secrecy rate is regarded as the lower bound of the secrecy capacity.

- **Ergodic Secrecy Capacity/Rate:** The secrecy capacity and the secrecy rate given above is for fixed channels, while time-varying channels are widely deployed in practice. When taking the fading of the wireless channels into account, the ergodic secrecy capacity is practically applied by assuming that the transmitted confidential message can be coded across a sufficiently large number of varying channel states, that is, under delay-tolerant applications. It indicates that the ergodic secrecy capacity evaluates the average performance of secrecy transmission over fading channels. Nevertheless, the optimal transmission scheme achieving the secrecy capacity is difficult to obtain for various fading channels in practical designs. Therefore, the secrecy rate is commonly deployed as the optimization objective in secure transmission designs with the consideration of channel fading, defined as the difference between the ergodic

rates of the main and wiretap channels with Gaussian codebook [241,274,275].

- **Secrecy Outage Probability:** Considering the imperfect CSI and the randomness of the communication channels resulting from the physical environment, such as the shadowing, the locations of nodes, and the multi-path fading, the observed signals change in a random manner. For transmission over quasi-static fading channels where classical information-theoretic secrecy is not always achievable, the secrecy outage probability measures the probability of failing to achieve classical information-theoretic secrecy [276, 277]. To be specific, it is defined as the probability that the instantaneous secrecy capacity C_s falls below a target secrecy rate R_s^0 as

$$P_{out}\left(R_s^0\right) = \Pr\left\{C_s < R_s^0\right\}. \tag{2.37}$$

  The expression above demonstrates that $C_s < R_s^0$ happens when the confidential message is not correctly decoded by intended receivers or is not perfectly secure. Consequently, reliable and secure transmission at a target secrecy rate R_s^0 can be ensured with the probability of $1 - P_{out}\left(R_s^0\right)$.

2.6 Open Problems and Future Work

This chapter has reviewed fundamental concepts and related works on security concerns in ISAC systems. Moreover, there are numerous open problems in this area.

Sensing-assisted physical layer security: In existing studies on secure ISAC systems, literature mainly focuses on a dual-functional BS emitting a waveform for both sensing and communication functionalities. The communication transmission is protected by related PLS approaches, while both the radar and communication systems still work individually. In order to improve energy efficiency and reduce power consumption, it is worthwhile to promote cooperation between sensing and communicating. This motivates the research on sensing-aided techniques for protecting communication data security, which exploits the active sensing functionality to identify the direction of the eavesdropper.

Target location protection: In the radar-communication coexistence scenario, the precoder containing the radar parameters in the design of mutual interference mitigation is passed to the communication system, resulting in risks to radar privacy. In general, it is possible to protect the angle information of the radar when the adversary does not employ the training-based technique to infer the radar information. However, recent research showed that machine-learning-based schemes are able to infer the location information contained in the precoding matrix. This motivates further studies on how to exchange parameters between radar and communication systems taking the privacy risk of each unit into consideration while maintaining a minimum level of mutual interference.

ISAC security design at a network level: Security mechanism design on the network level has been addressed for communication-only systems, where coverage probability and ergodic capacity are analyzed in a systematic manner. This network-level investigation advises networking planning and engineering design set out on the whole system. Note that the existing ISAC-related research is investigated in simple scenarios. The heterogeneity and high node density in future communication systems motivate fundamental research in network-level ISAC designs.

Chapter 3

Artificial Noise Aided Physical Layer Security in ISAC Systems

This chapter is based on our works published in [J1] and [C1].

3.1 Introduction

Given the dual-functional nature of the DFRC systems, the secrecy issue can be addressed in the aspect of either radar or communication. From the perspective of the radar system, existing works focus on radar privacy maintenance [278–280]. A functional architecture was presented in [278] for the control center aiming at coordinating the cooperation between radar and communication while maintaining the privacy of the radar system. In [279], obfuscation techniques have been proposed to counter the inference attacks in the scenario of spectrum sharing between military radars and commercial communication systems. Besides, the work of [280] showed the probability for an adversary to infer the radar's location by exploiting the communication precoding matrices. On the other hand, the works of [281, 282] have studied the secrecy problems from the viewpoint of communications. In [281], the MIMO radar transmits two different signals simultaneously, one of which is embedded with desired information for the legitimate receiver, and the other one consists of false information to confuse the eavesdroppers. Both of the signals are used to detect the target. Several optimization problems were presented, including secrecy rate maximization, target return SNR maximization and transmit power

minimization. Then, a unified joint system of passive radar and communication systems was considered in [282], where the communication receivers might be eavesdropped by the target of passive radar. As the radar system typically addresses uncooperative or even malicious targets, it is essential to guarantee the PLS in the safety-critical DFRC systems. To guarantee the secrecy of legitimate users in the communication system, the optimization problem was designed to maximize the SNR at the passive radar receiver (RR) while keeping the secrecy rate above a certain threshold. While the aforementioned approaches are well-designed by sophisticated techniques, the AN-aided PLS remains to be explored for the DFRC systems under practical constraints.

To the best of our knowledge, most of the present works regarding secure transmission in the DFRC system rely on the assumption of precisely known CSI at the transmitter. However, wireless communication channels are often impacted by interference from other users, devices, environmental factors, as well as thermal noise in practice. These factors can affect the accuracy of channel estimation and feedback, preventing the transmitter from obtaining perfect CSI. To address the beamforming design in a more general context, we take the imperfect CSI into account in our work, which includes instantaneous and statistical CSI with norm-bounded errors. Moreover, the well-known S-procedure and Lagrange dual function have been adopted to reformulate the optimization problem, which can be solved by Semi-definite Relaxation (SDR) approach. In addition to the CSI issues, we also explore the radar-specific target uncertainty, where we employ a robust adaptation technique for target tracking.

Accordingly, in this chapter, we propose several optimization problems aiming at ensuring information transmission security of the DFRC system. To be specific, we consider a MIMO DFRC BS that is serving multiple legitimate users while detecting targets. It should be noted that these targets are assumed to be potential eavesdroppers. Moreover, spatially focused AN is employed in our methods. Throughout the paper, we aim to minimize the SNR at the target while ensuring the SINR at each legitimate user. Within this scope, we summarize our contributions as follows:

- We first consider the ideal scenario under the assumptions of perfect CSI and the known precise location of targets. The beampattern is formed by approaching a given benchmark radar beampattern. By doing so, the formulated optimization problem can be firstly recast as Fractional programming (FP) problem [283], and then solved by the SDR.

- We investigate the problem under the practical condition of target location uncertainty, where we formulate a beampattern with a given angular interval that the targets might fall into.

- We impose the imperfect communication CSI to the optimization in addition to the above constraints, where worst-case FP problems are formulated to minimize the maximum SNR at the target with bounded CSI errors.

- We consider the statistical CSI, which is more practical due to significantly reduced feedback requirements [114]. To tackle this scenario, we further formulate the eavesdropper SNR minimization problem considering the error bound of statistical CSI.

- We derive the computational complexity for each proposed algorithm.

Moreover, for clarity, some important insights are listed as follows:

- When there is uncertainty on the target direction, the DFRC beam width inevitably needs to be widened, hence increasing the range of angles where the signal can be eavesdropped. Accordingly, ensuring security requires higher AN power, which impacts the power allocated to signal transmission, to transmit confidential information;

- When the peak to sidelobe ratio (PSLR) requirement for the radar increases with a fixed power budget, more power is spent on satisfying the radar requirement. Accordingly, the reduced power budget for communications deteriorates the secrecy rate;

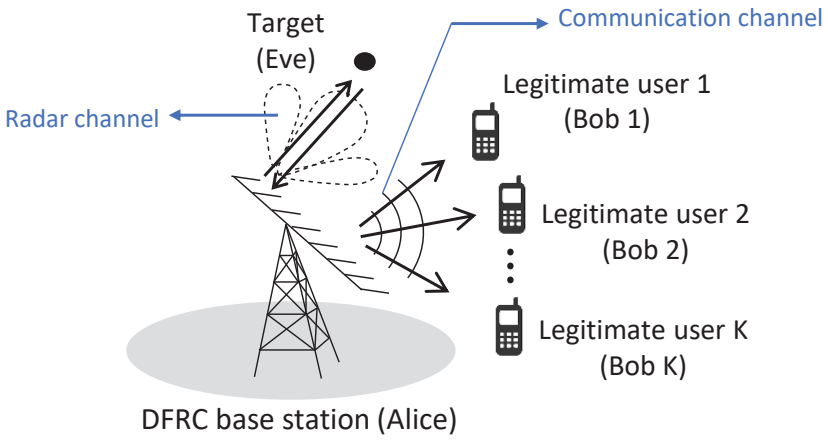

Figure 3.1: Dual-functional Radar-Communication system detecting target which comprises a potential eavesdropper.

- When the CSI is only imperfectly or statistically known, with a fixed power budget, the secrecy rate deteriorates. The system achieves a higher secrecy rate when both the target location and CSI are precisely known.

3.2 System Model

We consider a dual-functional MIMO DFRC system, which consists of a DFRC base station, legitimate users, and a target which is a potential eavesdropper, as shown in Fig. 3.1. The DFRC system is equipped with a uniform linear array (ULA) of N_t antennas, serving K single-antenna users, while detecting a point-like target, which is a single-antenna eavesdropper. For convenience, the multi-antenna transmitter, the legitimate users and the target will be referred to as Alice, Bobs, and Eve respectively.

3.2.1 Signal Model

In the scenario shown in Fig. 3.1, the DFRC base station Alice intends to send confidential information to single-antenna legitimate users, i.e. Bobs, with the presence of the potential eavesdropper, i.e. Eve. The received symbol vector at Bobs and Eve can be respectively modeled as

$$\begin{aligned} \mathbf{y} &= \mathbf{H}\mathbf{x} + \mathbf{z} \\ r &= \alpha \mathbf{a}^H(\theta)\mathbf{x} + e, \end{aligned} \tag{3.1}$$

where $\mathbf{H} = [\mathbf{h}_1, \mathbf{h}_2, \cdots, \mathbf{h}_K]^T \in \mathbb{C}^{K \times N_t}$ is the channel matrix, $\mathbf{x} \in \mathbb{C}^{N_t}$ is the transmitted signal vector, α represents the complex path-loss coefficient, θ is the angle of target, $\mathbf{a}(\theta) = \left[1 \quad e^{j2\pi\Delta\sin(\theta)} \quad \cdots \quad e^{j2\pi(N_t-1)\Delta\sin(\theta)}\right]^T \in \mathbb{C}^{N_t \times 1}$ denotes the steering vector of the transmit antenna array, with Δ being the normalized interval between adjacent antennas. $\mathbf{z}$ and e are the noise vector and scalar, respectively, with $z_k \sim \mathcal{CN}\left(0, \sigma_{z_k}^2\right)$, $e \sim \mathcal{CN}\left(0, \sigma_e^2\right)$.

Consider AN-aided transmit beamforming, the transmit vector $\mathbf{x}$ can be written as

$$\mathbf{x} = \mathbf{W}\mathbf{s} + \mathbf{n} \tag{3.2}$$

where $\mathbf{s} \in \mathbb{C}^K$ is the desired symbol vector of Bobs, where we assume $\mathbb{E}\left[\mathbf{s}\mathbf{s}^H\right] = \mathbf{I}$, $\mathbf{W} = [\mathbf{w}_1, \mathbf{w}_2, \cdots, \mathbf{w}_K] \in \mathbb{C}^{N_t \times K}$ is the beamforming matrix, each column of the beamforming matrix $\mathbf{W}$ represents the beamforming vector of each user, $\mathbf{n}$ is an artificial noise vector[1] generated by Alice to avoid leaking information to Eves. It is assumed that $\mathbf{n} \sim \mathcal{CN}(0, \mathbf{R}_N)$. Additionally, we assume that the desired symbol vector $\mathbf{s}$ and the artificial noise vector $\mathbf{n}$ are independent of each other.

According to [284], it is presumed that the above signal is used for both radar and communication operations, where each communication symbol is considered as a snapshot of a radar pulse. Then, the covariance matrix of the transmitted dual-functional waveform[2] can be given as

$$\mathbf{R}_X = \mathbb{E}\left[\mathbf{x}\mathbf{x}^H\right] = \sum_{k=1}^{K} \mathbf{W}_k + \mathbf{R}_N, \tag{3.3}$$

where $\mathbf{W}_k \triangleq \mathbf{w}_k \mathbf{w}_k^H$. Then, the beampattern can be expressed as

$$P_{bp} = \mathbf{a}^H(\theta)\mathbf{R}_X\mathbf{a}(\theta). \tag{3.4}$$

[1]Note that the generated AN is colored Gaussian noise, which has favorable auto-correlation properties, and will hence impose negligible impact on reconstructing the target at the radar receiver.

[2]In a general radar system, the transmitted waveform is required to be known at the receiver side in order to estimate the target. As the waveform changes symbol by symbol in DFRC systems, overhead generated by the sharing of the transmitted waveform with the receiver is significant. Thus, monostatic radar is assumed to be employed in our system model rather than bistatic radar, i.e., the transmitter and the receiver are collocated.

3.2.2 Metrics

To evaluate the performance of the system, we define a number of performance metrics in this subsection. Initially, based on the aforementioned system model, the SINR of the k-th user can be written as

$$\begin{aligned}\mathrm{SINR}_k^{\mathrm{CU}} &= \frac{\mathbb{E}\left[\left|\mathbf{h}_k^T \mathbf{w}_k s_k\right|^2\right]}{\sum_{i\neq k,i=1}^{K} \mathbb{E}\left[\left|\mathbf{h}_k^T \mathbf{w}_i s_i\right|^2\right] + \mathbb{E}\left[\left|\mathbf{h}_k^T \mathbf{n}\right|^2\right] + \sigma_{z_k}^2} \\ &= \frac{\mathbf{h}_k^T \mathbf{W}_k \mathbf{h}_k^*}{\sum_{i\neq k,i=1}^{K} \left(\mathbf{h}_k^T \mathbf{W}_i \mathbf{h}_k^*\right) + \left(\mathbf{h}_k^T \mathbf{R}_N \mathbf{h}_k^*\right) + \sigma_{z_k}^2}.\end{aligned} \tag{3.5}$$

Equation (3.5) can be simplified

$$\mathrm{SINR}_k^{\mathrm{CU}} = \frac{\mathrm{tr}\left(\mathbf{h}_k^* \mathbf{h}_k^T \mathbf{W}_k\right)}{\sum_{i\neq k,i=1}^{K} \mathrm{tr}\left(\mathbf{h}_k^* \mathbf{h}_k^T \mathbf{W}_i\right) + \mathrm{tr}\left(\mathbf{h}_k^* \mathbf{h}_k^T \mathbf{R}_N\right) + \sigma_{z_k}^2}. \tag{3.6}$$

The achievable transmission rate of legitimate users is given as

$$R_k^{\mathrm{CU}} = \log\left(1 + \mathrm{SINR}_k\right). \tag{3.7}$$

Likewise, based on the given signal model in (3.1) and (3.2), SNR at Eve can be given as [285]

$$\mathrm{SNR}^{\mathrm{E}} = \frac{|\alpha|^2 \mathbf{a}^H(\theta) \sum_{k=1}^{K} \mathbf{W}_k \mathbf{a}(\theta)}{|\alpha|^2 \mathbf{a}^H(\theta) \mathbf{R}_N \mathbf{a}(\theta) + \sigma_e^2}. \tag{3.8}$$

In practice, the precise location of the target is unlikely to be known in advance. Herewith, we define a region of target location angular uncertainty, which is given as $[\theta_0 - \Delta\theta, \theta_0 + \Delta\theta]$, with $\Delta\theta$ being the uncertainty region given a-priori. This scenario will be elaborated in Section 3.4. Then, the achievable transmission rate of Eve can be expressed as

$$R^{\mathrm{E}} = \log\left(1 + \mathrm{SNR}_E\right). \tag{3.9}$$

Additionally, the transmit power is expressed as

$$P_t = \mathrm{tr}(\mathbf{R}_X). \tag{3.10}$$

Given the achievable transmission rates of Bobs and Eve, the worst-case secrecy rate of the system is defined as[3] [286]

$$\mathrm{SR} = \min_k \left[R_k^{\mathrm{CU}} - R^{\mathrm{E}} \right]^+. \tag{3.11}$$

Note that since we focus on optimizing the covariance matrices of both the DFRC signal and the AN, the range sidelobe is not considered in this paper due to its reliance on symbol-level waveform designs, which is designated as our future work.

3.2.3 Channel Model with Imperfect CSI and Statistical CSI

3.2.3.1 Imperfect CSI

According to [287], an additive channel error model of k-th downlink user can be formulated as $\mathbf{h}_k = \tilde{\mathbf{h}}_k + \mathbf{e}_k$, where $\tilde{\mathbf{h}}_k$ is the estimated channel vector known at Alice, and $\mathbf{e}_k$ denotes the channel uncertainty within the spherical region $\Im_k = \{\mathbf{e}_k \mid \|\mathbf{e}_k\|^2 \leq \mu_k^2\}$.

3.2.3.2 Statistical CSI

As the statistical CSI is known to the BS instead of instantaneous CSI, we rewrite the SINR of the k-th user as

$$\mathrm{SINR}_k^{\mathrm{CU}} = \frac{\mathrm{tr}\left(\tilde{\mathbf{R}}_{h_k} \mathbf{W}_k\right)}{\sum_{i \neq k, i=1}^{K} \mathrm{tr}\left(\tilde{\mathbf{R}}_{h_k} \mathbf{W}_i\right) + \mathrm{tr}\left(\tilde{\mathbf{R}}_{h_k} \mathbf{R}_N\right) + \sigma_{z_k}^2}, \tag{3.12}$$

where $\tilde{\mathbf{R}}_{h_k} = \mathbf{E}\left\{\mathbf{h}_k^* \mathbf{h}_k^T\right\}$ denotes the k-th user's downlink channel covariance matrix with uncertainty. As a result, the true channel covariance matrix can be modeled

[3]The secrecy is defined as the worst-case secrecy against all potential Bob-Eve pairs in a multi-user multi-Eve scenario. We minimize the target's eavesdropping SNR subject to users' SNR thresholds, expressed as the minimum difference between the users' and the Eve's rates as we indicate in the following sections.

as $\mathbf{R}_{h_k} = \tilde{\mathbf{R}}_{h_k} + \mathbf{\Delta}_k, \forall k$, where $\mathbf{\Delta}_k, \forall k$ are the estimated error matrices. The Frobenius norm of the error matrix of the k-th user is assumed to be upper-bounded by a known constant δ_k, which can be expressed as $\|\mathbf{\Delta}_k\| \leq \delta_k$.

3.3 Minimize Eve's SNR with Perfect CSI and Target Angle

In this section, we aim to enhance the secrecy rate by minimizing Eve's SNR while guaranteeing the required SINR thresholds for legitimate users, i.e. the SINR of Bobs. Firstly, the formulated optimization problem is formulated based on the assumption that the channel information from Alice to Bobs in the communication system is perfectly known. Meanwhile, the precise direction of the detected target is assumed to be known to the transmitter, which will be further relaxed by considering the uncertainty in the target's location in the later sections. The complexity analysis is given at the end of this section.

3.3.1 Problem Formulation

Let us firstly consider the SNR^{E} minimization problem, which should guarantee: a) individual SINR requirement at each legitimate user, b) transmit power budget and c) a desired radar spatial beampattern. It is noteworthy that the time-domain metric peak-to-average power ratio (PAPR) in the DFRC system can be explicitly dealt with by including PAPR constraints in our optimization problems such as PAPR minimization convex optimization method adopted in [288], or constant modulus (CM) constraints in [144, 289, 290]. To keep the focus on the secrecy aspect, PAPR is not considered in our optimization problem throughout this chapter, which is designated as our future work. Note that an ideal radar beampattern should be obtained before designing the beamforming and artificial noise, which can be generated by solving the following constrained least-squares (LS) problem [284, 291]

as an example

$$\begin{aligned}\min_{\eta,\mathbf{R}_d} \ & \sum_{m=1}^{M} \left|\eta P_d(\theta_m) - \mathbf{a}^H(\theta_m)\mathbf{R}_d\mathbf{a}(\theta_m)\right|^2 \\ \text{s.t.} \ & \operatorname{tr}(\mathbf{R}_d) = P_0, \\ & \mathbf{R}_d \succeq 0, \mathbf{R}_d = \mathbf{R}_d^H, \\ & \eta \geq 0,\end{aligned} \tag{3.13}$$

where η is a scaling factor, P_0 represents the transmission power budget, $\{\theta_m\}_{m=1}^M$ denotes an angular grid covering the detection angular range in $[-\pi/2, \pi/2]$, $\mathbf{a}(\theta_m)$ denotes steering vector, $P_d(\theta_m)$ is the desired ideal beampattern gain at θ_m, $\mathbf{R}_d$ represents the desired waveform covariance matrix.

Given a covariance matrix $\mathbf{R}_d$ that corresponds to a well-designed MIMO radar beampattern, the fractional programming optimization problem of minimizing $\mathrm{SNR}^{\mathrm{E}}$ can be formulated as [4]

$$\min_{\mathbf{W}_k,\mathbf{R}_N} \frac{|\alpha|^2 \mathbf{a}^H(\theta_0) \sum_{k=1}^K \mathbf{W}_k \mathbf{a}(\theta_0)}{|\alpha|^2 \mathbf{a}^H(\theta_0)\mathbf{R}_N\mathbf{a}(\theta_0) + \sigma_e^2}, \tag{3.14a}$$

$$\text{s.t.} \ \ \|\mathbf{R}_X - \mathbf{R}_d\|^2 \leq \gamma_{bp}, \tag{3.14b}$$

$$\mathrm{SINR}_k^{\mathrm{CU}} \geq \gamma_b, \forall k, \tag{3.14c}$$

$$\operatorname{tr}(\mathbf{R}_X) = P_0, \tag{3.14d}$$

$$\mathbf{W}_k = \mathbf{W}_k^H, \mathbf{W}_k \succeq 0, \forall k, \tag{3.14e}$$

$$\operatorname{rank}(\mathbf{W}_k) = 1, \forall k, \tag{3.14f}$$

$$\mathbf{R}_N = \mathbf{R}_N^H, \mathbf{R}_N \succeq 0, \tag{3.14g}$$

where the constraints $\mathbf{W}_k = \mathbf{W}_k^H, \mathbf{W}_k \succeq 0, \operatorname{rank}(\mathbf{W}_k) = 1, \forall k$, are equivalent to constraining $\mathbf{W}_k = \mathbf{w}_k\mathbf{w}_k^H$ [13]. θ_0 represents the direction of Eve known at Alice[5], γ_{bp} is the pre-defined threshold that constraints the mismatch between designed covariance

[4]To simplify the optimization problem, we alternatively minimize the SNR at the target, while ensuring the SINR at each legitimate user is larger than a threshold.

[5]The MIMO radar is assumed to be with two working modes including searching and tracking. In the search mode, the radar transmits a spatially orthogonal waveform, which formulates the omnidirectional beampattern. Potential targets can be searched via the beampattern. Then, the radar is able to track potential targets via transmitting directional waveforms. Thus, the precise location is available to be known at Alice.

matrix $\mathbf{R}_X$ and the desired $\mathbf{R}_d$, and finally γ_b denotes the predefined SINR threshold of each legitimate user.

To solve the problem (3.14), let us employ the SDR approach by omitting the $\text{rank}(\mathbf{W}_k) = 1$ constraint in (3.14f), based on which we relax the optimization problem as

$$\min_{\mathbf{W}_k, \mathbf{R}_N} \frac{|\alpha|^2 \mathbf{a}^H(\theta_0) \sum_{k=1}^{K} \mathbf{W}_k \mathbf{a}(\theta_0)}{|\alpha|^2 \mathbf{a}^H(\theta_0) \mathbf{R}_N \mathbf{a}(\theta_0) + \sigma_e^2}, \tag{3.15a}$$

$$\text{s.t.} \quad \text{(3.14b) - (3.14e) and (3.14g).} \tag{3.15b}$$

By noting the fact that problem (3.15) is still non-convex due to the fractional objective function, we propose in the following an iterative approach to solve the problem efficiently.

3.3.2 Efficient Solver

Following [283], problem (3.15) is a single-ratio FP problem, which can be solved by employing the Dinkelbach's transform demonstrated in [292], where the globally optimal solution can be obtained by solving a sequence of SDPs. To develop the algorithm, we firstly introduce a scaling factor $c = \text{SNR}^{\text{E}}$, which is an auxiliary variable. We then define two scaling variables U and V, which are nonnegative and positive respectively, where $\text{U} = |\alpha|^2 \mathbf{a}^H(\theta) \sum_{k=1}^{K} \mathbf{W}_k \mathbf{a}(\theta), \forall k$, $\text{V} = |\alpha|^2 \mathbf{a}^H(\theta) \mathbf{R}_N \mathbf{a}(\theta) + \sigma_e^2$. As a result, the FP problem (3.15) is equivalent to

$$\min_{\mathbf{W}_k, \mathbf{R}_N} \text{U} - c\,\text{V}, \tag{3.16a}$$

$$\text{s.t. (3.14b) - (3.14e) and (3.14g),} \tag{3.16b}$$

where c can be iteratively updated by

$$c[t+1] = \frac{\text{U}[t]}{\text{V}[t]}, \tag{3.17}$$

where t is the index of iteration. For clarity, we summarize the above in Algorithm 3.1. According to [283], it is easy to prove the convergence of the algorithm given

the non-increasing property of c during each iteration. It is noted that the SDR approach generates an approximated solution to the optimization problem (3.14) by neglecting the rank-one constraint. Accordingly, eigenvalue decomposition or Gaussian randomization techniques are commonly employed to obtain a suboptimal solution. In our case, it is noteworthy that the solution obtained from the SDR solver can be guaranteed to be rank-1[6] [293].

3.3.3 Complexity Analysis

In this subsection, the computational complexity of Algorithm 3.1 is analyzed as follows. Note that SDP problems are commonly solved by the interior point method (IPM) [294], which obtains an ϵ-optimal solution after a sequence of iterations with the given ϵ. In problem (3.14), it is noted that the constraints are linear matrix inequality (LMI) except for (3.14b), which is a second-order cone (SOC) [295] constraint. Thus, we demonstrate the complexity in Table 3.1, where N_{iter} represents iteration times. For simplicity, the computational complexity can be given as $\mathcal{O}\left(\sqrt{2}N_{iter}\ln(1/\epsilon)K^{3.5}N^{6.5}\right)$ by reserving the highest order term.

Algorithm 3.1 Alogrithm for solving FP problem (3.15)

Input: $\mathbf{H}, \mathbf{a}(\theta_0), \sigma_e^2, \sigma_z^2, \alpha, \gamma_{bp}, \gamma_b, P_0, iter_{max} \geq 2, \varepsilon$
Output: $\mathbf{W}_k^{(t)}, \mathbf{R}_N^{(t)}, k = 1, \cdots, K$
1. Compute $\mathbf{R}_d$. Reformulate problem (3.15a) by (3.16a). Set the iteration threshold $\varepsilon > 0$. Initialize $c^{(0)}, c^{(1)}, \left|c^{(1)} - c^{(0)}\right| > \varepsilon$.

Repeat:
2. Obtain $\mathbf{W}_k^{(t)}, \mathbf{R}_N^{(t)}, k = 1, \cdots, K$ by solving the SDP problem (3.16).
3. Update c by (3.17).
4. $t = t + 1$.

Until:
$t \geq iter_{max}$ or $\left|c^{t+1} - c^t\right| < \varepsilon$

3.4 Minimize Eve's SNR with Robust Target Angle

In practice, the precise location of the target is difficult to be known at the transmitter. In this section, we consider the scenario where a rough estimate of the target's angle,

[6] Let k and m denote the number of $n \times n$ square matrix variables and linear constraints, separately. For a complex separable QCQP, the SDR is tight if $m \leq k + 2$, with the assumption that none of the solution $\left\{\mathbf{X}_i^*\right\}_{i=1}^k$ to SDR satisfies $\mathbf{X}_i^* = 0$ for some i [293].

instead of its precise counterpart, is available at Alice. Accordingly, the following beampattern design aims at achieving both a desired main-beam width covering the possible angle uncertainty interval of the target as well as a minimized sidelobe power in a prescribed region. First of all, the optimization problem is formulated to generate a wide main-beam beampattern, following which an efficient solver is proposed. Finally, the complexity analysis is given at the end of this section.

3.4.1 Problem Formulation

In this subsection, we consider the case that the angle uncertainty interval of the target is roughly known within the angular interval $[\theta_0 - \Delta\theta, \theta_0 + \Delta\theta]$. To this end, the target from every possible direction should be taken into consideration when formulating the optimization problem. Accordingly, the objective is given as the sum of Eve's SNR at all the possible locations as follows. Due to the uncertainty of target location, a wider beampattern needs to be formulated towards the uncertain angular interval to avoid missing the target. Inspired by the 3dB main-beam width beampattern design for MIMO radar [296], we propose a scheme aiming at keeping a constant power in the uncertain angular interval, which can be formulated as the following optimization problem

$$\min_{\mathbf{W}_k, \mathbf{R}_N} \sum_{\theta_m \in \Phi} \frac{|\alpha|^2 \mathbf{a}^H(\theta_m) \sum_{k=1}^{K} \mathbf{W}_k \mathbf{a}(\theta_m)}{|\alpha|^2 \mathbf{a}^H(\theta_m) \mathbf{R}_N \mathbf{a}(\theta_m) + \sigma_e^2} \tag{3.18a}$$

$$\text{s.t. } \mathbf{a}^H(\theta_0) \mathbf{R}_X \mathbf{a}(\theta_0) - \mathbf{a}^H(\theta_m) \mathbf{R}_X \mathbf{a}(\theta_m) \geq \gamma_s, \forall\, \theta_m \in \Omega \tag{3.18b}$$

$$\mathbf{a}^H(\theta_k) \mathbf{R}_X \mathbf{a}(\theta_k) \leq (1+\alpha) \mathbf{a}^H(\theta_0) \mathbf{R}_X \mathbf{a}(\theta_0), \forall \theta_k \in \Phi \tag{3.18c}$$

$$(1-\alpha) \mathbf{a}^H(\theta_0) \mathbf{R}_X \mathbf{a}(\theta_0) \leq \mathbf{a}^H(\theta_k) \mathbf{R}_X \mathbf{a}(\theta_k), \forall\, \theta_k \in \Phi \tag{3.18d}$$

$$\text{(3.14c) - (3.14g)}, \tag{3.18e}$$

where θ_0 is the main-beam location, Ω denotes the sidelobe region of interest, Φ denotes the wide main-beam region, γ_s is the bound of the sidelobe power.

Likewise, recall the problem (3.14), SDR technique is adopted. To solve the above sum-of-ratio problem, according to [283], we equivalently recast the

minimization problem by neglecting rank-1 constraint as

$$\max_{\mathbf{W}_i,\mathbf{R}_N} \sum_{\theta_m\in\Phi} \frac{|\alpha|^2\mathbf{a}^H(\theta_m)\mathbf{R}_N\mathbf{a}(\theta_m)+\sigma_e^2}{|\alpha|^2\mathbf{a}^H(\theta_m)\sum_{i=1}^K\mathbf{W}_i\mathbf{a}(\theta_m)} \tag{3.19a}$$

$$\text{s.t. (3.18b) - 3.18d), (13.4c) - (13.4e) and (13.4g),} \tag{3.19b}$$

It is noted that problem (3.19) is still non-convex. The approach to solving this sum-of-ratio FP problem is described in the following.

3.4.2 Efficient Solver

To present the solution to problem (3.19), we firstly refer to [283] and denote

$$A(\theta_m) = |\alpha|^2\mathbf{a}^H(\theta_m)\mathbf{R}_N\mathbf{a}(\theta_m)+\sigma_e^2$$
$$B(\theta_m) = |\alpha|^2\mathbf{a}^H(\theta_m)\sum\nolimits_{i=1}^K\mathbf{W}_i\mathbf{a}(\theta_m)$$

One step further, the sum-of-ratio problem is equivalent to the following optimization problem, which can be rewritten in the form

$$\max_{\mathbf{W}_i,\mathbf{R}_N,\mathbf{y}} \sum_{\theta_m\in\Phi} \Big(2y_m\sqrt{A(\theta_m)}-y_m^2B(\theta_m)\Big), \tag{3.20a}$$

$$\text{s.t. (3.18b) - (3.18d), (13.4c) - (13.4e) and (13.4g),} \tag{3.20b}$$

where $\mathbf{y}$ denotes a collection of variables $\{y_1,\cdots,y_M\}$. The optimal y_m can be obtained in the following closed form when θ_m is fixed

$$y_m^* = \frac{\sqrt{A(\theta_m)}}{B(\theta_m)}. \tag{3.21}$$

To this end, the reformulated optimization problem (3.20) can be solved. Then, eigenvalue decomposition or Gaussian randomization is required to get the approximated solution. [7] For clarity, the above procedure is summarized in Algorithm 3.2.

[7] It is known that the Charnes-Cooper transform is an effective approach for FP problems with low complexity. However, it comes with limitations, such as: (a) additional constraints are introduced; (b) the feasible regions of new variables are to be characterized, which may not be easy to do. We also remark that although the technique works very well for the single-ratio case (in fact converges to a global optimum solution of the concave-convex single-ratio FP problem), it cannot be easily

Algorithm 3.2 Algorithm for solving sum-of-ratio problem (3.19)

Input: $\mathbf{H}, \mathbf{a}(\theta_0)$, $\varepsilon > 0$, $\sigma_e^2, \sigma_z^2, \alpha, \gamma_b, \gamma_s, P_0, iter_{max} \geq 2$, $\Delta\theta$.
Output: $\mathbf{W}_k^{(t)}, \mathbf{R}_N^{(t)}, k = 1, \cdots, K$.
1. Reformulate problem (3.19) by (3.20).
Repeat:
2. Obtain $\mathbf{W}_k^{(t)}, \mathbf{R}_N^{(t)}, k = 1, \cdots, K$ by solving the new convex optimization problem (3.20).
3. Update $\mathbf{y}$ by (3.21).
4. $t = t + 1$.
Until:
$t \geq iter_{max}$ or $\left\|\mathbf{y}^{t+1} - \mathbf{y}^t\right\| < \varepsilon$

3.4.3 Complexity Analysis

We end this section by computing the complexity of solving problem (3.18). It is noted that all the constraints can be considered as LMIs in optimization problem (3.18). We denote $\Phi_0 = \text{card}(\Phi)$ and $\Omega_0 = \text{card}(\Omega)$ as the cardinality of Φ and Ω, respectively. Thus, referring to [294], we give the computational complexity in Table 3.1, which can be simplified as $\mathcal{O}\left(3\sqrt{2}N_{iter}\ln(1/\epsilon)K^{3.5}N^{6.5}\right)$ by reserving the highest order.

3.5 Robust Beamforming with Imperfect CSI

In this section, based on the models presented in the previous sections, we consider the case that the perfect channel information is not available at the base station. By relying on the method of robust optimization, we formulate an optimization problem aiming at designing the dual-functional beamformer that is robust to the channel uncertainty, which is bounded in a spherical region. Meanwhile, to guarantee the generality, we minimize the worst-case SNR received at the target in the angular interval of possible location of potential eavesdropper. Then, an efficient solver tailored for the considered fractional optimization problem is developed, following

extended to the multiple-ratio case, e.g., sum-of-ratios problem. To achieve better performance, we deploy the quadratic transform proposed in [297], which is inspired by Dinkelbach's transform. It is also proved in [297] that although the conventional Dinkelbach's transform may lead to a faster convergence rate than the proposed quadratic transform, the use of which is restricted to the single-ratio problem whereas the quadratic transform is capable of dealing with multiple ratios. Furthermore, for multiple-ratio FP problems where global convergence is not guaranteed, slower convergence can sometimes be advantageous as it allows the algorithm to fully explore the solution space.

by a detailed complexity analysis.

3.5.1 Problem Formulation

Recalling the channel model demonstrated in Section II, we formulate the optimization problem when the CSI is imperfectly known to the transmitter as follows. According to the well-known S-procedure [298], $\forall \mathbf{e}_k^H \mathbf{e}_k \leq \mu_k^2$, the constraint that guarantees the worst-case SINR of legitimates users can be reformulated as [287]

$$\left(\tilde{\mathbf{h}}_k + \mathbf{e}_k\right)^H \left(\mathbf{W}_k - \gamma_b \sum_{i=1, i\neq k}^{K} \mathbf{W}_i - \gamma_b \mathbf{R}_N\right)\left(\tilde{\mathbf{h}}_k + \mathbf{e}_k\right) - \gamma_b \sigma^2 \geq 0, \forall\, k. \tag{3.22}$$

Then, we minimize the possible maximum Eve's SNR in the main-beam region of interest, which yields the following robust optimization problem

$$\min_{\mathbf{W}_k, \mathbf{R}_N, t_k} \max_{\theta_m \in \Phi} \frac{|\alpha|^2 \mathbf{a}^H(\theta_m) \sum_{k=1}^{K} \mathbf{W}_k \mathbf{a}(\theta_m)}{|\alpha|^2 \mathbf{a}^H(\theta_m) \mathbf{R}_N \mathbf{a}(\theta_m) + \sigma_e^2} \tag{3.23a}$$

$$\text{s.t.} \begin{pmatrix} \tilde{\mathbf{h}}_k^T \mathbf{Y}_k \tilde{\mathbf{h}}_k^* - \gamma_b \sigma^2 - t_k \mu_k^2 & \tilde{\mathbf{h}}_k^T \mathbf{Y}_k \\ \mathbf{Y}_k \tilde{\mathbf{h}}_k^* & \mathbf{Y}_k + t_k \mathbf{I}_N \end{pmatrix} \geq 0, \forall\, k, \tag{3.23b}$$

$$\mathbf{Y}_k := \mathbf{W}_k - \gamma_b \left(\sum_{i\neq k} \mathbf{W}_i\right) - \gamma_b \mathbf{R}_N$$

$$t_k \geq 0, \forall k, \tag{3.23c}$$

$$\text{(3.18b) - (3.18d) and (3.14d) - (3.14g)}, \tag{3.23d}$$

where $\Phi = [\theta_0 - \Delta\theta, \theta_0 + \Delta\theta]$ is the main-beam region of interest, $m = 1, \cdots, M$. M represents the number of detecting angles in the interval Φ, and finally $\mathbf{t} = [t_1, \cdots, t_K]$ is an auxiliary vector relying on the S-procedure.

3.5.2 Efficient Solver

To solve problem (3.23), the SDR approach is adopted again by dropping the rank-1 constraint in (3.23i). Moreover, the objective function (3.23a) can be transformed to a max-min problem initially which is given as

$$\max_{\mathbf{W}_k, \mathbf{R}_N, t_k} \min_{\theta_m \in \Phi} \frac{|\alpha|^2 \mathbf{a}^H(\theta_m) \mathbf{R}_N \mathbf{a}(\theta_m) + \sigma_e^2}{|\alpha|^2 \mathbf{a}^H(\theta_m) \sum_{k=1}^{K} \mathbf{W}_k \mathbf{a}(\theta_m)}. \tag{3.24}$$

To verify this, we introduce a variable z and define $\mathbf{A}(\theta_m) = \mathbf{a}(\theta_m)\mathbf{a}^H(\theta_m)$. The objective function (3.24) can be rewritten as $\max_{\mathbf{W}_k,\mathbf{R}_N,t_k,z} z$, which subjects to $z \leq \left(\mathrm{tr}(\mathbf{A}(\theta_m)\mathbf{R}_N) + \sigma^2 \big/ |\alpha|^2\right) \big/ \mathrm{tr}\left(\mathbf{A}(\theta_m)\sum_{k=1}^{K}\mathbf{W}_k\right)$ and any other constraints in (3.23). Likewise, we denote

$$C(\theta_m) = \mathrm{tr}(\mathbf{A}(\theta_m)\mathbf{R}_N) + \sigma^2 \big/ |\alpha|^2$$
$$D(\theta_m) = \mathrm{tr}\left(\mathbf{A}(\theta_m)\sum\nolimits_{k=1}^{K}\mathbf{W}_k\right)$$

The aforementioned constraint is equivalent to

$$z \leq \max_{y_m}\left(2y_m\sqrt{C(\theta_m)} - y_m^2 D(\theta_m)\right),$$

which is a less-than-max inequality, so $\max_{y_m}$ can be integrated into the objective. Consequently, problem (3.23) is reformulated as

$$\max_{\mathbf{W}_k,\mathbf{R}_N,\mathbf{y},t_k,z} z, \tag{3.25a}$$

$$\text{s.t.} \quad 2y_m\sqrt{C(\theta_m)} - y_m^2 D(\theta_m) \geq z, \theta_m \in \Phi, \forall\, m, \tag{3.25b}$$

$$\begin{pmatrix} \tilde{\mathbf{h}}_k^T\mathbf{Y}_k\tilde{\mathbf{h}}_k^* - \gamma_b\sigma^2 - t_k\mu_k^2 & \tilde{\mathbf{h}}_k^T\mathbf{Y}_k \\ \mathbf{Y}_k\tilde{\mathbf{h}}_k^* & \mathbf{Y}_k + t_k\mathbf{I}_N \end{pmatrix} \geq 0, \forall\, k, \tag{3.25c}$$

$$\mathbf{Y}_k := \mathbf{W}_k - \gamma_b\left(\sum_{i\neq k}\mathbf{W}_i\right) - \gamma_b\mathbf{R}_N$$

$$\text{(3.23c) - (3.23f), (3.14d) - (3.14e), and (3.14g)} \tag{3.25d}$$

where y_m is an auxiliary variable, each y_m corresponds to the radar detecting angles θ_m in the main-beam region of interest Φ. We refer to the rest variables to the definitions which we presented in the previous sections. Note that problem (3.25) is convex and can be readily tackled. Here, we define a collection of variables $\mathbf{y} = \{y_1, \cdots, y_M\}$. To solve this problem, we apply the quadratic transform and optimize the primal variables $\mathbf{W}_k, \mathbf{R}_N, t_k$ and the auxiliary variable collection $\mathbf{y}$ in an alternating manner. When the primal variables are obtained by initializing the collection $\mathbf{y}$, the optimal y_m can be updated by

$$y_m^* = \frac{\sqrt{C(\theta_m)}}{D(\theta_m)}. \tag{3.26}$$

To this end, eigenvalue decomposition or Gaussian randomization is required to obtain approximated solutions. For clarity, the solution to problem (3.25) can be summarized as Algorithm 3.3.

Algorithm 3.3 Method for Solving multiple-ratio FP problem (3.24)

Input: $\mathbf{a}(\theta_0), \tilde{\mathbf{h}}_k, \sigma_e^2, \sigma_z^2, \alpha, \gamma_b, \gamma_s, P_0$, CSI estimation error threshold $\mu_k > 0$, $\Delta\theta$, iteration threshold $\varepsilon > 0$, $iter_{max} \geq 2$.

Output: $\mathbf{W}_k^{(t)}, \mathbf{R}_N^{(t)}, t_k, z, k = 1, \cdots, K$.

Initialization: Set initial values for $\mathbf{y}^{(0)}, \mathbf{y}^{(1)}$, which $\left\|\mathbf{y}^{(1)} - \mathbf{y}^{(0)}\right\| > \varepsilon$.

Repeat:

1. Reformulate problem (3.24) by replacing the fractional objective function with the form in (3.25b).
2. Reconstruct the problem with variable z.
3. Obtain $\mathbf{W}_k^{(t)}, \mathbf{R}_N^{(t)}, \forall k$ by solving the optimization problem, and then update $\mathbf{y}$ by (3.26).
4. Update the primal variables by (3.25), over $\mathbf{R}_N, \mathbf{W}_k, \forall k$ for fixed $\mathbf{y}$.
5. $t = t + 1$.

Until:

$t \geq iter_{max}$ or $\left\|\mathbf{y}^{(t)} - \mathbf{y}^{(t-1)}\right\| < \varepsilon$

3.5.3 Complexity Analysis

The complexity of Algorithm 3.3 is analyzed in this subsection. Similarly, Φ and Ω can be regarded as discrete domains. We denote $\Phi_0 = \text{card}(\Phi)$ and $\Omega_0 = \text{card}(\Omega)$ as the cardinality of Φ and Ω, respectively. All the constraints in problem (3.23) are LMIs. Specifically, we notice that the problem is composed by $3\Phi_0 + \Omega_0 + K + 1$ LMI constraints of size 1, $2K + 2$ LMI constraints of size N, and K LMI constraints of size $N + 1$. For simplicity, we reserve the highest order of computational complexity, which can be given as $\mathcal{O}\left(4\sqrt{3}N_{iter}\ln(1/\epsilon)K^{3.5}N^{6.5}\right)$.

3.6 Robust Beamforming With Statistical CSI

In this section, we consider the extension of the scenario in section V, where the channels from Alice to Bobs vary rapidly. As a result, the instantaneous CSI is difficult to be estimated. Note that the second-order channel statistics, which vary much more slowly, can be obtained by the BS through long-term feedback. Nevertheless, even in the event that the statistical CSI is known at Alice, uncertainty

is always inevitable. We therefore take the uncertainty matrix into consideration by employing additive errors to the channel covariance matrix. Likewise, the complexity analysis is given at the end of this section.

3.6.1 Problem Formulation

We firstly recall the reformulation of the SINR of the k-th user and the channel model with statistical CSI presented in Section 3.2. To this end, based on Lagrange dual function [114, 299], the constraint corresponding to QoS of k-th user can be formulated as

$$
\begin{aligned}
&-\delta_k \|\mathbf{A}_k + \mathbf{Z}_k\| - \mathrm{tr}\left(\tilde{\mathbf{R}}_{h_k}(\mathbf{Z}_k + \mathbf{A}_k)\right) - \gamma_b \mathrm{tr}\left(\tilde{\mathbf{R}}_{h_k}\mathbf{R}_N\right) - \gamma_b \sigma_z^2 \geq 0 \\
&\mathbf{Z}_k = \mathbf{Z}_k^H, \mathbf{Z}_k \succeq \mathbf{0}, \forall\, k
\end{aligned}
$$

where $\mathbf{A}_k = \gamma_b \sum_{i=1, i\neq k}^{K} \mathbf{W}_i - \mathbf{W}_k, \forall\, k$. Recalling the optimization problem in Section 3.5, likewise, the robust beamforming problem with erroneous statistical CSI is given as

$$
\min_{\mathbf{W}_k, \mathbf{R}_N, \mathbf{Z}_k} \max_{\theta_m \in \Phi} \frac{|\alpha|^2 \mathbf{a}^H(\theta_m) \sum_{k=1}^{K} \mathbf{W}_k \mathbf{a}(\theta_m)}{|\alpha|^2 \mathbf{a}^H(\theta_m) \mathbf{R}_N \mathbf{a}(\theta_m) + \sigma_e^2} \tag{3.27a}
$$

$$
\text{s.t.} \quad -\delta_k \|\mathbf{A}_k + \mathbf{Z}_k\| - \mathrm{tr}\left(\tilde{\mathbf{R}}_{h_k}(\mathbf{Z}_k + \mathbf{A}_k)\right) - \gamma_b \mathrm{tr}\left(\tilde{\mathbf{R}}_{h_k}\mathbf{R}_N\right) - \gamma_b \sigma_z^2 \geq 0, \forall\, k, \tag{3.27b}
$$

$$
\mathbf{Z}_k = \mathbf{Z}_k^H, \mathbf{Z}_k \succeq \mathbf{0}, \forall\, k \tag{3.27c}
$$

$$
\text{(3.18b) - (3.18d) and (3.14d) - (3.14g).} \tag{3.27d}
$$

We note that the problem (3.27) can be solved with SDR approach by dropping the rank-one constraint in (3.27). One step further, similar to (3.23), problem (3.27) can be reformulated in a similar way, given by

$$
\max_{\mathbf{W}_k, \mathbf{R}_N, \mathbf{Z}_k, z} z \tag{3.28a}
$$

$$
\text{s.t.} \quad 2y_m \sqrt{C(\theta_m)} - y_m^2 D(\theta_m) \geq z, \theta_m \in \Phi, \forall m, \tag{3.28b}
$$

$$
\text{(3.27b)-(3.27c), (3.18b) - (3.18d), (3.14d) - (3.14e) and (3.14g).} \tag{3.28c}
$$

Note that problem (3.28) is SDP feasibility and can be solved in polynomial time using interior-point algorithms[8] [114].

3.6.2 Complexity Analysis

The complexity of problem (3.27) is given as follows. As is noted in problem (3.28), almost all the constraints are LMI except for the SOC constraint (3.27b). Likewise, we denote $\Phi_0 = \text{card}(\Phi)$ and $\Omega_0 = \text{card}(\Omega)$ as the cardinality of Φ and Ω. Note that the problem is composed by K SOC constraints of size 1, $\Omega_0 + 3\Phi_0 + 1$ LMI constraints of size 1, and $4K + 2$ LMIs of size N. Accordingly, we compute the complexity as shown in Table 3.1. When the CSI is statistically known, the computational complexity can be simply demonstrated as $\mathcal{O}\left(5\sqrt{2}N_{iter}\ln(1/\epsilon)K^{3.5}N^{6.5}\right)$. which is the complexity of each iteration. Then, The calculated complexities of all the proposed optimizations are summarised in Table 3.1.

	Complexity
Perfect CSI and Precise Target Location	$\mathcal{O}\left(\sqrt{2}N_{iter}\ln(1/\epsilon)K^{3.5}N^{6.5}\right)$
Perfect CSI and Target Location Uncertainty	$\mathcal{O}\left(3\sqrt{2}N_{iter}\ln(1/\epsilon)K^{3.5}N^{6.5}\right)$
Imperfect CSI and Target Location Uncertainty	$\mathcal{O}\left(4\sqrt{3}N_{iter}\ln(1/\epsilon)K^{3.5}N^{6.5}\right)$
Statistical CSI and Target Location Uncertainty	$\mathcal{O}\left(5\sqrt{2}N_{iter}\ln(1/\epsilon)K^{3.5}N^{6.5}\right)$

Table 3.1: Complexity Analysis

3.7 Numerical Results

To evaluate the proposed methods, numerical results based on Monte Carlo simulations are shown in this section to validate the effectiveness of the proposed beamforming method. Without loss of generality, each entry of channel matrix $\mathbf{H}$ is assumed to obey standard Complex Gaussian distribution, i.e. $h_{i,j} \sim \mathcal{CN}(0,1)$. We assume that the DFRC base station employs a ULA with half-wavelength spacing between adjacent antennas. In the following simulations, the number of antennas is set as $N_t = 18$ and the number of legitimate users is $K = 4$. Moreover, for convenience,

[8] Since solutions $\mathbf{W}_k, k = 1, \cdots, K$ obtained from solving the convex relaxation problems (3.15), (3.19), (3.24) and (3.28) are all rank-one, the rank-one approximation procedures, e.g., eigenvalue decomposition or Gaussian randomization, can be omitted in general for our study.

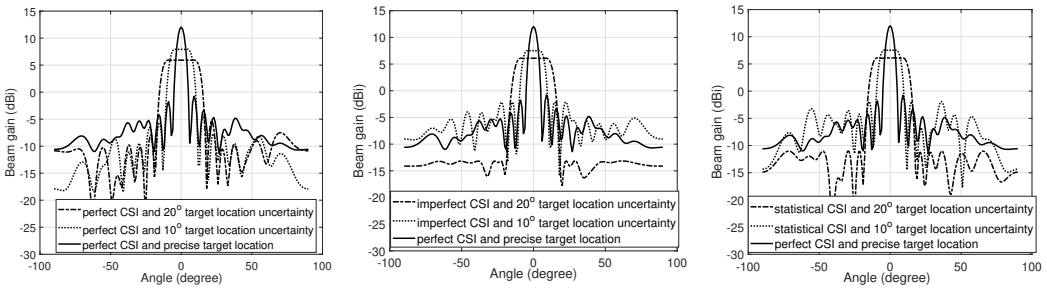

(a) (b) (c)

Figure 3.2: Beampatterns with various target direction uncertainty interval when (a) CSI is known, (b) CSI is imperfectly known and (c) statistical CSI is imperfectly known.

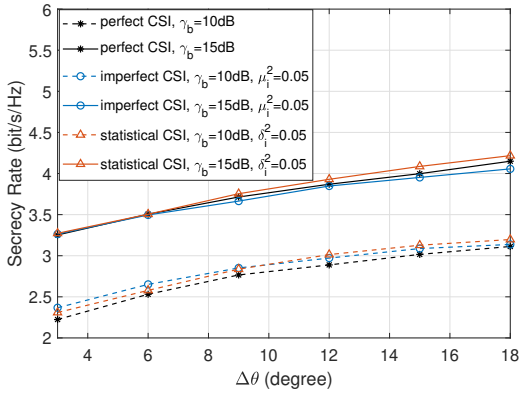

Figure 3.3: Secrecy rate with different angular intervals, $N = 18, K = 4, P_0 = 30$ dBm, with $\gamma_b = 10$ dB and $\gamma_b = 15$ dB, respectively.

the noise level of the eavesdropper is assumed to be the same as that of the intended receivers. The constrained beamforming design problems in Section 3.3-Section 3.6 are solved by the classic SDR technique using the CVX toolbox [300].

3.7.1 Beam Gain

We first show the resultant radar beampattern in Fig. 3.2 with different angular interval of target location uncertainty, i.e. $[-5°, 5°]$ and $[-10°, 10°]$. The SINR threshold of each legitimate user is set as $\gamma_b = 10$ dB. The narrow beampattern when the target location is precisely known at the BS is set as a benchmark. It is found that the desired beampattern with a wide main beam is obtained by solving the proposed algorithms, which maintain the same power in the region of the possible target location. Additionally, it is noted that with the expansion of location uncertainty angular interval, the power gain of the main beam reduces.

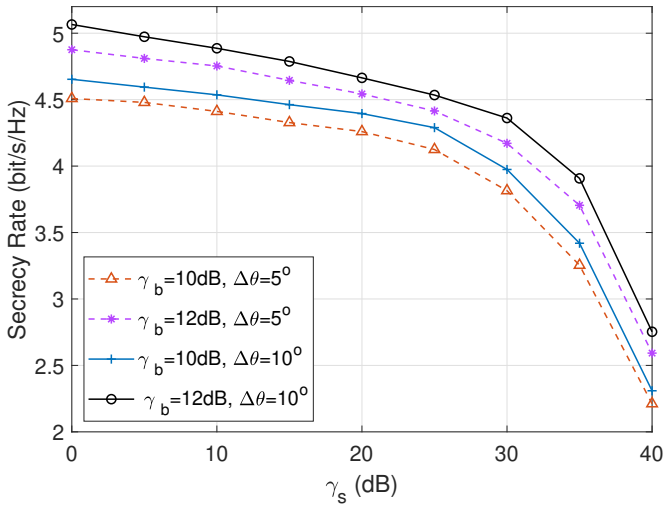

Figure 3.4: Worst-case secrecy rate versus the sidelobe power with various SINR threshold of legitimate users for the Algorithm 2, $N = 18, K = 4, P_0 = 30$ dBm, $\Delta\theta = 5°$.

3.7.2 Trade-off Between the Performance of Radar and Communication System

In this subsection, we evaluate the performance trade-off between radar and communication systems. Fig. 3.3 shows the secrecy rate performance with various angular intervals for $\gamma_b = 10$ dB and $\gamma_b = 15$ dB. The main-beam power decreases when the target uncertainty increases, then the leaking information would get less, which improves the secrecy rate. As is demonstrated in Fig. 3.3, the secrecy rate increases with the growth of the target uncertainty interval. Besides, with 5 dB growth of legitimate user SINR threshold, the secrecy rate increases 0.5 bit/s/Hz approximately.

Fig. 3.4 demonstrates the secrecy rate performance versus the threshold of sidelobe with $P_0 = 30$ dBm, $\Delta\theta = 5°$, which reveals the trade-off between the performance of radar and communication systems. In Algorithm 3.2, the power difference between the main beam and sidelobe increases with the growth of γ_s, which results in the increasing possibility of information leaking. As the numerical result shown in Fig. 3.4, it is notable that the secrecy rate decreases with the growth of γ_s, especially the tendency gets obvious when γ_s is greater than 30 dB.

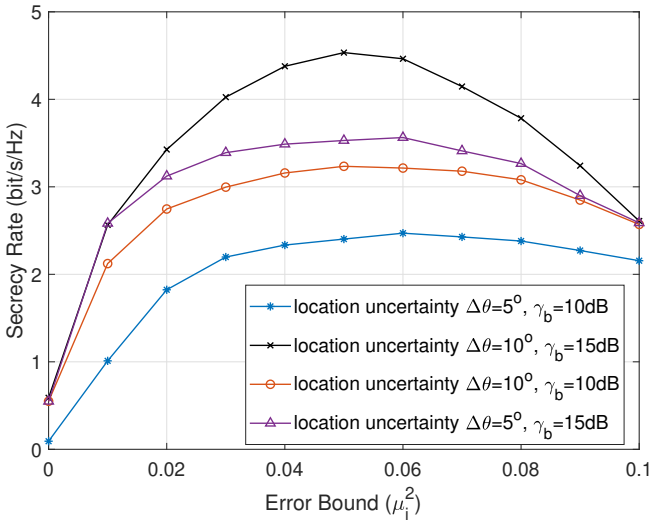

Figure 3.5: Achieved secrecy rate with different error bounds in the scenario of known imperfect CSI, $N = 18, K = 4, P_0 = 30$ dBm.

3.7.3 Robust Beamforming Performance

As the norm of CSI error is bounded by a constant, the secrecy rate performance versus error bound is illustrated in Fig. 3.5, with different location uncertainty. With the growth of error bound, the achievable SINR at each legitimate user keeps being above the given threshold but not a constant according to constraints (3.25c) and (3.27b). We note that the worst-case secrecy rate reduces after a certain value with the increasing error bound, because of the different changing rate between target SNR and user SINR corresponding to various error bounds in Fig. 3.5. Whereas, as is shown in Fig. 3.6, the secrecy rate keeps increasing with the growth of error bound. In addition, the robust beamforming designs achieve a higher secrecy rate when the location uncertainty is limited in a larger interval.

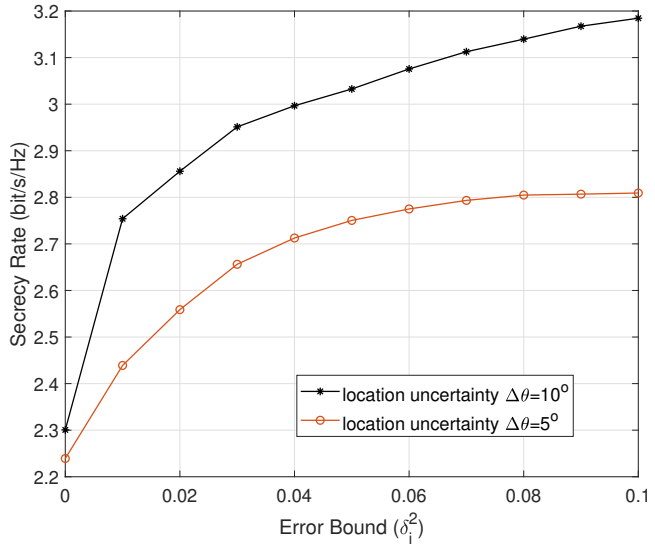

Figure 3.6: Worst-case secrecy rate versus different error bounds when statistical CSI is imperfectly known, $N = 18, K = 4, P_0 = 30$ dBm, $\gamma_b = 10$ dB.

3.8 Conclusions

In this chapter, optimization-based beamforming designs have been addressed for the MIMO DFRC system, which aimed at ensuring the security of information transmission in case of leaking to targets by adding AN at the transmitter to confuse the potential eavesdropper. Specifically, we have minimized the SNR of the target which is regarded as the potential eavesdropper while keeping each legitimate user's SINR above a certain constant to ensure the secrecy rate of the DFRC system. Throughout this paper, the optimization beamforming problem has been designed with perfect CSI and imperfect CSI, as well as with accurate and inaccurate target location information.

First of all, both the precise location of the target and perfect CSI have been assumed to be known at BS, which gained the highest secrecy rate according to the numerical results. When the target location was uncertain, the main-beam power decreased with the growth of the uncertainty angular interval. Moreover, the secrecy rate versus different thresholds of sidelobe has been demonstrated, which revealed the trade-off between radar and communication system performance. Then, we formulated a target SNR minimization problem with imperfect instantaneous CSI and statistical CSI known to the base station respectively. As shown in the numerical

results, the beamforming design has been feasible in both robust scenarios. Finally, simulation results have been presented to show the secrecy rate tendency affected by error bound with various target location uncertainty.

Chapter 4

Ensure the PLS of ISAC Systems by Deploying the Constructive/Destructive Interference Technique

This chapter is based on our works published in [J2], [C2], and [C3].

4.1 Introduction

The AN-aided secure DFRC systems have been presented in the previous chapter. However, the AN indeed degrades SINR at both CUs and eavesdroppers, which requires a higher power budget to ensure the QoS. In view of the redundant power consumption caused by AN, DM has attracted growing research attention as an emerging hardware-efficient approach to secure wireless communication systems in recent years [16–18].

The DM transmitter sends confidential information to the CUs such that the malicious eavesdroppers cannot intercept the transmitted messages [19]. Unlike the SR-based methods, the DM technique adjusts the amplitude and phase of the symbols at the users of interest directly while scrambling the symbols in other undesired directions, which implies that the modulation happens at the antenna level instead of at the baseband level. As a result, a low SER can be endorsed at the CUs, while

the received symbols of the eavesdropper are randomized in the signal constellation. Since the expensive and power-consuming RF chains and digital-to-analog converter (DAC) deployed in conventional beamforming design are not required, the DM-based scheme is efficient on aspects of both cost and energy. The DM approach is based on the principles of exploiting CI [2, 20–22], where the received signal is not necessary to be aligned with the intended symbols, but is pushed away from the detection thresholds of the signal constellation.

To the best of our knowledge, all the existing studies on DFRC security are based on SR maximization, with the assumption of Gaussian symbol transmission and perfect or imperfect CSI knowledge. To address DFRC security in broader scenarios, it is worth studying the CI-based waveform design for the reason that a) MUI is commonly treated as a detrimental impact that needs to be mitigated, while it becomes beneficial and further contributes to the useful signal power in CI design; b) CI based precoding can support a larger number of data streams with a significantly improved SER performance [301].

Moreover, motivated by the demand for power-efficient and cost-effective MIMO systems, we deploy constant envelope (CE) waveform design in our problem formulations. To be specific, CE waveforms maintain a constant amplitude, allowing power amplifiers to operate at or near saturation, improving power efficiency and minimizing energy consumption [302]. Besides, CE waveforms have a low PAPR, which reduces the likelihood of signal clipping, simplifies the design of power amplifiers, and improves overall system performance. In practice, digital phase shifters (PSs) are mostly deployed, which provide a discrete set of phase states which are controlled by a string of binary digits [303].

In this chapter, we propose several designs, which aim at maximizing the received SINR of the radar in secure DFRC systems. Specifically, we consider an MU-MISO DFRC BS which serves CUs and detects a point-like target simultaneously, where the transmit waveform and the receive beamformer are jointly designed to improve PLS following the CI approach. Note that the target is treated as a potential eavesdropper. As a further consideration on communication data secrecy,

MUI is designed to be constructive at the CUs, while disrupting the data at the radar target, which deteriorates the target receive signals and thus increases the SER at the target. Also, discrete phase CE and 1-bit DACs constraints are taken into account for hardware cost reduction. Throughout this chapter, the proposed problems above are firstly studied in an ideal scenario where the target location is known to the BS, and are then extended to the more practical case where the location is uncertain to the BS.

Within this scope, the contributions of our work are summarized as follows:

- We design the transmit waveform and receive beamformer jointly for the secure ISAC system, where the DM technique is employed to maximize the received SINR of the radar system under the constraints of power budget and CI for security.
- We propose an FP algorithm to solve the radar SINR maximization problem and compare the resulting performance with benchmark techniques, and alternative solvers including semidefinite relaxation (SDR), and successive Quadratically Constrained Quadratic Program (SQ) methods.
- We investigate the problem under the practical condition of target location uncertainty, where the ISAC waveform is designed to maximize the minimum radar SINR within a given angular interval that the targets might fall into.
- We further consider an advanced secure CI design for the proposed ISAC system, where the MUI is designed to be constructive to CUs, while destructive to the target.
- We also take the hardware efficiency into account, imposing discrete phase CE and 1-bit DACs constraints into the waveform optimization design by exploiting the full destructive region.

4.2 System Model

We consider an ISAC MU-MISO system with a BS equipped with N_T transmit antennas and N_R receive antennas, which is serving K single-antenna users and

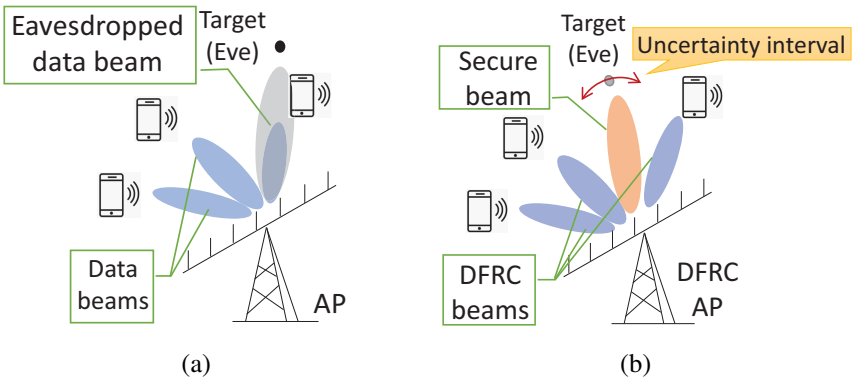

Figure 4.1: (a) ISAC System imposed a potential eavesdropper, which might eavesdrop on the information from the access point (AP) to CUs. (b) Secure ISAC system.

detecting a point-like target simultaneously. As shown in Fig. 4.1, the target can be regarded as a potential eavesdropper which might intercept the information sent from the BS to legitimate users. Due to the existence of I clutter sources, the target return interferes with the BS's receiver. Additionally, the communication channel is considered to be a narrowband slow time-varying block fading Rician fading channel. Based on the assumptions above, below we elaborate on the radar and communication signal models.

4.2.1 Radar Signal Model

Let $\mathbf{x} \in \mathbb{C}^{N_T \times 1}$ denote the transmit signal vector, the received waveform at the receive array is given as

$$\mathbf{r} = \underbrace{\alpha_0 \mathbf{U}(\theta_0)\mathbf{x}}_{\text{signal}} + \underbrace{\sum_{i=1}^{I} \alpha_i \mathbf{U}(\theta_i)\mathbf{x}}_{\text{signal - dependent clutter}} + \underbrace{\mathbf{z}}_{\text{noise}}, \tag{4.1}$$

where α_0 and α_i denote the complex amplitudes of the target and the i-th interference source, θ_0 and θ_i are the angle of the target and the i-th signal-dependent clutter source, respectively, and $\mathbf{z} \in \mathbb{C}^{N_R \times 1}$ is the additive white Gaussian noise (AWGN) vector, with the variance of σ_R^2. $\mathbf{U}(\theta)$ is the steering matrix of a uniform linear array (ULA) antenna with a half-wavelength spaced element, defined as

$$\mathbf{U}(\theta) = \mathbf{a}_r(\theta)\mathbf{a}_t^T(\theta), \tag{4.2}$$

where

$$\mathbf{a}_t(\theta) = \frac{1}{\sqrt{N_T}}\left[1, e^{j\pi\sin\theta}, \cdots, e^{j\pi(N_T-1)\sin\theta}\right]^T$$
$$\mathbf{a}_r(\theta) = \frac{1}{\sqrt{N_R}}\left[1, e^{j\pi\sin\theta}, \cdots, e^{j\pi(N_R-1)\sin\theta}\right]^T.$$

Then, the output of the filter can be given as

$$\begin{aligned} r_f &= \mathbf{w}^H\mathbf{r} \\ &= \alpha_0\mathbf{w}^H\mathbf{U}(\theta_0)\mathbf{x} + \sum_{i=1}^{I}\alpha_i\mathbf{w}^H\mathbf{U}(\theta_i)\mathbf{x} + \mathbf{w}^H\mathbf{z}, \end{aligned} \tag{4.3}$$

where $\mathbf{w} \in \mathbb{C}^{N_R\times 1}$ denotes the receive beamforming vector. Accordingly, the output SINR can be expressed as

$$\begin{aligned} \mathrm{SINR}_{rad} &= \frac{\left|\alpha_0\mathbf{w}^H\mathbf{U}(\theta_0)\mathbf{x}\right|^2}{\mathbf{w}^H\sum\limits_{i=1}^{I}|\alpha_i|^2\mathbf{U}(\theta_i)\mathbf{x}\mathbf{x}^H\mathbf{U}^H(\theta_i)\mathbf{w} + \mathbf{w}^H\mathbf{w}\sigma_R^2} \\ &= \frac{\mu\left|\mathbf{w}^H\mathbf{U}(\theta_0)\mathbf{x}\right|^2}{\mathbf{w}^H\left(\mathbf{\Sigma}(\mathbf{x}) + \mathbf{I}_{N_R}\right)\mathbf{w}}, \end{aligned} \tag{4.4}$$

where $\mu = |\alpha_0|^2/\sigma_R^2$, $\mathbf{\Sigma}(\mathbf{x}) = \sum\limits_{i=1}^{I} b_i\mathbf{U}(\theta_i)\mathbf{x}\mathbf{x}^H\mathbf{U}^H(\theta_i)$, and $b_i = |\alpha_i|^2/\sigma_R^2$.

Since $\mathbf{x}$ is the intended information signal, the received signal at target (eavesdropper's receiver) can be given as

$$y_R = \alpha_0\mathbf{a}_t^H(\theta_0)\mathbf{x} + e, \tag{4.5}$$

where $e \sim \mathcal{CN}\left(0, \sigma_T^2\right)$ denotes the AWGN. Then, eavesdropping SNR at radar target can be expressed as

$$\mathrm{SNR}_T = \frac{\left|\alpha_0\mathbf{a}_t^H(\theta_0)\mathbf{x}\right|^2}{\sigma_T^2}. \tag{4.6}$$

4.2.2 Communication Signal Model

The received signal at the k-th CU can be written as

$$y_k = \mathbf{h}_k^H\mathbf{x} + n_k, \tag{4.7}$$

where $\mathbf{h}_k \in \mathbb{C}^{N_T \times 1}$ denotes the multiple-input-single-output (MISO) channel vector between the BS and the k-th CU. Similarly, n_k is the AWGN of the CU k with the variance of $\sigma^2_{C_k}$. Following the typical mmWave channel proposed in [304], we assume that $\mathbf{h}_k$ is a slow time-varying block Rician fading channel, i.e., the channel is constant in a block but varies slowly from one block to another. Thus, the channel vector of the k-th user can be expressed as a combination of a deterministic strongest line-of-sight (LoS) channel vector and a multiple-path scattered channel vector, which is expressed as

$$\mathbf{h}_k = \sqrt{\frac{v_k}{1+v_k}}\mathbf{h}^{\text{LoS}}_{L,k} + \sqrt{\frac{1}{1+v_k}}\mathbf{h}^{\text{NLoS}}_{S,k}, \tag{4.8}$$

where $v_k > 0$ is the Rician K-factor of the k-th user, $\mathbf{h}^{\text{LoS}}_{L,k} = \sqrt{N_T}\mathbf{a}_t(\omega_{k,0})$ is the LoS deterministic component. $\mathbf{a}(\omega_{k,0})$ denotes the array steering vector, where $\omega_{k,0} \in \left[-\frac{\pi}{2}, \frac{\pi}{2}\right]$ is the angle of departure (AOD) of the LoS component from the BS to user k [304, 305]. The scattering component $\mathbf{h}^{\text{NLoS}}_{S,k}$ can be expressed as $\mathbf{h}^{\text{NLoS}}_{S,k} = \sqrt{\frac{N_T}{L}}\sum_{l=1}^{L} c_{k,l}\mathbf{a}_t(\omega_{k,l})$, where L denotes the number of propagation paths, $c_{k,l} \sim \mathcal{CN}(0,1)$ is the complex path gain and $\omega_{k,l} \in \left[-\frac{\pi}{2}, \frac{\pi}{2}\right]$ is the AOD associated to the (k,l)-th propagation path.

Additionally, we note that the intended symbol varies at a symbol-by-symbol basis in CI precoding designs. Let s_k denote the intended symbol of the k-th CU, which is M-PSK modulated. To this end, we define $s_k \in \mathcal{A}_M$, where $\mathcal{A}_M = \left\{a_m = e^{j(2m-1)\phi}, m = 1, \cdots, M\right\}$, $\phi = \pi/M$, and M denotes the modulation order.

4.3 $SINR_{rad}$ Maximization with Known Target Location

With the knowledge of precise target location, in this section, we design the transmit waveform aiming at maximizing the received radar SINR and subject to the information secrecy constraint in the wireless communication system deploying the CI method. For clarity, we remark here that the known target location is quite a typical assumption in the radar literature, especially for target-tracking algorithm designs.

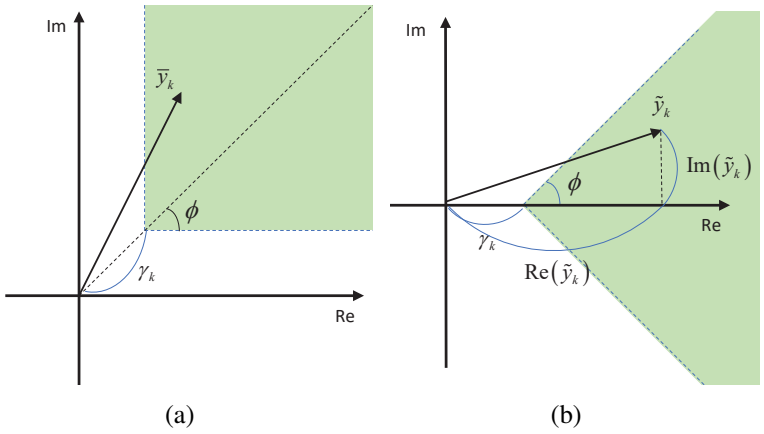

(a) (b)

Figure 4.2: QPSK illustration. (a) Relaxed phase DM. (b) Rotation by $\arg\left(s_k^*\right)$.

This can be interpreted as to optimize the transmit waveform and receive beamformer towards a specific direction of interest, or to track the movement of the target with predicted location information inferred from the previous estimates. Note that this also applies to the clutter sources, whose angles are assumed to be pre-estimated.

In light of the above system setting, we then propose two algorithms to tackle the optimization problem, namely, the SQ method proposed in Section III-B and the FP method proposed in Section III-C. Finally, the SDR approach is adopted to analyze the upper-bound performance, and is presented in Section 4.3.

4.3.1 Problem Formulation

As demonstrated in [57], the study of the DM technique can be based on strict phase and relaxed phase constraints. For the strict phase-based waveform design, the received signal y_k should have exactly the same phase as the induced symbol of the k-th CU (i.e., s_k), which constrains the degrees of freedom (DoFs) in designing the waveform $\mathbf{x}$. Hence, inspired by the concept of CI [2, 151], the optimization problem is proposed to locate the received symbol for each CU within a constructive region rather than restrict the symbol in the proximity of the constellation point, namely the relaxed phase based design.

The CI technique has been widely investigated in recent work. To avoid deviating our focus, we will omit the derivation of the CI constraints, and refer the reader to [2] for more details. Since CI-based waveform design aims to transform the

undesirable MUI into useful power by pushing the received signal further away from the M-PSK decision boundaries, all interference contributes to the useful received power [306]. Herewith, the SNR of the k-th user is expressed as [1]

$$\mathrm{SNR}_k = \frac{\left|\mathbf{h}_k^H \mathbf{x}\right|^2}{\sigma_{C_k}^2}. \tag{4.9}$$

With the knowledge of the channel information, all CUs' data, as well as the location of target and clutter resources is readily available at the transmitter, we formulate the following optimization problem aiming at maximizing the SINR of the target return

$$\begin{aligned} \max_{\mathbf{w},\mathbf{x}} \quad & \mathrm{SINR}_{rad} \\ \text{s.t.} \quad & \|\mathbf{x}\|^2 \leq P_0 \\ & \left|\arg\left(\mathbf{h}_k^H \mathbf{x}\right) - \arg\left(s_k\right)\right| \leq \xi, \forall\, k, \\ & \mathrm{SNR}_k \geq \Gamma_k, \forall\, k, \end{aligned} \tag{4.10}$$

where P_0 denotes the transmit power budget, Γ_k is the given SNR threshold, and ξ is the phase threshold where the noise-less received symbols are supposed to lie.

As illustrated in Fig. 4.2, by taking one of the QPSK constellation points as an example, the constructive region is given as the green area. In Fig. 4.2(a), $\bar{y}_k$ denotes the noise-excluding signal and the SNR-related scalar γ_k is the threshold distance to the decision region of the received symbol at the k-th CU. Then, in order to express the constructive region geometrically, we rotate the noise-free received signal $\bar{y}_k$ and project it onto real and imaginary axes, which are illustrated in Fig. 4.2(b). By

[1] We note that the CI technique adjusts the received signal at the receiver side directly at the symbol level, thus the transmit signal is assumed to be finite-alphabet symbols. As the achievable secrecy rate for a finite-alphabet input scenario would differ from the secrecy rate achieved by a Gaussian codebook [307], we deploy the SER as a performance metric to evaluate the information security instead of the secrecy rate.

noting $|s_k| = 1$, the rotated signal $\tilde{y}_k$ can be given in the form of

$$\begin{aligned}\tilde{y}_k = (y_k - n_k)\frac{s_k^*}{|s_k|} &= \mathbf{h}_k^H \mathbf{x} s_k^* \\ &= \tilde{\mathbf{h}}_k^H \mathbf{x},\end{aligned} \tag{4.11}$$

where $\tilde{\mathbf{h}}_k = \mathbf{h}_k s_k^*$. Let us represent $\mathrm{Re}(\tilde{y}_k) = \mathrm{Re}\left(\tilde{\mathbf{h}}_k^H \mathbf{x}\right)$ and $\mathrm{Im}(\tilde{y}_k) = \mathrm{Im}\left(\tilde{\mathbf{h}}_k^H \mathbf{x}\right)$. Then, the SINR_{rad} maximization problem (4.10) can be recast as [2]

$$\max_{\mathbf{w},\mathbf{x}} \ \mathrm{SINR}_{rad} \tag{4.12a}$$

$$\text{s.t.} \quad \|\mathbf{x}\|^2 \le P_0 \tag{4.12b}$$

$$\left|\mathrm{Im}\left(\tilde{\mathbf{h}}_k^H \mathbf{x}\right)\right| \le \left(\mathrm{Re}\left(\tilde{\mathbf{h}}_k^H \mathbf{x}\right) - \sqrt{\sigma_{C_k}^2 \Gamma_k}\right)\tan\phi, \forall\, k \tag{4.12c}$$

where $\phi = \pm\pi/M$. Till now, the constraints (4.12b) and (4.12c) are both convex. In particular, the CI constraint (4.12c) is essentially linear with respect to the variable $\mathbf{x}$. In the following subsections, we will transform the non-convex objective function to tackle the optimization problem.

4.3.2 Solve (4.12) by SQ Approach

It is noted that problem (4.12) is still non-convex since the clutter is signal-dependent, where the quadratic form of optimizing variable $\mathbf{x}$ is included in both the numerator and denominator. To address this issue, in this section we develop an SQ approach to extract a suboptimal solution. Firstly, note that problem (4.12) can be viewed as the classical minimum variance distortionless response (MVDR) beamforming problem with respect to $\mathbf{w}$, which can be expressed as a function of $\mathbf{x}$ as

$$\mathbf{w} = \frac{[\mathbf{\Sigma}(\mathbf{x}) + \mathbf{I}]^{-1}\mathbf{U}(\theta_0)\mathbf{x}}{\mathbf{x}^H \mathbf{U}^H(\theta_0)[\mathbf{\Sigma}(\mathbf{x}) + \mathbf{I}]^{-1}\mathbf{U}(\theta_0)\mathbf{x}}. \tag{4.13}$$

By substituting (4.13) into (4.4), the optimization problem (4.12) can be rewritten as [308, 309]

$$\begin{aligned}&\max_{\mathbf{x}} \ \mathbf{x}^H \mathbf{\Phi}(\mathbf{x})\mathbf{x} \\ &\text{s.t. (4.12b) and (4.12c),}\end{aligned} \tag{4.14}$$

where $\mathbf{\Phi}(\mathbf{x}) = \mathbf{U}^H(\theta_0)[\mathbf{\Sigma}(\mathbf{x}) + \mathbf{I}]^{-1}\mathbf{U}(\theta_0)$ is a positive-semidefinite SINR matrix. To solve problem (4.14), we adopt the sequential optimization algorithm (SOA) presented in [309]. To be specific, let us firstly ignore the dependence of $\mathbf{\Phi}(\mathbf{x})$ on $\mathbf{x}$, i.e., fixing the signal-dependent matrix $\mathbf{\Phi}(\mathbf{x}) = \mathbf{\Phi}$ for a given $\mathbf{x}$. To start with, we initialize $\mathbf{\Phi} = \mathbf{\Phi}_0$, where $\mathbf{\Phi}_0$ is a constant positive-semidefinite matrix. By using SOA, the waveform $\mathbf{x}$ is optimized iteratively with the updated $\mathbf{\Phi}$ till convergence. By doing so, in each SOA iteration, we solve the following problem

$$\begin{aligned} &\max_{\mathbf{x}} \ \mathbf{x}^H\mathbf{\Phi}\mathbf{x} \\ &\text{s.t. (4.12b) and (4.12c).} \end{aligned} \tag{4.15}$$

Note that problem (4.15) is easily converted to a convex Quadratically Constrained Quadratic Program (QCQP) problem by recasting the signal-independent matrix $\mathbf{\Phi}$ to be negative-semidefinite as follows [308]

$$\begin{aligned} &\max_{\mathbf{x}} \ \mathbf{x}^H\mathbf{Q}\mathbf{x} \\ &\text{s.t. (4.12b) and (4.12c),} \end{aligned} \tag{4.16}$$

where $\mathbf{Q} = (\mathbf{\Phi} - \lambda\mathbf{I})$, $\lambda \geq \lambda_{\max}(\mathbf{\Phi})$, where $\lambda_{\max}(\mathbf{\Phi})$ is the largest eigenvalue of $\mathbf{\Phi}$ [2] It is straightforward to see that $\mathbf{Q}$ is negative-semidefinite, thus the objective function is concave, and then it can be tackled efficiently by CVX toolbox [310]. Here, we denote $\mathbf{w}^*$ and $\mathbf{x}^*$ as the optimal receive beamformer and waveform, respectively. Furthermore, as the expression given in (4.13), the receive beamforming vector $\mathbf{w}^*$ can be updated by the optimal waveform $\mathbf{x}^*$. Therefore, the suboptimal solutions are obtained until convergence by updating $\mathbf{x}$ and $\mathbf{w}$ iteratively. The generated solution will serve as a baseline in Section 4.6 named as SQ. For clarity, we summarize the SQ approach in Algorithm 4.1. The computational complexity of solving problem (4.16) at each iteration is given by $\mathcal{O}\left(N_T^3\sqrt{K}\right)$ [311].

In SQ approach, we note that the reformulation of the objective function in

[2]Note that the objective function (4.16) can be transformed into the form of Rayleigh quotient, which is a typical optimization formulation with a closed-form solution. However, it does not admit a simple closed-form solution due to CI constraints. Accordingly, the Rayleigh quotient theorem cannot be trivially applied to solve the optimization problem.

(4.16) actually relaxes the one given in (4.15). To be specific, we have $\mathbf{x}^H\mathbf{Q}\mathbf{x} = \mathbf{x}^H(\mathbf{\Phi} - \lambda\mathbf{I})\mathbf{x} = \mathbf{x}^H\mathbf{\Phi}\mathbf{x} - \lambda\mathbf{x}^H\mathbf{x}$, while the power constraint (4.12b) indicates that $\mathbf{x}^H\mathbf{x}$ in the second term is not constant. In the following subsection, we adopt the FP algorithm to solve problem (4.15), which aims to tackle the problem without relaxation in the objective function.

Algorithm 4.1 SQ Algorithm for solving problem (4.12)

Input: $P_0, \mathbf{h}_k, \sigma_{C_k}^2, \sigma_R^2, \theta_i, \theta_0, \alpha_0, b_i, \Gamma_k, \forall\ k, \forall\ i, \varepsilon > 0$, and the maximum iteration number m_{max}

Output: $\mathbf{x}$

1. Reformulate problem (4.12) by (4.16).
2. Initialize the positive-semidefinite matrix $\mathbf{\Phi}^0$, $m = 1$.

Repeat:

3. Calculate $\mathbf{Q}^{m-1}$, solve problem (16) to obtain the optimal waveform $\mathbf{x}^m$.
4. Update $\mathbf{\Phi}^m$ by $\mathbf{x}^m$.
5. Transform $\mathbf{\Phi}^m$ into the negative-semidefinite matrix $\mathbf{Q}^m$.
6. $m = m + 1$.

Until:

$m \geq m_{max}$ or $\left|\mathrm{SINR}_{rad}^m - \mathrm{SINR}_{rad}^{m-1}\right| < \varepsilon$

4.3.3 Solve (4.12) by FP Approach

The original radar SINR maximization problem can also be written as

$$\begin{aligned} &\max_{\mathbf{x}} \ \frac{\mu\left|\mathbf{w}^H\mathbf{U}(\theta_0)\mathbf{x}\right|^2}{\mathbf{w}^H(\mathbf{\Sigma}(\mathbf{x}) + \mathbf{I}_{N_R})\mathbf{w}} \\ &\text{s.t. (4.12b) and (4.12c).} \end{aligned} \tag{4.17}$$

We note that the non-convexity lies only in the objective function in the problem above, and one can stay in the convex feasible region by exploiting various linear iteration schemes. Thus, it can be solved by converting the objective function into its linear approximation form. Following the *Dinkelbach's transform* of FP problem presented in [297], we firstly reformulate the objective function as

$$\begin{aligned} &\max_{\mathbf{x}} \ \mu\left|\mathbf{w}^H\mathbf{U}(\theta_0)\mathbf{x}\right|^2 - u\mathbf{w}^H(\mathbf{\Sigma}(\mathbf{x}) + \mathbf{I}_{N_R})\mathbf{w} \\ &\text{s.t. (4.12b) and (4.12c).} \end{aligned} \tag{4.18}$$

Here, the objective function is still non-concave because of the first term. To proceed with optimization problem (4.18), let us firstly denote $f(\mathbf{x}) = \left|\mathbf{w}^H\mathbf{U}(\theta_0)\mathbf{x}\right|^2$. Then, we approximate the objective function $f(\mathbf{x})$ by its first-order Taylor expansion with respective to $\mathbf{x}$ at $\mathbf{x}' \in \mathcal{D}$, where $\mathcal{D}$ denotes the feasible region of (4.17).

$$\begin{aligned} f(\mathbf{x}) &\approx f(\mathbf{x}') + \nabla f^H(\mathbf{x}')(\mathbf{x}-\mathbf{x}') \\ &= f(\mathbf{x}') + \mathrm{Re}\left(\left(2\left(\mathbf{x}'^H\mathbf{U}^H(\theta_0)\mathbf{w}\right)\mathbf{U}^H(\theta_0)\mathbf{w}\right)^H(\mathbf{x}-\mathbf{x}')\right), \end{aligned} \tag{4.19}$$

where $\nabla f(\cdot)$ denotes the gradient of $f(\cdot)$. For simplicity, we omit the constant term $f(\mathbf{x}')$ and denote

$$g(\mathbf{x}) = \mathrm{Re}\left(\left(2\left(\mathbf{x}^{m-1}{}^H\mathbf{U}^H(\theta_0)\mathbf{w}\right)\mathbf{U}^H(\theta_0)\mathbf{w}\right)^H\left(\mathbf{x}-\mathbf{x}^{m-1}\right)\right). \tag{4.20}$$

Herewith, the m-th iteration of the FP algorithm can be obtained by solving the following convex optimization problem

$$\begin{aligned} &\max_{\mathbf{x}} \ \mu g(\mathbf{x}) - u\mathbf{w}^H\left(\mathbf{\Sigma}(\mathbf{x}) + \mathbf{I}_{N_R}\right)\mathbf{w} \\ &\text{s.t. (4.12b) and (4.12c),} \end{aligned} \tag{4.21}$$

where $\mathbf{x}^{m-1} \in \mathcal{D}$ is the point obtained at the $(m-1)$-th iteration. The optimal solution $\mathbf{x}^m \in \mathcal{D}$ can be obtained by solving problem (4.21), and then the receive beamformer $\mathbf{w}^m$ can be obtained by substituting $\mathbf{x}^m$ in (4.13). Furthermore, u is an auxiliary variable, which is updated iteratively by

$$u^{m+1} = \frac{\mu\left|\mathbf{w}^H\mathbf{U}(\theta_0)\mathbf{x}^m\right|^2}{\mathbf{w}^H\left(\mathbf{\Sigma}(\mathbf{x}^m) + \mathbf{I}_{N_R}\right)\mathbf{w}}. \tag{4.22}$$

It is easy to prove the convergence of the algorithm given the non-increasing property of u during each iteration [297]. For clarity, we summarize the above in Algorithm 4.2. We note that the computational complexity of solving problem (4.21) at each iteration is given by $\mathcal{O}\left(N_T^3\sqrt{K}\right)$ [311].

4.3.4 Upper Bound Performance

In this subsection, we derive a new optimization problem to analyze the upper-bound performance of problem (4.12). According to the reformulation given in problem (4.14), the objective function is equivalent to

$$y(\mathbf{x}) = \mathbf{x}^H \mathbf{U}^H(\theta_0)\left[\mathbf{\Sigma}(\mathbf{x}) + \mathbf{I}\right]^{-1}\mathbf{U}(\theta_0)\mathbf{x}. \tag{4.23}$$

It is obvious that $\mathbf{\Sigma}(\mathbf{x}) + \mathbf{I} \succeq \mathbf{I}$, and thereby, $[\mathbf{\Sigma}(\mathbf{x}) + \mathbf{I}]^{-1} \preceq \mathbf{I}$, which indicates that $y(\mathbf{x}) \leq \mathbf{x}^H \mathbf{U}^H(\theta_0)\mathbf{U}(\theta_0)\mathbf{x}$. So we firstly relax the objective function as

$$\begin{aligned} &\max_{\mathbf{x}} \ \mathbf{x}^H \mathbf{U}^H(\theta_0)\mathbf{U}(\theta_0)\mathbf{x} \\ &\text{s.t. (4.12b) and (4.12c).} \end{aligned} \tag{4.24}$$

It is noted that problem (4.24) is an inhomogeneous QCQP [312] problem. We firstly define $\mathbf{X} = \mathbf{x}\mathbf{x}^H$ and let

$$\tilde{\mathbf{X}} = \begin{bmatrix} \mathbf{X} & \mathbf{x} \\ \mathbf{x}^H & 1 \end{bmatrix}. \tag{4.25}$$

Afterwards, problem (4.24) can be recast as

$$\begin{aligned} &\max_{\mathbf{x},\mathbf{X}} \ \mathrm{tr}\left(\mathbf{X}\hat{\mathbf{U}}_0\right) \\ &\text{s.t. } \ \tilde{\mathbf{X}} \succeq 0, \mathrm{rank}\left(\tilde{\mathbf{X}}\right) = 1 \\ &\quad \text{(4.12b) and (4.12c),} \end{aligned} \tag{4.26}$$

where $\hat{\mathbf{U}}_0 = \mathbf{U}^H(\theta_0)\mathbf{U}(\theta_0)$. Note that problem (4.26) is ready to be solved by the SDR technique [313]. To start with, we relax the above optimization problem by dropping the rank-1 constraint, yielding

$$\begin{aligned} &\max_{\mathbf{x},\mathbf{X}} \ \mathrm{tr}\left(\mathbf{X}\hat{\mathbf{U}}_0\right) \\ &\text{s.t. } \ \tilde{\mathbf{X}} \succeq 0 \\ &\quad \text{(4.12b) and (4.12c).} \end{aligned} \tag{4.27}$$

Problem (4.27) is convex and can be optimally solved. Here, we define $\mathbf{X}^*$ and $\mathbf{x}^*$ as the approximate solution to the problem above. By substituting the $\mathbf{X}^*$ in the objective function in (4.25), the optimal objective value is an upper bound of the optimal value in problem (4.12). Note that the computational complexity of solving problem (4.27) is given as $\mathcal{O}\left(N_T^4\sqrt{2N_T+K}\right)$ [311]. For clarity, the computational complexities of proposed algorithms in Sec. 4.3 are summarized in Table 4.1.

Algorithms	Complexity
SQ	$\mathcal{O}\left(N_T^3\sqrt{K}\right)$
FP	$\mathcal{O}\left(N_T^3\sqrt{K}\right)$
SDP	$\mathcal{O}\left(N_T^4\sqrt{2N_T+K}\right)$

Table 4.1: Complexity Analysis

Remark 1. *In problem (4.27), the constraint* $\tilde{\mathbf{X}} \succeq 0$ *implies* $\mathbf{X} \succeq \mathbf{x}\mathbf{x}^H$. *Based on the relaxations above, we have the following inequalities*

$$\mathrm{tr}\left(\mathbf{X}^*\hat{\mathbf{U}}_0\right) \geq \mathrm{tr}\left(\mathbf{x}^*\mathbf{x}^{*H}\hat{\mathbf{U}}_0\right) \geq \mathbf{x}^{*H}\boldsymbol{\Phi}\left(\mathbf{x}^*\right)\mathbf{x}^*$$

Therefore, the objective value in (4.27) is larger than the achievable $SINR_{rad}$, *of which performance is presented as the upper bound of radar receive SINR in our simulation results.*

Algorithm 4.2 The Proposed FP Algorithm for solving problem (4.12)

Input: $P_0, \mathbf{h}_k, \sigma_{C_k}^2, \sigma_R^2, \theta_i, \theta_0, \alpha_0, b_i, \Gamma_k, \forall\ k, \forall\ i, \varepsilon > 0$, and the maximum iteration number m_{max}

Output: $\mathbf{x}$

1. Reformulate the objective function as given in (4.21).
2. Initialize $\mathbf{x}^0 \in \mathcal{D}$ randomly, $m = 1$.

Repeat:

3. Solve problem (4.21) to obtain the optimal waveform $\mathbf{x}^m$.
4. Obtain the receive beamformer $\mathbf{w}^m$ by substituting $\mathbf{x}^m$ in (4.13).
5. Update u by (4.22).
6. $m = m + 1$.

Until:

$m \geq m_{max}$ or $\left|\mathrm{SINR}_{rad}^m - \mathrm{SINR}_{rad}^{m-1}\right| < \varepsilon$

4.4 SINR$_{rad}$ Maximization with Target Angle Uncertainty

In a practical target tracking scenario, the target location is not perfectly known to the BS due to its movement and random fluctuation, and we therefore consider the scenario where a rough estimation of the target's angle is available at the BS. That is, the target is assumed to locate in an uncertain angular interval. In the following waveform design, we aim to maximize the minimum SINR$_{rad}$ with regard to all possible locations within the interval, while taking the CI technique and power budget into account. Finally, an efficient solver is proposed to tackle the worst-case optimization problem.

4.4.1 Problem Formulation

Let us denote the uncertain interval as $\Psi = [\theta_0 - \Delta\theta, \theta_0 + \Delta\theta]$. It is noteworthy that the target from every possible direction should be taken into account when formulating the optimization problem. To this end, we therefore consider the following worst-case problem, which is to maximize the minimum SINR$_{rad}$ with respect to all the possible target locations within Ψ. For the sake of simplicity, let $\theta_p \in \mathrm{card}(\Psi)$ denote the p-th possible location in the given region, where $\mathrm{card}(\cdot)$ represents the cardinality of $(\cdot)$.

$$\max_{\mathbf{x}} \min_{\theta_p \in \mathrm{card}(\Psi)} \frac{\mu\left|\mathbf{w}^H \mathbf{U}\left(\theta_p\right)\mathbf{x}\right|^2}{\mathbf{w}^H\left(\mathbf{\Sigma}(\mathbf{x}) + \mathbf{I}_{N_R}\right)\mathbf{w}} \quad \text{s.t. (4.12b) and (4.12c).} \tag{4.28}$$

Note that the problem above is non-convex since the point-wise maximum of concave functions is not convex. In the following subsection, we will work on solving the problem (4.28).

4.4.2 Efficient Solver

As is detailed in [297], the straightforward extension of Dinkelbach's transform which is deployed in Section III does not guarantee the equivalence to problem (4.28). Thus, we give the equivalent quadratic transformation of the *the max-min-*

ratio problem (4.28), which is rewritten as

$$\begin{aligned} &\max_{\mathbf{x},\mathbf{u}} \min_{\beta_p \in \text{card}(\Psi)} 2u_p \sqrt{\mu \left| \mathbf{w}^H \mathbf{U}\left(\theta_p\right) \mathbf{x} \right|^2} - u_p^2 \mathbf{w}^H \left(\mathbf{\Sigma}\left(\mathbf{x}\right) + \mathbf{I}_{N_R}\right) \mathbf{w} \\ &\text{s.t. (4.12b) and (4.12c).} \end{aligned} \tag{4.29}$$

Here, we denote $\mathbf{u}$ as a collection of variables $\{u_1, \cdots, u_P\}, u_p \in \mathbb{R}$. The objective above is a sequence of ratios for $\theta_p \in \text{card}\left(\Psi\right)$. To proceed[3], we rewrite problem (4.29) in an epigraph form by introducing the variable $a, a \in \mathbb{R}$, which yields the following formulation

$$\max_{\mathbf{x},\mathbf{u},a} \quad a \tag{4.30a}$$

$$\text{s.t. } 2u_p \sqrt{\mu \left| \mathbf{w}^H \mathbf{U}\left(\theta_p\right) \mathbf{x} \right|^2} - u_p^2 \mathbf{w}^H \left(\mathbf{\Sigma}\left(\mathbf{x}\right) + \mathbf{I}_{N_R}\right) \mathbf{w} \geq a, \forall\ \theta_p \in \text{card}\left(\Psi\right) \tag{4.30b}$$

$$\text{(4.12b) and (4.12c).} \tag{4.30c}$$

By observing problem (4.30), it is noted that the constraint (4.30b) is non-convex. To tackle the problem, likewise, we substitute $\mu \left| \mathbf{w}^H \mathbf{U}\left(\theta_p\right) \mathbf{x} \right|^2$ in the first term of (4.30b) with its first-order Taylor expansion approximation with respective to $\mathbf{x}$ at $\mathbf{x}' \in \mathcal{D}$ as is given in (4.19), which is expressed as

$$\begin{aligned} &\max_{\mathbf{x},\mathbf{u},a} \quad a \\ &\text{s.t. } 2u_p \sqrt{\mu \text{Re}\left(\left(2\left(\mathbf{x}'^H \mathbf{U}^H\left(\theta_p\right) \mathbf{w}\right) \mathbf{U}^H\left(\theta_0\right) \mathbf{w}\right)^H \left(\mathbf{x} - \mathbf{x}'\right)\right)} - \\ &\qquad u_p^2 \mathbf{w}^H \left(\mathbf{\Sigma}\left(\mathbf{x}\right) + \mathbf{I}_{N_R}\right) \mathbf{w} \geq a, \ \ \forall\ \theta_p \in \text{card}\left(\Psi\right) \\ &\quad \text{(4.12b) and (4.12c).} \end{aligned} \tag{4.31}$$

It is noted that at the m-th iteration, $\mathbf{x}'$ in problem (4.31) denotes $\mathbf{x}^{m-1} \in \mathcal{D}$, which is the point obtained at the $(m-1)$-th iteration. When the optimal waveform $\mathbf{x}$ is

[3]As given in the expression (4.4), it can be found that the objective function is independent with the amplitude coefficient α_0, therefore, when the target location is imperfectly known, the uncertainty of amplitude can be neglected in the problem formulation.

obtained, the variable u_p can be updated by the following closed form as

$$u_p^{m+1} = \frac{\sqrt{\mu\left|\mathbf{w}^H\mathbf{U}\left(\theta_p\right)\mathbf{x}^m\right|^2}}{\mathbf{w}^H\left(\mathbf{\Sigma}\left(\mathbf{x}^m\right)+\mathbf{I}_{N_R}\right)\mathbf{w}}. \tag{4.32}$$

Now, problem (4.31) can be solved by interior point methods at a worst-case computational complexity of $\mathcal{O}\left(N_T^3\sqrt{\Psi_0+K+1}\right)$ at each iteration [314], where we denote Ψ_0 as the number of elements in card(Ψ). For clarity, the proposed method of solving (4.28) is summarized in Algorithm 4.3.

Algorithm 4.3 The Proposed Algorithm for solving multiple-ratio FP problem (4.28)

Input: $P_0, \mathbf{h}_k, \sigma_{C_k}^2, \sigma_R^2, \theta_i, \theta_0, \alpha_0, b_i, \Gamma_k, \Delta\theta, \forall\, k, \forall\, i, \varepsilon > 0$, and the maximum iteration number m_{max}

Output: $\mathbf{x}$

1. Reformulate the problem by (4.29).
2. Transform the problem to epigraph form following (4.30).
3. Reformulate the non-convex constraint by (4.31).
4. Initialize $\mathbf{x}^0 \in \mathcal{D}$ randomly, $m = 1$.

Repeat:

5. Solve problem (4.31) to obtain the optimal waveform $\mathbf{x}^m$.
6. Obtain the receive beamformer $\mathbf{w}^m$ by substituting $\mathbf{x}^m$ in (4.13).
7. Update $\mathbf{u}$ by (4.32).
8. $m = m + 1$.

Until:

$m \geq m_{max}$ or $\|\mathbf{u}^m - \mathbf{u}^{m-1}\| < \varepsilon$

4.5 CI precoding with DI for the Radar Receiver

In this section, we consider the information transmission security of the DFRC system. We assume that the communication users are legitimate, and treat the point-like target as a potential eavesdropper which might surveille the information from BS to CUs. Accordingly, in the following design, we aim to maximize the SINR at the radar receiver like the proposed formulation in Section 4.3 and Section 4.4, while confining the received signal at the target into the destructive region of the constellation, in order to ensure the PLS for DFRC transmission. This problem will be studied under the circumstances that the target location is known to the BS perfectly and imperfectly, respectively.

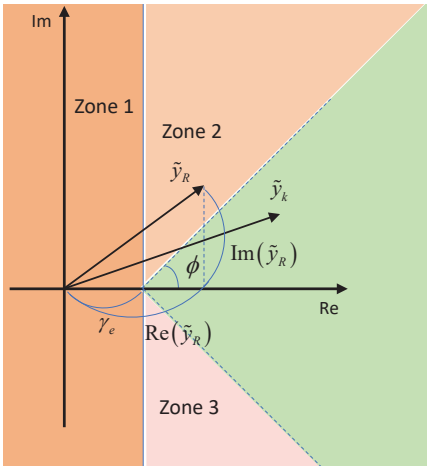

Figure 4.3: The constructive and destructive region division for QPSK.

4.5.1 With Knowledge of Precise Target Location

In prior work with respect to DM technique, such as algorithms proposed in [57], the problems are designed based on the CSI of legitimate users, where the symbols received by potential eavesdroppers are scrambled due to the channel disparity. However, PLS cannot be explicitly guaranteed in this way. To be specific, taking QPSK modulation as an example, the intended symbol can be intercepted with a $\frac{1}{4}$ probability at the target when the target's channel is independent of the CUs' channels, while more importantly, the probability of the target intercepting increases when the target and CUs' channels are correlated. The simulation result will be shown in Section 4.6.

While the CI-based precoding guarantees low SER at CUs, we still need to focus on the detection performance at the target in order to prevent the transmitted information from being decoded. Thus, the following problem is designed to improve the SER at the target. In detail, we define the region out of the constructive region as a destructive region and aim at restricting the received signal of the potential eavesdropper in the destructive area.

We firstly take s_1 as a reference. Likewise, the received noise-excluding signal

at the target can be expressed as

$$\begin{aligned}\tilde{y}_R = (y_R - e)\frac{s_1^*}{|s_1|} &= \alpha_0 \mathbf{a}_t^H(\theta_0)\mathbf{x}s_1^* \\ &= \alpha_0 \tilde{\mathbf{a}}_t^H(\theta_0)\mathbf{x},\end{aligned} \tag{4.33}$$

where $\tilde{\mathbf{a}}_t^H(\theta_0) = \mathbf{a}_t^H(\theta_0)\, s_1^*$. Accordingly, the destructive region can be described by

$$|\mathrm{Im}(\tilde{y}_R)| \geq \left(\mathrm{Re}(\tilde{y}_R) - \sqrt{\sigma_T^2 \Gamma_T}\right)\tan\phi, \tag{4.34}$$

where the scalar Γ_T denotes the desired maximum SNR for the potential eavesdropper and $\sqrt{\sigma_T^2\Gamma_T}$ corresponds to γ_e in Fig. 4.3. As illustrated in Fig. 4.3, the destructive region can be divided to three zones and the inequality (4.34) holds when any one of the following constraints is fulfilled.

$$\textit{zone } 1 : \mathrm{Re}\left(\alpha_0 \tilde{\mathbf{a}}_t^H(\theta_0)\mathbf{x}\right) - \sqrt{\sigma_T^2\Gamma_T} \leq 0 \tag{4.35a}$$

$$\begin{aligned}\textit{zone } 2 : \mathrm{Im}\left(\alpha_0 \tilde{\mathbf{a}}_t^H(\theta_0)\mathbf{x}\right) &\geq \left(\mathrm{Re}\left(\alpha_0 \tilde{\mathbf{a}}_t^H(\theta_0)\mathbf{x}\right) - \sqrt{\sigma_T^2\Gamma_T}\right)\tan\phi \\ \text{and } \mathrm{Re}\left(\alpha_0 \tilde{\mathbf{a}}_t^H(\theta_0)\mathbf{x}\right) &> \sqrt{\sigma_T^2\Gamma_T}\end{aligned} \tag{4.35b}$$

$$\begin{aligned}\textit{zone } 3 : -\mathrm{Im}\left(\alpha_0 \tilde{\mathbf{a}}_t^H(\theta_0)\mathbf{x}\right) &\geq \left(\mathrm{Re}\left(\alpha_0 \tilde{\mathbf{a}}_t^H(\theta_0)\mathbf{x}\right) - \sqrt{\sigma_T^2\Gamma_T}\right)\tan\phi \\ \text{and } \mathrm{Re}\left(\alpha_0 \tilde{\mathbf{a}}_t^H(\theta_0)\mathbf{x}\right) &> \sqrt{\sigma_T^2\Gamma_T}.\end{aligned} \tag{4.35c}$$

For simplicity, we denote (4.35) as destructive interference (DI) constraints. By taking the full region of destructive interference into consideration, the optimization problem can be formulated as

$$\begin{aligned}\max_{\mathbf{x}} \quad & \frac{\mu\left|\mathbf{w}^H\mathbf{U}(\theta_0)\mathbf{x}\right|^2}{\mathbf{w}^H(\boldsymbol{\Sigma}(\mathbf{x}) + \mathbf{I}_{N_R})\mathbf{w}} \\ \text{s.t. } & \text{(4.12b) and (4.12c)} \\ & \text{(4.35a) or (4.35b) or (4.35c).}\end{aligned} \tag{4.36}$$

Note that problem (4.36) is again an FP problem, which can be converted to

$$\begin{aligned} &\max_{\mathbf{x}} \ \mu g(\mathbf{x}) - u\mathbf{w}^H(\mathbf{\Sigma}(\mathbf{x}) + \mathbf{I}_{N_R})\mathbf{w} \\ &\text{s.t. (4.12b) and (4.12c)} \\ &\quad \text{(4.35a) or (4.35b) or (4.35c).} \end{aligned} \tag{4.37}$$

One step further, since all of the constraints given in (4.35) are linear, the reformulation above can be tackled following the solving method proposed in Section 4.3. Then, the formulation (4.37) is converted into a convex optimization problem which includes three subproblems. By solving the problems above, we can obtain optimal waveforms $\mathbf{x}_1^*, \mathbf{x}_2^*, \mathbf{x}_3^*$. Then, we substitute each of them in the objective function, the one resulting in maximum SINR_{rad} will be the final solution to problem (4.36).

4.5.2 With Target Location Uncertainty

In this subsection, we study the scenario where the target location is known imperfectly. Similar to Section 4.4, the target is assumed to locate within a given angular interval $\Psi = [\theta_0 - \Delta\theta, \theta_0 + \Delta\theta]$ and $\beta_p \in \text{card}(\Psi)$ denotes the p-th possible target angle. In order to guarantee secrecy, we confine the received signal at every possible angle in the destructive area. Hence, the problem is given as follows

$$\max_{\mathbf{x}} \ \min_{\theta_p \in \text{card}(\Psi)} \frac{\mu\left|\mathbf{w}^H\mathbf{U}\left(\theta_p\right)\mathbf{x}\right|^2}{\mathbf{w}^H(\mathbf{\Sigma}(\mathbf{x}) + \mathbf{I}_{N_R})\mathbf{w}} \tag{4.38a}$$

$$\text{s.t.} \quad \|\mathbf{x}\|^2 \le P_0 \tag{4.38b}$$

$$\left|\text{Im}\left(\tilde{\mathbf{h}}_k^H\mathbf{x}\right)\right| \le \left(\text{Re}\left(\tilde{\mathbf{h}}_k^H\mathbf{x}\right) - \sqrt{\sigma_{C_k}^2\Gamma_k}\right)\tan\phi, \forall\ k \tag{4.38c}$$

$$\left|\text{Im}\left(\alpha_0\tilde{\mathbf{a}}_t^H\left(\beta_p\right)\mathbf{x}\right)\right| \ge \left(\text{Re}\left(\alpha_0\tilde{\mathbf{a}}_t^H\left(\beta_p\right)\mathbf{x}\right) - \sqrt{\sigma_T^2\Gamma_T}\right)\tan\phi, \forall\ p, \tag{4.38d}$$

which is however not convex. When we take the possible target locations into account, the approach proposed in Section 4.5 would be complicated and time-consuming. Therefore, in order to reduce the computational complexity, we solve problem (4.38) by following the given steps below. Firstly, it is noteworthy that (4.38d) holds when

any one of the following inequalities is satisfied for each p.

$$\mathrm{Im}\left(\alpha_0\tilde{\mathbf{a}}_t^H\left(\beta_p\right)\mathbf{x}\right) \geq \left(\mathrm{Re}\left(\alpha_0\tilde{\mathbf{a}}_t^H\left(\beta_p\right)\mathbf{x}\right) - \sqrt{\sigma_T^2\Gamma_T}\right)\tan\phi, \forall\ p \tag{4.39a}$$

$$-\mathrm{Im}\left(\alpha_0\tilde{\mathbf{a}}_t^H\left(\beta_p\right)\mathbf{x}\right) \geq \left(\mathrm{Re}\left(\alpha_0\tilde{\mathbf{a}}_t^H\left(\beta_p\right)\mathbf{x}\right) - \sqrt{\sigma_T^2\Gamma_T}\right)\tan\phi, \forall\ p. \tag{4.39b}$$

One step further, according to the big-M continuous relaxation method proposed in [315], we introduce binary variables $\eta_p \in \{0,1\}, \forall\ p$ and a sufficiently large constant $\Omega > 0$, the reformulated either-or constraints in (4.39) can be converted to

$$\left(\mathrm{Re}\left(\alpha_0\tilde{\mathbf{a}}_t^H\left(\beta_p\right)\mathbf{x}\right) - \sqrt{\sigma_T^2\Gamma_T}\right)\tan\phi - \mathrm{Im}\left(\alpha_0\tilde{\mathbf{a}}_t^H\left(\beta_p\right)\mathbf{x}\right) - \eta_p\Omega \leq 0, \forall\ p \tag{4.40a}$$

$$\left(\mathrm{Re}\left(\alpha_0\tilde{\mathbf{a}}_t^H\left(\beta_p\right)\mathbf{x}\right) - \sqrt{\sigma_T^2\Gamma_T}\right)\tan\phi + \mathrm{Im}\left(\alpha_0\tilde{\mathbf{a}}_t^H\left(\beta_p\right)\mathbf{x}\right) - \left(1-\eta_p\right)\Omega \leq 0, \forall\ p. \tag{4.40b}$$

Note that in the either-or constraints above, (4.40a) is active when $\eta_p = 0$, which corresponds to (4.39a), and (4.40b) is fulfilled anyway due to the sufficiently large constant Ω. Likewise, when $\eta_p = 1$, (40b) is activated. Accordingly, problem (4.38) can be recast as [306]

$$\begin{aligned} \max_{\mathbf{x}}\ & \min_{\theta_p\in\mathrm{card}(\Psi)} \frac{\mu\left|\mathbf{w}^H\mathbf{U}\left(\theta_p\right)\mathbf{x}\right|^2}{\mathbf{w}^H\left(\boldsymbol{\Sigma}\left(\mathbf{x}\right)+\mathbf{I}_{N_R}\right)\mathbf{w}} \\ \text{s.t.}\ & \text{(4.12b), (4.12c), (4.40a) and (4.40b)} \\ & \eta_p \in \{0,1\}, \forall\ p, \end{aligned} \tag{4.41}$$

We firstly reformulate the problem into the following equivalent form

$$\begin{aligned} \min_{\mathbf{x}}\ & \max_{\beta_p\in\mathrm{card}(\Psi)} \frac{\mathbf{w}^H\left(\boldsymbol{\Sigma}\left(\mathbf{x}\right)+\mathbf{I}_{N_R}\right)\mathbf{w}}{\mu\left|\mathbf{w}^H\mathbf{U}\left(\beta_p\right)\mathbf{x}\right|^2} \\ \text{s.t.}\ & \text{(4.12b), (4.12c), (4.40a) and (4.40b)} \\ & \eta_p \in \{0,1\}, \forall\ p, \end{aligned} \tag{4.42}$$

Henceforth, we will work on solving (4.42). Based on the formulation proposed

in Section 4.4, we firstly give the epigraph form of problem (4.42), which is shown in (4.43).

$$\min_{\mathbf{x},\eta_p,a} \quad a \tag{4.43a}$$

$$\text{s.t. } 2u_p\sqrt{\mathbf{w}^H\left(\mathbf{\Sigma}\left(\mathbf{x}\right)+\mathbf{I}_{N_R}\right)\mathbf{w}}- u_p^2\mu\,\mathrm{Re}\left(\left(2\left(\mathbf{x}'^H\mathbf{U}^H\left(\theta_p\right)\mathbf{w}\right)\mathbf{U}^H\left(\theta_0\right)\mathbf{w}\right)^H\left(\mathbf{x}-\mathbf{x}'\right)\right)\leq a, \forall\ \theta_p\in\mathrm{card}\left(\Psi\right) \tag{4.43b}$$

$$\text{(4.12b), (4.12c), (4.40a) and (4.40b)} \tag{4.43c}$$

$$\eta_p\in\{0,1\},\forall\ p. \tag{4.43d}$$

It is noted that (4.43) is a mixed-integer optimization problem with no polynomial-time computational complexity. To reach a lower complexity, we give the equivalent form of the above problem as [306, 316]

$$\begin{aligned}\min_{\mathbf{x},\eta_p,a}\quad & a+\omega\left(\sum_{p=1}^{2\Delta\theta+1}\eta_p-\sum_{p=1}^{2\Delta\theta+1}\eta_p^2\right)\\ \text{s.t. }\quad & \text{(4.43b)}\\ & \text{(4.12b), (4.12c), (4.40a) and (4.40b)}\\ & 0\leq\eta_p\leq 1,\forall\ p,\end{aligned} \tag{4.44}$$

where ω denotes a large penalty factor for penalizing the objective function for any η_p that is not equal to 0 or 1. The problem above can be solved by the successive convex approximation (SCA) method firstly aiming to obtain the optimal η_p. Then, $\mathbf{x}, a$ can be tackled by optimal η_p iteratively following the FP algorithm. To start with, we initially let $s\left(\eta_p\right)=\sum_{p=1}^{2\Delta\theta+1}\eta_p^2$, and the first-order Taylor expansion of $s\left(\eta_p\right)$ is given as

$$\tilde{s}\left(\eta_p,\eta'_p\right)\approx\sum_{p=1}^{2\Delta\theta+1}\left(\eta'_p\right)^2+2\sum_{p=1}^{2\Delta\theta+1}\eta'_p\left(\eta_p-\eta'_p\right). \tag{4.45}$$

Herewith, problem (4.44) is solvable by adopting the SCA algorithm so as to generate

the optimal η_p. Eventually, the reformulation is given as

$$\min_{\mathbf{x},\eta_p,a} \quad a+\omega\left(\sum_{p=1}^{2\Delta\theta+1}\eta_p-\tilde{s}\left(\eta_p,\eta_p^{n-1}\right)\right) \tag{4.46a}$$

$$\text{s.t. } 2u_p\sqrt{\mathbf{w}^H\left(\mathbf{\Sigma}\left(\mathbf{x}\right)+\mathbf{I}_{N_R}\right)\mathbf{w}}-$$

$$u_p^2\mu\,\mathrm{Re}\left(\left(2\left(\mathbf{x}^{m-1}{}^H\mathbf{U}^H\left(\theta_p\right)\mathbf{w}\right)\mathbf{U}^H\left(\theta_0\right)\mathbf{w}\right)^H\left(\mathbf{x}-\mathbf{x}^{m-1}\right)\right)\leq a,\forall\ p \tag{4.46b}$$

$$\text{(4.12b), (4.12c), (4.40a) and (4.40b)} \tag{4.46c}$$

$$0\leq\eta_p\leq 1,\forall\ p. \tag{4.46d}$$

where n is the iteration index of η_p. To tackle this problem, η_p is updated until convergence, and then the optimal waveform $\mathbf{x}$ can be obtained by updating $u_p,\forall\ p$ iteratively by

$$u_p^{m+1}=\frac{\sqrt{\mathbf{w}^H\left(\mathbf{\Sigma}\left(\mathbf{x}^m\right)+\mathbf{I}_{N_R}\right)\mathbf{w}}}{\mu\left|\mathbf{w}^H\mathbf{U}\left(\theta_p\right)\mathbf{x}^m\right|^2}. \tag{4.47}$$

Let us denote the number of iterations required for generating the optimal η_p by N_n. Accordingly, the total complexity of can be given as $\mathcal{O}\left(4N_nN_T^6\Psi_0\right)$ by reserving the highest order term [314]. For simplicity, the proposed method of solving problem (4.41) is summarized in Algorithm 4.4.

4.6 Hardware efficient Design

4.6.1 Security Design with 1-bit DACs

We proceed to the optimization-based non-linear mapping scheme with 1-bit DACs [317] by taking the full region of destructive interference into consideration. The

resulting optimization problem can be formulated as

$$\max_{\mathbf{x}} \ \frac{\mu\left|\mathbf{w}^H\mathbf{U}(\theta_0)\mathbf{x}\right|^2}{\mathbf{w}^H(\mathbf{\Sigma}(\mathbf{x})+\mathbf{I}_{N_R})\mathbf{w}} \tag{4.48a}$$

$$\text{s.t. } |x_n| \in \left\{\pm\sqrt{\frac{P_0}{2N_T}} \pm \sqrt{\frac{P_0}{2N_T}}j\right\}, n = 1, \cdots, N_T \tag{4.48b}$$

$$\left|\text{Im}\left(\tilde{\mathbf{h}}_k^H\mathbf{x}\right)\right| \le \left(\text{Re}\left(\tilde{\mathbf{h}}_k^H\mathbf{x}\right) - \sqrt{\sigma_{C_k}^2\Gamma_k}\right)\tan\phi, \forall k \tag{4.48c}$$

$$\text{(4.35a) or (4.35b) or (4.35c).} \tag{4.48d}$$

Note that the non-convexity lies in (4.48a) and (4.48b). The objective function was recast linearly and readily solvable in Section 4.3.3, which refers to problem (4.21). With respect to the non-convex constraint lies in (4.48b), we then relax the strict modulus constraints on $x_n, \forall n$ and recast the problem above as [144]

$$\max_{\hat{\mathbf{x}}} \ \mu g(\hat{\mathbf{x}}) - u\mathbf{w}^H(\mathbf{\Sigma}(\hat{\mathbf{x}})+\mathbf{I}_{N_R})\mathbf{w} \tag{4.49a}$$

$$\text{s.t. } |\text{Re}(\hat{x}_n)| \le \sqrt{\frac{P_0}{2N_T}}, |\text{Im}(\hat{x}_n)| \le \sqrt{\frac{P_0}{2N_T}}, \forall n \tag{4.49b}$$

$$\text{(4.48c) and (4.48d).} \tag{4.49c}$$

We note that the problem above is convex and can be solved by CVX toolbox [298]. However, the elements in the resultant waveform $\hat{\mathbf{x}}$ cannot guarantee strict equality for the real and imaginary parts of $\hat{x}_n$. Thus, we normalize the optimal 1-bit DAC waveform following

$$x_n = \text{sgn}[\text{Re}(\hat{x}_n)]\sqrt{\frac{P_0}{2N_T}} + \text{sgn}[\text{Im}(\hat{x}_n)]\sqrt{\frac{P_0}{2N_T}}j, \forall\ n, \tag{4.50}$$

where $\text{sgn}[\cdot]$ denotes the sign function.

Till now, problem (4.48) is converted into a convex optimization problem which includes three subproblems. By solving the problems above, we can obtain optimal waveforms $\mathbf{x}_1^*, \mathbf{x}_2^*, \mathbf{x}_3^*$ corresponding to the aforementioned constraints (4.35a), (4.35b) and (4.35c), respectively. Then, we substitute each of them in the objective function, the one resulting in maximum SINR_{rad} will be the final solution to problem (4.48).

Algorithm 4.4 The Proposed Algorithm for solving the mixed-integer optimization problem (4.41)

Input: $P_0, \mathbf{h}_k, \sigma_{C_k}^2, \sigma_R^2, \theta_i, b_i, \theta_0, \alpha_0, \Delta\theta, \Gamma_k, \forall\, k, \forall\, i, \varepsilon > 0, \varepsilon_0 > 0$, and the maximum iteration number m_{max}

Output: $\mathbf{x}$

1. Reformulate the problem by (4.43).
2. Transform the problem to epigraph form following (4.31).
3. Initialize $\eta_p^0 \in [0,1]$, $\mathbf{x}^0 \in \mathcal{D}$ randomly, $n = 1$, $m = 1$.

Repeat:

4. When $\mathbf{x}$ is fixed, solve problem (4.47) iteratively by updating η_p^n until $\left| \sum_{p=1}^{2\Delta\theta+1} \eta_p^{n-1} \left(\eta_p - \eta_p^{n-1} \right) \right| < \varepsilon_0$.
5. Fix the optimal η_p^*, solve problem (4.47) to obtain the optimal waveform $\mathbf{x}^m$.
6. Obtain the receive beamformer $\mathbf{w}^m$ by substituting $\mathbf{x}^m$ in (4.13).
7. Update $\mathbf{u}$ by (4.46).
8. $m = m + 1$.

Until:

$m \geq m_{max}$ or $\|\mathbf{u}^m - \mathbf{u}^{m-1}\| < \varepsilon$

4.6.2 1-bit Quantization Constant Modulus Design

Since the extreme case of 1-bit DACs represents a special case of coarsely quantized CE signals [318,319], we explore the 1-bit quantized CE precoding in this subsection. Herewith, the optimization problem is formulated as

$$\max_{\mathbf{x}} \ \frac{\mu \left| \mathbf{w}^H \mathbf{U}(\theta_0) \mathbf{x} \right|^2}{\mathbf{w}^H (\mathbf{\Sigma}(\mathbf{x}) + \mathbf{I}_{N_R}) \mathbf{w}} \tag{4.51a}$$

$$\text{s.t. } |x_n| = \sqrt{\frac{P_0}{N_T}}, n = 1, \cdots, N_T \tag{4.51b}$$

$$\text{(4.48c) and (4.48d).} \tag{4.51c}$$

In this case, we relax CE constraints and recast the problem as

$$\max_{\tilde{\mathbf{x}}} \ \mu g(\tilde{\mathbf{x}}) - u \mathbf{w}^H (\mathbf{\Sigma}(\tilde{\mathbf{x}}) + \mathbf{I}_{N_R}) \mathbf{w} \tag{4.52a}$$

$$\text{s.t. } |\tilde{x}_n| \leq \sqrt{\frac{P_0}{N_T}}, n = 1, \cdots, N_T \tag{4.52b}$$

$$\text{(4.48c) and (4.48d).} \tag{4.52c}$$

We note that the relaxed form above is a second-order cone program (SOCP) and can be effectively solved. In order to achieve a full CE waveform design for all the antennas at the BS we need to force the equality constrained before transmission. More specifically, we normalize the optimal waveform $\tilde{\mathbf{x}}$ following

$$\bar{x}_n = \begin{cases} \tilde{x}_n \Big/ \left(\sqrt{\dfrac{P_0}{N_T}} |\tilde{x}_n| \right) & \text{if } |\tilde{x}_n| \neq \sqrt{P_0/N_T}, \forall\, n \\ \tilde{x}_n & \text{if } |\tilde{x}_n| = \sqrt{P_0/N_T}, \forall\, n \end{cases} \tag{4.53}$$

We consider that phase shifters (PSs) are controlled digitally in practical applications and the weight of each PS is assumed to be a finite number of values depending on the quantization bits. Thus, when we deploy 1-bit resolution PSs, we discrete the phase of $\bar{x}_n, \forall\, n$ by (4.50).

4.7 Numerical Results

In this section, we evaluate the proposed methods via Monte Carlo-based simulation results given as follows. We assume that both the DFRC BS and the radar receiver are equipped with uniform linear arrays (ULAs) with the same number of elements with half-wavelength spacing between adjacent antennas. In the following simulations, the power budget is set as $P_0 = 30$ dBm, and the Rician coefficient is given as $v_k = 1$. The target is located at $\theta_0 = 0^\circ$ with a reflecting power of $|\alpha_0|^2 = 10$ dB and clutter sources are located at $\theta_1 = -50^\circ, \theta_2 = -20^\circ, \theta_3 = 20^\circ, \theta_4 = 50^\circ$ reflecting a power of $|\alpha_1|^2 = |\alpha_2|^2 = |\alpha_3|^2 = |\alpha_4|^2 = 20$ dB. The SNR threshold Γ_T is set as -1dB as the default unless it is presented specifically.

4.7.1 The Resultant Beampattern

The resultant beampattern is firstly given in Fig. 4.4 with different number of DFRC BS antennas, where we set the DFRC precoder design proposed by Chen et al. [5] as the benchmark, namely 'DFRC-PD', and the proposed methods in this paper are denoted as 'DFRC-CI' and 'DFRC-CI-DI' in our results, respectively. The SNR threshold $\Gamma_k, \forall\, k$ is fixed as 15dB. The nulls at the locations of clutter sources are clearly illustrated. It can be observed that the performance of beampattern gets

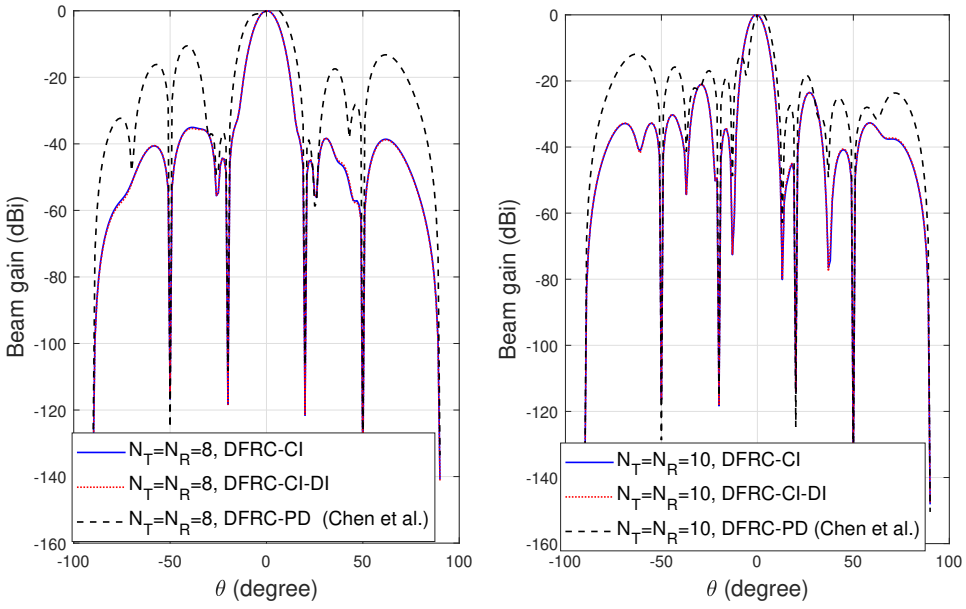

(a) (b)

Figure 4.4: Optimized beampatterns with different numbers of DFRC BS antennas, where the beamformer design approach proposed in [5] is set as benchmarks and $K = 5$.

better from the viewpoint of the radar, and the main beam width decreases with the increasing number of BS antennas. Additionally, compared with the beamformer design method proposed in [5], the peak to sidelobe ratio (PSLR) of the resultant beampattern generated from our proposed waveform design method is higher, and it can be found that the null in the main beam is mitigated in our design. It can also be noted that the beampattern generated by the CI-DI method overlaps with the one obtained by employing CI constraints only.

Furthermore, when the radar target location is not known to the BS perfectly, the generated beampattern is shown in Fig. 4.5 with the different angular intervals of possible target locations. It is noteworthy that the power gain of the main beam reduces and the PSLR decreases with the expansion of the target location uncertainty interval.

4.7.2 Radar SINR Performance

In this subsection, we evaluate the performance of radar receive SINR versus SNR threshold of the communication system, number of CUs, and target location uncer-

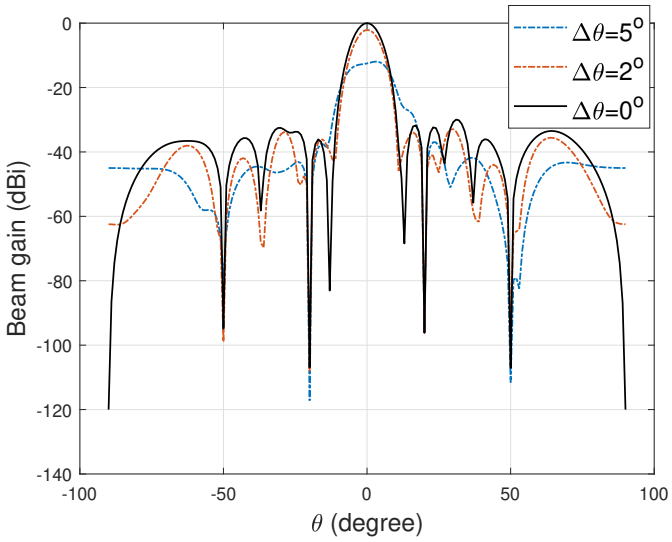

Figure 4.5: The resultant beampattern with different angular interval.$N_T = N_R = 10, K = 5$.

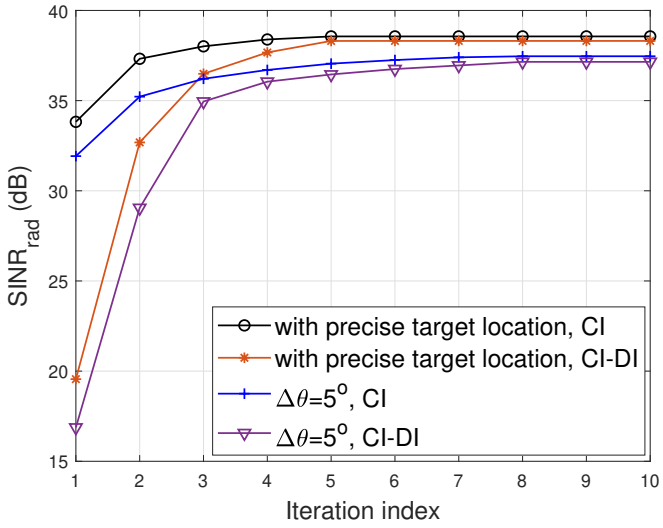

Figure 4.6: Convergence analysis.

tainty. Firstly, Fig. 4.6 illustrates the convergence analysis of the proposed methods. It can be found that the algorithm converges fast when the target location is precisely known to the BS. The optimal solution is generated with 5 iterations with the knowledge of the precise target location, while it converges with around 9 iterations when the target location is uncertain.

The average performance of the tradeoff between the given SNR threshold of CU and the SINR of radar is illustrated in Fig. 4.7, including benchmark algorithms. Specifically, with respect to the benchmarks, SQ denotes the method

proposed in [308], and SDR without Gaussian Rand denotes the upper bound of the objective function as we have given in Section 4.3. To satisfy the rank-1 constraint, a Gaussian randomization procedure is commonly required, the simulation result of which is given in Fig. 4.7 denoted as 'SDR after Gaussian Rand'. It is found that the received SINR of radar increases with the growth of Γ_k when we adopt SQ method and the SDR technique after the Gaussian randomization procedure, while SINR_{rad} decreases when we deploy the other methods. This is for the reason that the optimized system power increases with the growth of Γ_k, which is less than the given power budget P_0, under the circumstance when the SQ method or SDR solver with Gaussian randomization procedure is deployed. That is, the SQ approach and SDR after Gaussian randomization fail to formulate an appropriate tradeoff between the radar system and the communication system. Moreover, the proposed waveform design method reaches a higher SINR_{rad} compared with the beamformer design in [5], especially when Γ_k is above 22dB. Furthermore, the radar receives SINR is deteriorated when the destructive interference constraints are taken into account. Moreover, when deploying the hardware-efficient constraints, we note that the hardware-efficient designs, i.e., both the discrete phase CE and 1-bit DACs approaches, deteriorate the performance of radar SINR. Specifically, the 1-bit quantized CE outperforms the 1-bit DAC technique, which is for the reason that the feasible region of problem (5.51) is larger than that of problem (5.48). It also demonstrates that the hardware efficiency design is achieved at the expense of the target sensing performance.

Fig. 4.8 depicts the radar SINR versus the number of CUs with the different numbers of BS antennas, which reveals the tradeoff between radar and communication system. It can be also noted that the received SINR of the radar system gets lower when DI constraints are taken into account.

In Fig. 4.9, we explore the effect of correlation between the target and CU LoS channels in the radar eavesdropping performance with various angular uncertainty intervals $\Delta\theta$ when the angle difference between the CU and the target (i.e. '$\Delta\phi$' in Fig. 4.9) varies from 0.5° to 25°. It indicates the tradeoff between SINR_{rad} and target

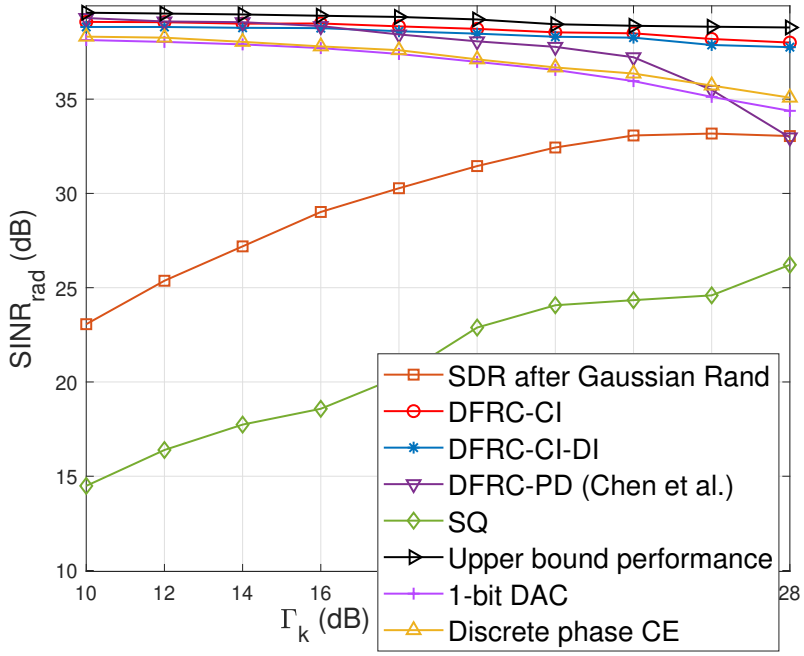

Figure 4.7: The performance of radar SINR versus CU's SNR with different solving methods, $N_T = N_R = 10, K = 5$.

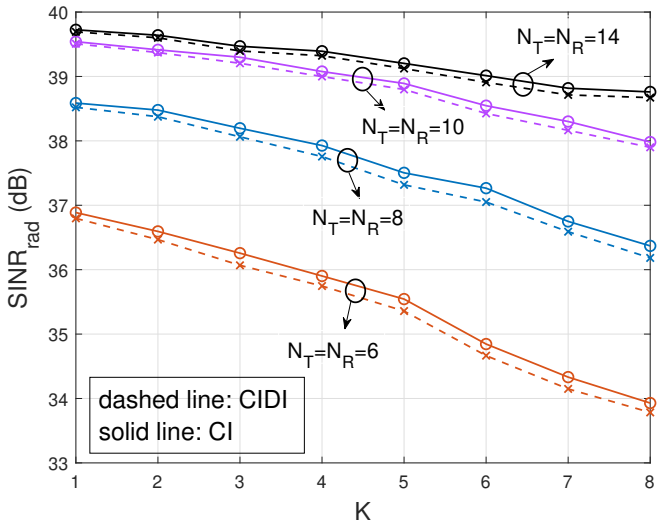

Figure 4.8: The received SINR of radar versus the number of CUs with the different number of DFRC BS antennas.

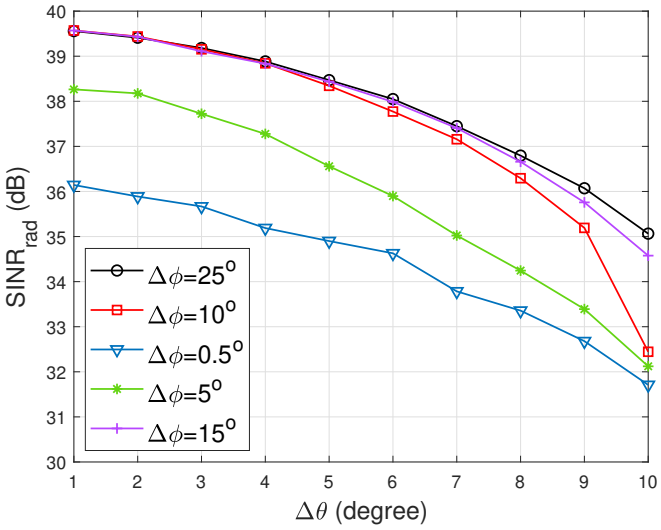

Figure 4.9: Average SINR of radar versus angular interval of target location uncertainty for different angular differences $\Delta\phi$ between the target and communication users, $N_T = N_R = 10, K = 5$.

uncertainty. In addition, it can be found that the radar SINR is slightly impacted by the CU location when the angle difference is larger than 15°.

4.7.3 Communications Security Performance

The distribution of received symbols at CUs (denoted by blue markers) and the target (denoted by blue markers) is shown in Fig. 4.10, where QPSK and 8PSK modulated symbols are taken as examples. It illustrates that the received symbols are randomized at the target when only CI is considered, while the signals received by the target are conveyed into the destructive region when deploying DI constraints. In Fig. 4.11, the average SER of CUs versus threshold SNR Γ_k is depicted when the BS is equipped with a different number of antennas, with and without DI constraints, respectively. It is found that the SER decreases with the growth of Γ_k. Furthermore, when the received symbols at the target are constructed in the destructive region, CUs decode the received symbols with a lower probability, which means the SER performance of the CUs is deteriorated to some extent when DI constraints are taken into account.

Furthermore, in Fig. 4.12, we take one CU as a reference to evaluate the SER performance of the radar target versus the angle difference between the target and the CU. It is noted that the target decode probability converges to 0.75 with the

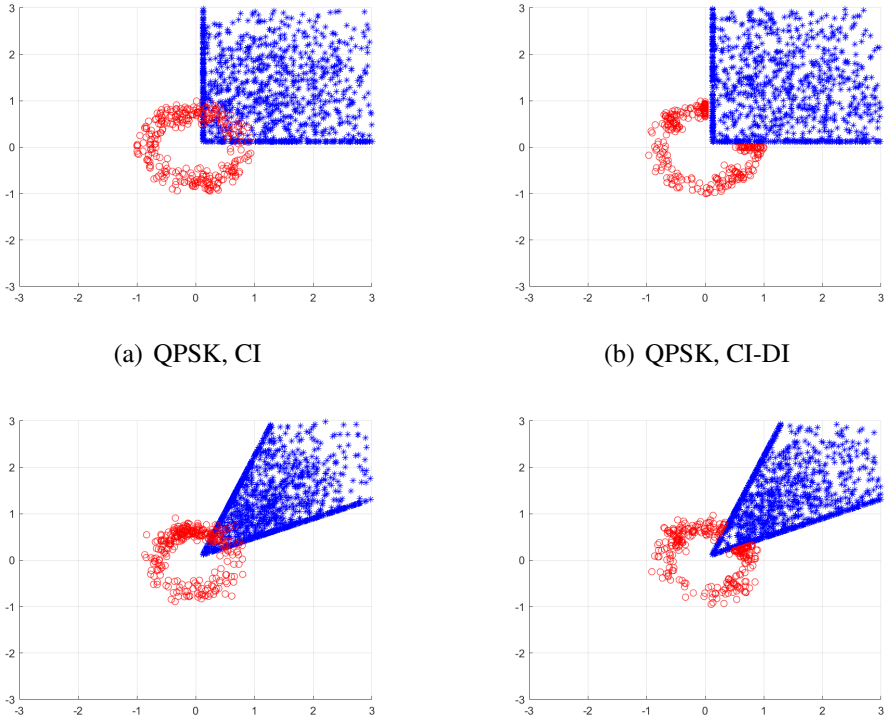

(a) QPSK, CI (b) QPSK, CI-DI

(c) 8PSK, CI (d) 8PSK, CI-DI

Figure 4.10: The constellation of received signals with DI constraints when the target location is known to the BS precisely, where the received signal at CUs and the target are denoted by blue dots and red dots, respectively. QPSK and 8PSK modulated signal, $N_T = N_R = 10, K = 5$.

increasing angular difference from the CU to the target when only the CI constraint is considered. For generality, the simulation result is obtained on average of target location ranging in the angular interval $\left[-\frac{\pi}{2}, \frac{\pi}{2}\right]$. Moreover, it can be found that the SER at the target increases obviously when the DI constraints are considered, which is close to 1 when the angle difference is getting larger. Thus, it indicates that the deployment of the DI method prevents the radar target from eavesdropping communication data efficiently when the CU and the target channels are correlated.

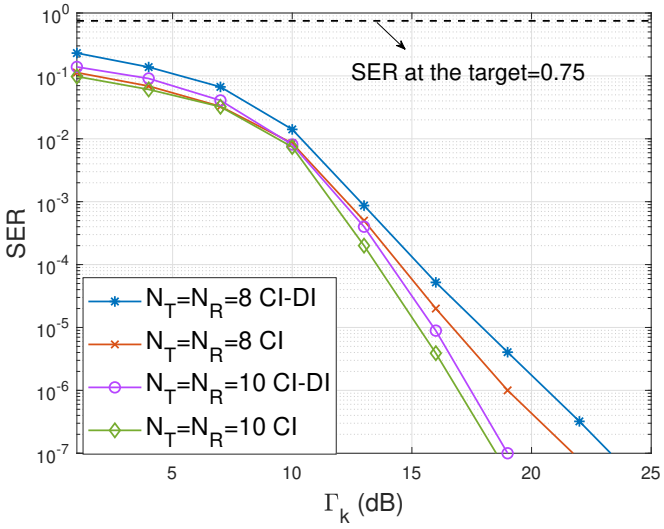

Figure 4.11: SER of CU versus SNR threshold Γ_k with the different number of antennas equipped by BS when target location is known precisely. $K = 5$.

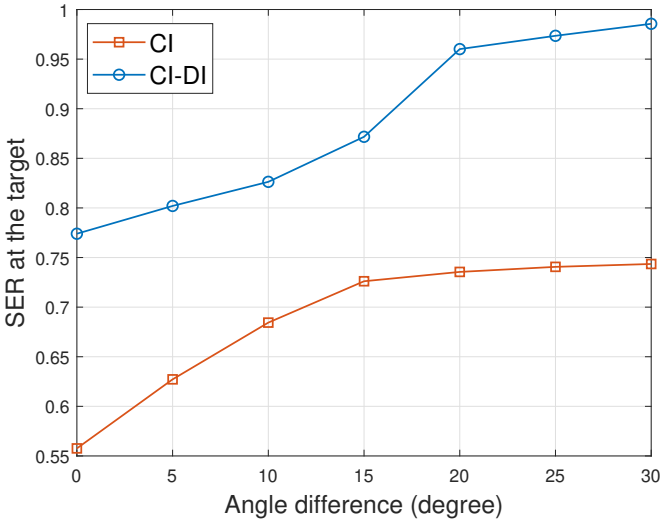

Figure 4.12: SER at the target versus the angle difference between the target and the CU with and without DI constraint when the target location is known precisely. $K = 5, N_T = N_R = 10$.

4.8 Conclusions

In this chapter, we have considered the sensing-aided secure ISAC systems, where the dual-functional BS emitted waveforms to estimate the amplitudes and the directions of potential eavesdroppers and send confidential communication data to CUs simultaneously. The proposed design has promoted the cooperation between sensing and communication rather than conventionally individual functionalities. The weighted optimization problem has been designed to optimize the normalized CRB and secrecy rate while constraining the system power budget. Our numerical results have demonstrated that the secrecy rate was enhanced with the decreasing CRB in both single and multi-Eve scenarios.

Chapter 5

Sensing-assisted PLS in ISAC Systems

5.1 Introduction

We note that in the above works on secure ISAC transmission, the radar and communication systems work individually over separate end goals rather than cooperating with each other. To further promote the integration of S&C functionalities to improve the security of the ISAC systems, we propose a novel approach to ensure the PLS for communication data transmission, which is assisted by the sensing functionality. To be specific, we still consider a dual-functional access point (AP) that emits waveforms, aiming at estimating targets' parameters and communicating with users simultaneously. As the waveform carries confidential information intended for CUs, while the beampattern is designed to point to the angles of targets, this system faces the risk of information leakage if targets act as eavesdroppers. Differing from the scenario in the previous Chapters, we here obtain the channel information of Eves with the assistance of the sensing functionality. Besides, apart from the single-target scenario, we further implement the proposed method in the multi-target scenario.

The proposed algorithm includes two stages. At the first stage, the dual-functional AP emits an omnidirectional waveform for Eve detection, which then receives echoes reflected from both CUs and Eves located within the sensing range. Suppose that all CUs are cooperative users. That is, the location information of each is acknowledged to the AP. Thus, it is possible to obtain angle estimates of Eves contained in the reflected echo by removing known CUs' angles. The estimation

performance is measured by the CRB [320].

In the next stage, we formulate a weighted optimization problem to minimize the CRB of targets/Eves and maximize the secrecy rate, subject to beampattern constraints as well as a transmit power budget. A key novelty in this setup is that the channel information in the secrecy rates is a function of the sensing performance. Specifically, to avoid any false dismissal detection, the main lobe of the beampattern is designed to be wide, with a width depending on the estimation accuracy. Afterwards, by improving estimation accuracy, the sensing and security functionalities provide mutual benefits, resulting in improvement of the mutual performances with every iteration of the optimization, until convergence.

Within this scope, the contributions of our work are summarized as follows:

- We present a sensing-assisted PLS algorithm of the ISAC system, where the CRB and secrecy rate are employed to measure the sensing and secrecy performance, respectively. Specifically, the secrecy rate is updated with the increasing accuracy of the Eve angle estimation iteratively.

- We analyze the lower bound of CRB and the upper bound of the secrecy rate with the constraint of power budget in our proposed ISAC system.

- We iteratively maximize the determinant of the Fisher Information Matrix (FIM) and the secrecy rate of the ISAC system by jointly designing the beamforming matrix and the AN.

- We further consider the Eve location uncertainty, where the main beam of the sensing beampattern is designed to be sufficiently wide to illuminate the possible angular region that an Eve may appear with high probability, which is indicated by the CRB value obtained from the previous iteration. This implies that secrecy needs to be provided throughout the angle range.

- We design a fractional programming (FP) algorithm to solve the proposed weighted optimization problem and verify the efficiency of the solver for both single-Eve and multi-Eve detection.

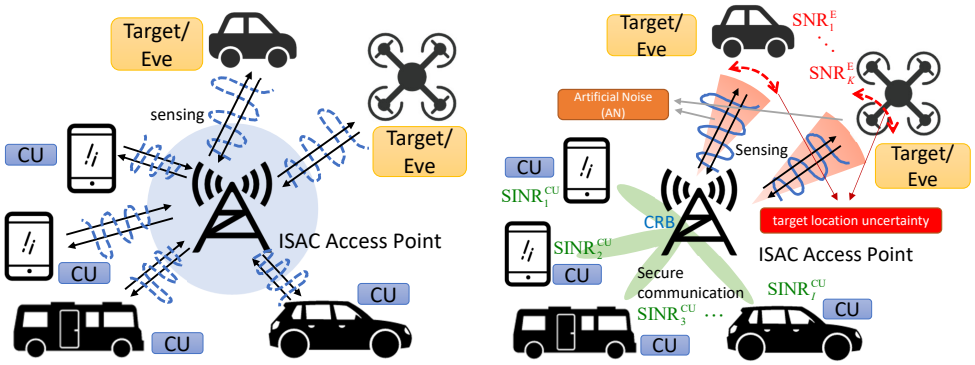

(a) Stage 1–The ISAC AP emits omnibeampat-tern for Eve estimations

(b) Stage 2–Sensing-aided secure ISAC system

Figure 5.1: Architecture of the proposed secure ISAC system assisted by the sensing functionality.

5.2 System Model

We consider a mmWave ISAC system equipped with co-located antennas and let N_t and N_r denote the number of transmit antennas and receive antennas, where the base station communicates with K communication users (CUs) and detects M targets/Eves simultaneously as depicted in Fig. 5.1. We assume the BS has knowledge of the CUs and their channels, and has no knowledge of the Eves.

5.2.1 Communication Signal Model and Metrics

Let the rows of $\mathbf{X} \in \mathbb{C}^{N_t \times L}$ denote the transmit waveforms, where L is the number of time-domain snapshots. By transmitting the dual-functional waveforms to K CUs, the received signal matrix at the receivers can be expressed as

$$\mathbf{Y}_C = \mathbf{H}\mathbf{X} + \mathbf{Z}_C, \tag{5.1}$$

where $\mathbf{Z}_C \in \mathbb{C}^{K \times L}$ is the additive white Gaussian noise (AWGN) matrix and with the variance of each entry being σ_C^2. $\mathbf{H} = [\mathbf{h}_1, \mathbf{h}_2, \ldots, \mathbf{h}_K]^H \in \mathbb{C}^{K \times N_t}$ represents the communication channel matrix, which is assumed to be known to the BS, with each entry being independently distributed. Following the typical mmWave channel model in [304, 321], we assume that $\mathbf{h}_k$ is a slow-fading block Rician fading channel. The

channel vector of the k-th user can be expressed as

$$\mathbf{h}_k = \sqrt{\frac{v_k}{1+v_k}}\mathbf{h}_{L,k}^{\text{LoS}} + \sqrt{\frac{1}{1+v_k}}\mathbf{h}_{S,k}^{\text{NLoS}}, \tag{5.2}$$

where $v_k > 0$ is the Rician K-factor of the k-th user, $\mathbf{h}_{L,k}^{\text{LoS}} = \sqrt{N_t}\mathbf{a}_t(\omega_{k,0})$ is the LoS deterministic component. $\mathbf{a}(\omega_{k,0})$ denotes the array steering vector, where $\omega_{k,0} \in \left[-\frac{\pi}{2}, \frac{\pi}{2}\right]$ is the angle of departure (AOD) of the LoS component from the BS to the user k [304, 305]. The scattering component $\mathbf{h}_{S,k}^{\text{NLoS}}$ can be expressed as $\mathbf{h}_{S,k}^{\text{NLoS}} = \sqrt{\frac{N_t}{L_p}}\sum_{l=1}^{L_p} c_{k,l}\mathbf{a}_t(\omega_{k,l})$, where L_p denotes the number of propagation paths, $c_{k,l} \sim \mathcal{CN}(0,1)$ is the complex path gain and $\omega_{k,l} \in \left[-\frac{\pi}{2}, \frac{\pi}{2}\right]$ is the AOD associated to the (k,l)-th propagation path.

The waveform $\mathbf{X}$ in (5.1) can be expressed as

$$\mathbf{X} = \mathbf{WS} + \mathbf{N}, \tag{5.3}$$

where $\mathbf{W} \in \mathbb{C}^{N_t \times K}$ is the dual-functional beamforming matrix to be designed, each row of $\mathbf{S} \in \mathbb{C}^{K \times L}$ denotes the k-th unit-power data stream intended to CUs, and $\mathbf{N} \in \mathbb{C}^{N_t \times L}$ is the AN matrix generated by the transmitter to interfere potential eavesdroppers. We assume that $\mathbf{N} \sim \mathcal{CN}(\mathbf{0}, \mathbf{R}_N)$, where $\mathbf{R}_N \succeq \mathbf{0}$ denotes the covariance matrix of the AN that is to be designed. We further assume that the data streams are approximately orthogonal to each other, yielding

$$\frac{1}{L}\mathbf{S}_C\mathbf{S}_C^H \approx \mathbf{I}_{K\times K}. \tag{5.4}$$

Note that (5.4) is asymptotically achievable when L is sufficiently large. Then, we denote the beamforming matrix as $\mathbf{W} = [\mathbf{w}_1, \ldots, \mathbf{w}_K]$, where each column $\mathbf{w}_k$ is the

beamformer for the k-th CU. Accordingly, the SINR of the k-th user is given as

$$\begin{aligned}\mathrm{SINR}_k^{\mathrm{CU}} &= \frac{\left|\mathbf{h}_k^H \mathbf{w}_k\right|^2}{\sum\limits_{i=1,i\neq k}^{K}\left|\mathbf{h}_k^H \mathbf{w}_i\right|^2+\left|\mathbf{h}_k^H \mathbf{R}_N \mathbf{h}_k\right|+\sigma_C^2} \\ &= \frac{\mathrm{tr}\left(\tilde{\mathbf{H}}_k \tilde{\mathbf{W}}_k\right)}{\sum\limits_{i=1,i\neq k}^{K}\mathrm{tr}\left(\tilde{\mathbf{H}}_k \tilde{\mathbf{W}}_i\right)+\mathbf{tr}\left(\tilde{\mathbf{H}}_k \mathbf{R}_N\right)+\sigma_C^2},\end{aligned} \tag{5.5}$$

where we denote $\tilde{\mathbf{H}}_k = \mathbf{h}_k \mathbf{h}_k^H$ and $\tilde{\mathbf{W}}_k = \mathbf{w}_k \mathbf{w}_k^H$.

5.2.2 Radar Signal Model

By emitting the waveform $\mathbf{X}$ to sense Eves, the reflected echo signal matrix at the BS receive array is given as

$$\mathbf{Y}_R = \sum_{m=1}^{M} \mathbf{a}^*(\theta_m)\beta_m \mathbf{b}^T(\theta_m)\mathbf{X} + \mathbf{Z}_R, \tag{5.6}$$

where $\mathbf{a}(\theta) \in \mathbb{C}^{N_r \times 1}$ and $\mathbf{b}(\theta) \in \mathbb{C}^{N_t \times 1}$ represent the steering vectors for the receive and transmit arrays, which are assumed to be a uniform linear array (ULA) with half-wavelength antenna spacing. β_m is the complex amplitude of the m-th Eve. We assume the number of antennas is even and define the receive steering vector as

$$\mathbf{a}(\theta) = \left[e^{-j\frac{N_r-1}{2}\pi\sin\theta}, e^{-j\frac{N_r-3}{2}\pi\sin\theta}, \cdots, e^{j\frac{N_r-1}{2}\pi\sin\theta}\right]^T. \tag{5.7}$$

It is noted that we choose the center of the ULA antennas as the reference point. To this end, it is easy to verify that

$$\mathbf{a}^H(\theta)\dot{\mathbf{a}}(\theta) = 0. \tag{5.8}$$

Finally, $\mathbf{Z}_R$ denotes the interference and the AWGN term. We assume that the columns of $\mathbf{Z}_R$ are independent and identically distributed circularly symmetric complex Gaussian random vectors with mean zero and a covariance matrix $\mathbf{Q} = \sigma_R^2 \mathbf{I}$.

Similar to the expression in (5.5), the eavesdropping SNR received at the m-th

Eve is written as

$$\mathrm{SNR}_m^{\mathrm{E}} = \frac{|\alpha_m|^2 \mathbf{a}^H(\theta_m) \sum_{k=1}^{K} \tilde{\mathbf{W}}_k \mathbf{a}(\theta_m)}{|\alpha_m|^2 \mathbf{a}^H(\theta_m) \mathbf{R}_N \mathbf{a}(\theta_m) + \sigma_0^2}, \tag{5.9}$$

where σ_0^2 denotes the covariance of AWGN received by each Eve.

For simplicity, the reflected echo signal given in (5.6) can be recast as

$$\mathbf{Y} = \mathbf{A}^*(\boldsymbol{\theta}) \boldsymbol{\Lambda} \mathbf{B}^T(\boldsymbol{\theta}) \mathbf{X} + \mathbf{Z}_R, \tag{5.10}$$

where we denote $\mathbf{A}(\boldsymbol{\theta}) = [\mathbf{a}(\theta_1), \ldots, \mathbf{a}(\theta_M)]$, $\mathbf{B}(\boldsymbol{\theta}) = [\mathbf{b}(\theta_1), \ldots, \mathbf{b}(\theta_M)]$, and $\boldsymbol{\Lambda} = \mathrm{diag}(\beta_m)$.

5.2.3 CRB and Secrecy Rate

In this subsection, we elaborate on the radar detection and communication security metrics. Particularly, the target/Eve estimation is measured by the CRB, which is a lower bound on the variance of unbiased estimators [322], and the security performance is evaluated by the secrecy rate.

In the multi-Eve detection scenario, the CRB with respect to the unknown Eve parameters $\theta_1, \ldots, \theta_M$ and $\beta_1, \ldots, \beta_M$ was derived in [323] in detail, and the Fisher information matrix (FIM) for $\theta_m, \forall\, m$ as well as real and imaginary parts of $\beta_m, \forall\, m$ is given as

$$\mathbf{J} = 2L \begin{bmatrix} \mathrm{Re}(\mathbf{J}_{11}) & \mathrm{Re}(\mathbf{J}_{12}) & -\mathrm{Im}(\mathbf{J}_{12}) \\ \mathrm{Re}^T(\mathbf{J}_{12}) & \mathrm{Re}(\mathbf{J}_{22}) & -\mathrm{Im}(\mathbf{J}_{22}) \\ -\mathrm{Im}^T(\mathbf{J}_{12}) & -\mathrm{Im}^T(\mathbf{J}_{22}) & \mathrm{Re}(\mathbf{J}_{22}) \end{bmatrix}, \tag{5.11}$$

where the elements of the matrix in (5.11) are given as

$$\begin{aligned} \mathbf{J}_{11} = &\left(\dot{\mathbf{A}}^H \mathbf{Q}^{-1} \dot{\mathbf{A}}\right) \odot \left(\boldsymbol{\Lambda}^* \mathbf{B}^H \mathbf{R}_X^* \mathbf{B} \boldsymbol{\Lambda}\right) + \left(\dot{\mathbf{A}}^H \mathbf{Q}^{-1} \mathbf{A}\right) \odot \left(\boldsymbol{\Lambda}^* \mathbf{B}^H \mathbf{R}_X^* \dot{\mathbf{B}} \boldsymbol{\Lambda}\right) + \\ &\left(\mathbf{A}^H \mathbf{Q}^{-1} \dot{\mathbf{A}}\right) \odot \left(\boldsymbol{\Lambda}^* \dot{\mathbf{B}}^H \mathbf{R}_X^* \mathbf{B} \boldsymbol{\Lambda}\right) + \left(\mathbf{A}^H \mathbf{Q}^{-1} \mathbf{A}\right) \odot \left(\boldsymbol{\Lambda}^* \dot{\mathbf{B}}^H \mathbf{R}_X^* \dot{\mathbf{B}} \boldsymbol{\Lambda}\right) \end{aligned} \tag{5.12a}$$

$$\mathbf{J}_{12} = \left(\dot{\mathbf{A}}^H \mathbf{Q}^{-1} \mathbf{A}\right) \odot \left(\boldsymbol{\Lambda}^* \mathbf{B}^H \mathbf{R}_X^* \mathbf{B}\right) + \left(\mathbf{A}^H \mathbf{Q}^{-1} \mathbf{A}\right) \odot \left(\boldsymbol{\Lambda}^* \dot{\mathbf{B}}^H \mathbf{R}_X^* \mathbf{B}\right) \tag{5.12b}$$

$$\mathbf{J}_{22} = \left(\mathbf{A}^H \mathbf{Q}^{-1} \mathbf{A}\right) \odot \left(\mathbf{B}^H \mathbf{R}_X^* \mathbf{B}\right), \tag{5.12c}$$

with $\odot$ denoting the Hadamard (element-wise) matrix product, and $\dot{\mathbf{A}} = \left[, \frac{\partial \mathbf{a}(\theta_1)}{\partial \theta_1} \quad \frac{\partial \mathbf{a}(\theta_2)}{\partial \theta_2} \quad \cdots \quad \frac{\partial \mathbf{a}(\theta_M)}{\partial \theta_M} \right], \dot{\mathbf{B}} = \left[\frac{\partial \mathbf{b}(\theta_1)}{\partial \theta_1} \quad \frac{\partial \mathbf{b}(\theta_2)}{\partial \theta_2} \quad \cdots \quad \frac{\partial \mathbf{b}(\theta_M)}{\partial \theta_M} \right].$

Also, the covariance matrix $\mathbf{R}_X$ is given as

$$\begin{aligned} \mathbf{R}_X &= \frac{1}{L}\mathbf{X}\mathbf{X}^H = \mathbf{W}\mathbf{W}^H + \mathbf{R}_N \\ &= \sum_{k=1}^{K} \tilde{\mathbf{W}}_k + \mathbf{R}_N. \end{aligned} \tag{5.13}$$

As per the above, the corresponding CRB matrix is expressed as

$$\mathrm{CRB}\left(\boldsymbol{\theta}, \boldsymbol{\beta}\right) = \mathbf{J}^{-1} \tag{5.14}$$

and

$$\begin{aligned} \mathrm{CRB}\left(\boldsymbol{\theta}\right) &= \left[\mathbf{J}^{-1}\right]_{11} \\ \mathrm{CRB}\left(\boldsymbol{\beta}\right) &= \left[\mathbf{J}^{-1}\right]_{22} + \left[\mathbf{J}^{-1}\right]_{33}. \end{aligned} \tag{5.15}$$

Moreover, the achievable secrecy rate at the legitimate user is defined as the difference between the achievable rates at the legitimate receivers and the eavesdroppers. Thus, we give the expression of the worst-case secrecy rate as [324, 325]

$$\mathrm{SR}\left(\tilde{\mathbf{W}}_k, \mathbf{R}_N\right) = \min_{k,m} \left[R_k^{\mathrm{CU}} - R_m^{\mathrm{E}}\right]^+, \tag{5.16}$$

where $R_k^{\mathrm{CU}}, \forall\, k$ and $R_m^{\mathrm{E}}, \forall\, m$ represent the achievable transmission rate of the k-th CU and the m-th Eve, which can be expressed as (17a) and (17b), respectively.

$$R_k^{\mathrm{CU}}\left(\tilde{\mathbf{W}}_k, \mathbf{R}_N\right) = \log\left(1 + \mathrm{SINR}_k^{\mathrm{CU}}\right) \tag{5.17a}$$

$$R_m^{\mathrm{E}}\left(\tilde{\mathbf{W}}_k, \mathbf{R}_N\right) = \log\left(1 + \mathrm{SNR}_m^{\mathrm{E}}\right). \tag{5.17b}$$

5.3 Benchmark Schemes: Isotropic AN

In the scenario considered with no knowledge of the Eves, a typical method to avoid the information inception is to transmit AN. To be specific, partial transmit power is allocated to emit the AN to interfere with the Eves, where the AN is

isotropically distributed on the orthogonal complement subspace of CUs' channels [326]. To elaborate on this, we firstly take the l-th snapshot as a reference, i.e., (5.1) is simplified as

$$\mathbf{y}_C[l] = \mathbf{H}\mathbf{x}[l] + \mathbf{z}_C[l]. \tag{5.18}$$

where $\mathbf{x}[l] = \mathbf{W}\mathbf{s}[l] + \mathbf{n}[l]$. For simplicity, the snapshot index l will be omitted in the following descriptions. We further rewrite the AN vector $\mathbf{n}$ as

$$\mathbf{n} = \mathbf{V}\bar{\mathbf{n}}, \tag{5.19}$$

where $\mathbf{V} = \mathbf{P}_{\mathbf{H}}^{\perp} = \mathbf{I}_{N_t} - \mathbf{H}^H\left[\mathbf{H}\mathbf{H}^H\right]^{-1}\mathbf{H}$ denotes the orthogonal complement projector of the $\mathbf{H}$, and $\bar{\mathbf{n}}$ is the zero-mean colored noise vector with a covariance matrix $\mathbf{R}_{\bar{n}} = \mathbb{E}\left\{\bar{\mathbf{n}}\bar{\mathbf{n}}^H\right\}$ [119, 327]. Accordingly, the covariance matrix is given as

$$\bar{\mathbf{R}}_x = \sum_{k=1}^{K}\tilde{\mathbf{W}}_k + \mathbf{V}\mathbf{R}_{\bar{n}}\mathbf{V}^H. \tag{5.20}$$

Then, the received signal vector of legitimate CUs is written as

$$\mathbf{y}_C = \mathbf{H}\mathbf{W}\mathbf{s} + \mathbf{z}_C. \tag{5.21}$$

It is noted that the AN does not interfere the CUs' channels and the SINR of the k-th user is given as

$$\overline{\mathrm{SINR}}_k^{\mathrm{CU}} = \frac{\mathrm{tr}\left(\tilde{\mathbf{H}}_k\tilde{\mathbf{W}}_k\right)}{\sum\limits_{i=1,i\neq k}^{K}\mathrm{tr}\left(\tilde{\mathbf{H}}_k\tilde{\mathbf{W}}_i\right) + \sigma_C^2}. \tag{5.22}$$

Likewise, the SNR of the m-th Eve is given as

$$\begin{aligned}\overline{\mathrm{SNR}}_m^{\mathrm{E}} &= \frac{\mathbb{E}\left\{\mathbf{g}_m^H\mathbf{W}\mathbf{s}\right\}}{\mathbb{E}\left\{\mathbf{g}_m^H\mathbf{n}\right\} + \sigma_0^2} = \frac{\mathbf{g}_m^H\sum\limits_{k=1}^{K}\tilde{\mathbf{W}}_k\mathbf{g}_m}{\mathbf{g}_m^H\mathbf{V}\mathbf{R}_{\bar{n}}\mathbf{V}^H\mathbf{g}_m + \sigma_0^2} \\ &= \frac{\mathrm{tr}\left(\mathbf{G}_m\sum\limits_{k=1}^{K}\tilde{\mathbf{W}}_k\right)}{\mathrm{tr}\left(\mathbf{G}_m\mathbf{V}\mathbf{R}_{\bar{n}}\mathbf{V}^H\right) + \sigma_0^2},\end{aligned} \tag{5.23}$$

where $\mathbf{g}_m$ denotes the channel from the transmitter to the m-th Eve. Note that the covariance matrix of the colored noise vector, i.e., $\mathbf{R}_{\bar{n}}$, is set as the identity matrix when Eves' channels are unknown to the ISAC BS.

5.3.1 AN Refinement Based on Eves' Information

The AN design could be further refined if more information about Eve's channels $\mathbf{g}_m$ is known to the BS. In this case, we assume that the instantaneous channel realizations of Eves are known to the transmitter, which is defined as $\mathbf{G}_m = \mathbb{E}\left\{\mathbf{g}_m \mathbf{g}_m^H\right\} = \bar{\mathbf{g}}_m \bar{\mathbf{g}}_m^H + \sigma_{G,m}^2 \mathbf{I}_{N_t}$, where $\bar{\mathbf{g}}_m$ and $\sigma_{G,m}^2 \mathbf{I}_{N_t}$ denote the mean and covariance matrix of $\mathbf{g}_m$, respectively. In particular, to obtain a fair comparison with our approach that assumes no Eves' information, we consider the extreme setting that $\mathbf{G}_m = \sigma_{g,m}^2 \mathbf{I}_{N_t}$, $\sigma_{g,m}^2 > 0$. Besides, we assume that $\mathbf{g}_m$ and $\mathbf{s}$ are independent and identically distributed (i.i.d.). To this end, the expression of the secrecy rate can be accordingly obtained as given in Section 5.2, which is written as

$$\mathrm{SR}_{\mathrm{IST}} = \min_{k,m} \left[\log\left(1 + \overline{\mathrm{SINR}}_k^{\mathrm{CU}}\right) - \log\left(1 + \overline{\mathrm{SNR}}_m^{\mathrm{E}}\right) \right]^+. \tag{5.24}$$

In light of the above assumptions, the secrecy rate maximization problem with the omnidirectional beampattern design is given as

$$\begin{aligned} \max_{\tilde{\mathbf{W}}_k, \mathbf{R}_{\bar{n}}} \quad & \mathrm{SR}_{\mathrm{IST}} \\ \text{s.t.} \quad & \bar{\mathbf{R}}_X = \frac{P_0}{N_t} \mathbf{I}_{N_t} \\ & \tilde{\mathbf{W}}_k \succeq \mathbf{0}, \mathbf{R}_{\bar{n}} \succeq \mathbf{0}, \forall\, k. \end{aligned} \tag{5.25}$$

Note that the non-convexity of the problem above only lies in the objection function, while it can be regarded as a typical secrecy rate maximization problem, which has been solved efficiently as studied in [213, 328]. The simulation results will be given in Section 5.7 as benchmarks.

5.4 Eves' Parameters Estimation

To avoid redundancy, we briefly present the method to estimate amplitudes and angles of Eves based on our signal models proposed in Section 5.2, namely the combined Capon and approximate maximum likelihood (CAML) approach [329, 330]. Specifically, Capon is initially applied to estimate the peak directions, and then approximate maximum likelihood (AML) is used to estimate the amplitudes of all Eves.

We firstly give the expression of signal model $\mathbf{Y}$ [331], where we let $\hat{\theta}_m, m = 1,\ldots,M$ denote the estimated Eves' directions. Similar to the receive signal model in (5.6), we here have

$$\mathbf{Y} = \mathbf{A}^*\left(\hat{\boldsymbol{\theta}}\right)\hat{\boldsymbol{\Lambda}}\mathbf{B}^T\left(\hat{\boldsymbol{\theta}}\right)\mathbf{X} + \tilde{\mathbf{Z}}, \tag{5.26}$$

where $\hat{\boldsymbol{\Lambda}} = \text{diag}\left[\beta\left(\hat{\theta}_1\right),\ldots,\beta\left(\hat{\theta}_M\right)\right]$ and $\tilde{\mathbf{Z}}$ denotes the residual term. By employing the AML algorithm, the estimate of amplitudes can be written in a closed form given as [330]

$$\boldsymbol{\beta} = \frac{1}{L}\left[\left(\mathbf{A}^H\mathbf{T}^{-1}\mathbf{A}\right)\odot\left(\mathbf{B}^H\hat{\mathbf{R}}_X^*\mathbf{B}\right)\right]^{-1}\cdot\text{vecd}\left(\mathbf{A}^H\mathbf{T}^{-1}\mathbf{Y}\mathbf{X}^H\mathbf{B}^*\right), \tag{5.27}$$

where vecd$(\cdot)$ denotes a column vector with the elements being the diagonal of a matrix and

$$\mathbf{T} = L\hat{\mathbf{R}} - \frac{1}{L}\mathbf{Y}\mathbf{X}^H\mathbf{B}^*\left(\mathbf{B}^T\hat{\mathbf{R}}_X\mathbf{B}^*\right)^{-1}\mathbf{B}^T\mathbf{X}\mathbf{Y}^H, \tag{5.28}$$

where $\hat{\mathbf{R}}$ is the sample covariance of the observed data samples and $\hat{\mathbf{R}} = \frac{1}{L}\mathbf{Y}\mathbf{Y}^H$.

At the first step of the Eve parameter estimation, we design our transmission so that the AP emits an omnidirectional waveform, which is usually employed by the MIMO radar for initial probing. Thus, the covariance matrix is given as $\tilde{\mathbf{R}}_X = \frac{P_0}{N_t}\mathbf{I}_{N_t}$. The CRBs for angles and amplitudes of targets can be accordingly calculated by substituting $\tilde{\mathbf{R}}_X$ into (5.12) and (5.15), where we denote them as $\text{CRB}_0\left(\hat{\boldsymbol{\theta}}\right)$ and $\text{CRB}_0\left(\hat{\boldsymbol{\beta}}\right)$. Assume that the probability density function (PDF) of the angle estimated error is modeled as Gaussian distribution, zero mean and a variance of $\text{CRB}_0\left(\hat{\boldsymbol{\theta}}\right)$. That is, $\text{E}_{est,m} \sim \mathcal{CN}\left(0, \text{CRB}_0\left(\hat{\theta}_m\right)\right)$, where $\text{E}_{est,k}$ denotes the angle estimation error of the k-th Eve. As a consequence, the probability that the real direction of the k-th Eve

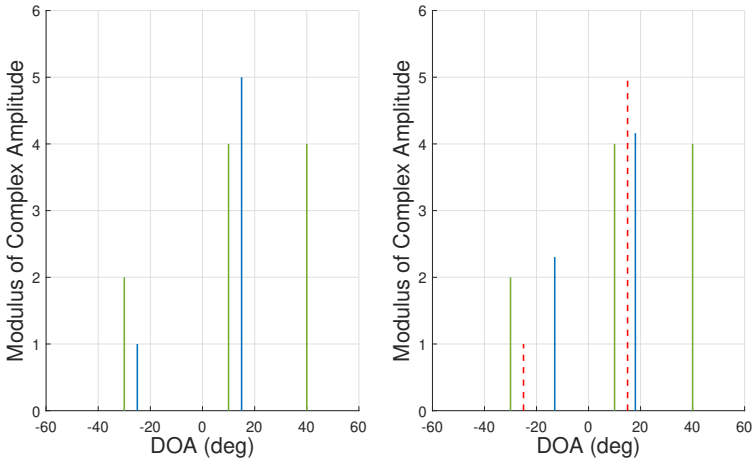

(a) (b)

Figure 5.2: Spatial spectral estimates with CAML approach, when Eves locate at $\theta_1 = -25°, \theta_2 = 15°$ (blue lines), and CUs locate at $\theta_3 = 40°, \theta_4 = 10°$ and $\theta_5 = -30°$ (green lines). The red dashed lines in (b) denote the real directions and amplitudes of Eves. (a) SNR=20dB. (b) SNR=-15dB.

falls in the range $\Xi_m^{(0)} = \left[\hat{\theta}_m - 3\sqrt{\mathrm{CRB}_0\left(\hat{\theta}_m\right)}, \hat{\theta}_m + 3\sqrt{\mathrm{CRB}_0\left(\hat{\theta}_m\right)}\right]$ is approximately 0.9973 [332]. Thus, the main lobe width of the radar beampattern will be initially designed as $\Xi^{(0)}$, and then it will be iteratively updated based on the optimized CRB.

For clarity, we present the spatial spectrum of the direction of angle (DOA) estimation by deploying the CAML technique in Fig. 5.2. It is assumed that two Eves are located at $\theta_1 = -25°, \theta_2 = 15°$ (denoted by blue lines) and three CUs locate at $\theta_3 = 40°, \theta_4 = 10°, \theta_5 = -30°$ (denoted by green lines), with the modulus of complex amplitudes $\beta_1 = 1, \beta_2 = 5, \beta_3 = 4, \beta_4 = 5$ and $\beta_5 = 2$, where directions of CUs are known to the transmitter. Fig. 5.2(a) and Fig. 5.2(b) demonstrate the CAML performance when SNR=20dB and SNR=-15dB, respectively. It is noted that the CAML approach estimates the DOA precisely when SNR is 20dB, while errors of the angle estimation happen when the SNR decreases to -15 dB. To further illustrate the performance of the CAML estimation method, the root means square error (RMSE) versus the SNR of the echo signal is shown in Fig. 5.3 with the CRB as a baseline. As expected, the CRB is shown as the lower bound of the RMSE obtained by CAML estimation, in particular, the CRB gets tight in the high-SNR regime.

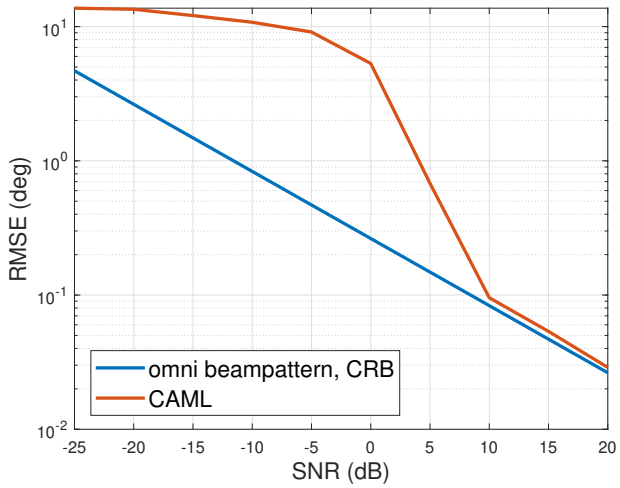

Figure 5.3: Target/Eve estimation performance by applying CAML method, with the CRB obtained by omni directional beampattern design as a benchmark.

5.5 Bounds for CRB and Secrecy Rate

The design of a weighted optimization between the radar CRB and the communication secrecy rate presents the challenge that the two performance metrics have different units and potentially different magnitudes. To overcome this challenge we need to normalize them each with their respective upper/lower bound. To obtain these bounds, in this section we present the CRB minimization problem and the secrecy rate maximization problem with the system power budget constraint. Considering the further design of the weighted objective function in the following section, the CRB minimization problem can be approximated as the FIM determinant maximization problem. To this end, the optimal solutions generate the upper bounds of the FIM determinant and the secrecy rate, both of which will be employed to normalize the metrics in Section 5.6.

5.5.1 Upper-bound of the FIM Determinant

We denote $\boldsymbol{\eta}$ as the sensing parameters, thus the MSE can be expressed as $\mathbf{M}(\boldsymbol{\eta}) \triangleq \mathbb{E}\left\{(\boldsymbol{\eta}-\hat{\boldsymbol{\eta}})(\boldsymbol{\eta}-\hat{\boldsymbol{\eta}})^T\right\} \succeq \mathbf{J}^{-1}$. For the m-th parameter η_i to be estimated, it has $\mathbb{E}\left\{\|\eta_i-\hat{\eta}_i\|^2\right\} \geq \left[\mathbf{J}^{-1}\right]_{ii}$ [333]. Thus, it is common to minimize the trace or the determinant of the CRB matrix, i.e., $\mathrm{tr}\left(\mathbf{J}^{-1}\right)$ or $\left|\mathbf{J}^{-1}\right|$. Since the CRB matrix is the inverse of the FIM matrix, the problem of minimizing $\left|\mathbf{J}^{-1}\right|$ is equivalent to maximizing $|\mathbf{J}|$,

which is given as [323]

$$\max_{\tilde{\mathbf{W}}_k, \mathbf{R}_N} \quad |\mathbf{J}| \tag{5.29a}$$

$$\text{s.t.} \ \ \mathbf{R}_N \succeq \mathbf{0}, \tilde{\mathbf{W}}_k \succeq \mathbf{0}, \forall\, k \tag{5.29b}$$

$$\text{tr}\left(\sum_{k=1}^{K} \tilde{\mathbf{W}}_k + \mathbf{R}_N\right) = P_0, \tag{5.29c}$$

where P_0 denotes the power budget of the proposed system. It is noted that the optimization above is convex and can be efficiently solved by CVX toolbox [310,334]. Consequently, by substituting the optimal $\tilde{\mathbf{W}}_k, \mathbf{R}_N$ in (5.11), the upper-bound of FIM determinant is obtained.

5.5.2 Secrecy Rate Bound

To derive the upper bound of the secrecy rate, we only consider the communication security metric in this subsection. Assuming that the CSI is perfectly known to the BS, the secrecy rate maximization problem can be formulated as

$$\text{SR}^\star = \max_{\tilde{\mathbf{W}}_k, \mathbf{R}_N} \min_{k,m} \ \text{SR}\left(\tilde{\mathbf{W}}_k, \mathbf{R}_N\right) \tag{5.30a}$$

$$\text{s.t.} \ \ \text{(5.29b), (5.29c).} \tag{5.30b}$$

It is noted that the non-convexity lies in the objective function of (5.30), which makes the optimization problem above difficult to solve. To resolve this issue, we introduce an auxiliary variable b, where (5.30) has the same optimal solutions as the reformulation below

$$\begin{aligned} \text{SR}^\star = \max_{\tilde{\mathbf{W}}_k, \mathbf{R}_N, b} \ & \min_{k,m} \ \left[R_{C_k}\left(\tilde{\mathbf{W}}_k, \mathbf{R}_N\right) - \log b\right] \\ \text{s.t.} \ \ & \log\left(1 + \frac{|\alpha_m|^2 \mathbf{a}^H(\theta_m) \sum_{i=k}^{K} \tilde{\mathbf{W}}_k \mathbf{a}(\theta_m)}{|\alpha_m|^2 \mathbf{a}^H(\theta_m) \mathbf{R}_N \mathbf{a}(\theta_m) + \sigma_R^2}\right) \le \log b, \forall\, m \\ & \text{(5.29b), (5.29c).} \end{aligned} \tag{5.31}$$

The above problem can be simply relaxed into a convex SDP problem. For brevity, we refer readers to [213] for more details.

5.6 Weighted Optimization Problem

In this section, we propose a normalized weighted optimization problem that reveals the performance tradeoff between the communication security and Eve parameters estimation. Additionally, recall that the ISAC access point firstly emits an omnidirectional beampattern as given in Section 5.4, where imprecise angles of Eves have been obtained at the given SNR, with the angular uncertainty interval of the m-th Eve is denoted as $\Xi_m^{(0)}$. To reduce angle estimation errors, we also take the wide main beam design into account, which covers all possible directions of Eves.

5.6.1 Problem Formulation

To achieve the desired tradeoff between the communication data security and the radar estimation CRB, while taking the estimation errors of Eves' angles and the system power budget into account, we formulate the weighted optimization problem as follows

$$\max_{\tilde{\mathbf{W}}_m, \mathbf{R}_N} \ \rho \frac{|\mathbf{J}|}{|\mathbf{J}|_{UB}} + (1-\rho)\frac{\mathrm{SR}}{\mathrm{SR}_{UB}} \tag{5.32a}$$

$$\text{s.t. } \mathbf{a}^H(\vartheta_{m,0})\mathbf{R}_X\mathbf{a}(\vartheta_{m,0}) - \mathbf{a}^H\left(\vartheta_{m,p}\right)\mathbf{R}_X\mathbf{a}\left(\vartheta_{m,p}\right) \geq \gamma_s, \forall\, \vartheta_{m,p} \in \mathrm{card}(\Psi_m), \forall\, m \tag{5.32b}$$

$$\mathbf{a}^H(\vartheta_{m,n})\mathbf{R}_X\mathbf{a}(\vartheta_{m,n}) \leq (1+\alpha)\mathbf{a}^H(\vartheta_{m,0})\mathbf{R}_X\mathbf{a}(\vartheta_{m,0}), \forall\, \vartheta_{m,n} \in \mathrm{card}(\Omega_m), \forall\, m \tag{5.32c}$$

$$\mathbf{a}^H(\vartheta_{m,n})\mathbf{R}_X\mathbf{a}(\vartheta_{m,n}) \geq (1-\alpha)\mathbf{a}^H(\vartheta_{m,0})\mathbf{R}_X\mathbf{a}(\vartheta_{m,0}), \forall\, \vartheta_{m,n} \in \mathrm{card}(\Omega_m), \forall\, m \tag{5.32d}$$

$$(5.29b)\ ,\ (5.29c), \tag{5.32e}$$

where $|\mathbf{J}|_{UB}$ and SR_{UB} denote the upper bounds of the FIM matrix determinant and the secrecy rate which were obtained in Section 5.4, respectively. $0 \leq \rho \leq 1$ denotes the weighting factor that determines the weights for the Eve estimation performance

Algorithm 5.1 Iterative optimization of the CRB and the secrecy rate

Initialization: $\Xi_m^{(0)}$ obtained from initial target/Eve estimation and CRB in Section 5.4; $r = 1$

Repeat:

1: $\Omega_m^{(r)} = \Xi_m^{(r-1)}$, $\Psi_m^{(r)}$ is accordingly obtained;

2: substitute $\Omega_m^{(r)}$ and $\Psi_m^{(r)}$ into problem (5.32);

Repeat:

3: solve problem (5.32) by FP algorithm;

Until: find the optimal $c \in \left[\left(\min\limits_k \ 1 + P_0\|\mathbf{h}_k\|^2\right)^{-1}, 1\right]$ which generates the maximum value of the objective function deploying the golden search;

4: the optimal variables $\tilde{\mathbf{W}}_k^\star, \mathbf{R}_N^\star$ are obtained;

5: calculate the $\mathrm{CRB}^{(r)}\left(\hat{\theta}\right)$ and the secrecy rate in the r-th iteration;

6: $\Xi_m^{(r)}$ can be accordingly obtained;

7: update $r = r + 1$,

Until: Convergence.

and the secrecy rate. α denotes a given scalar associated with the wide main beam fluctuation. $\vartheta_{m,n}$ is the n-th possible direction of the m-th Eve, $\vartheta_{k,0}$ is the angle which was estimated by the algorithm proposed in Section 5.4. Ω_m and Φ_m denote the main beam region and sidelobe region, respectively. Note that $\mathrm{card}\,(\cdot)$ denotes the the cardinality of $(\cdot)$.

Remark 2. *It is important to highlight that the secrecy rate given by (5.16) is a function of the estimation accuracy of Eve's parameters, including θ_m and α_m. Accordingly, beyond the tradeoff in the weighted optimization in this section, the improvement in the sensing performance directly results in an improvement in the secrecy performance.*

5.6.2 Efficient Solver

To tackle problem (5.32), we firstly recast the complicated secrecy rate term in the objective function. For simplicity, we denote $\Sigma_k = \sum_{i=1}^{K} \mathrm{tr}\left(\tilde{\mathbf{H}}_k \tilde{\mathbf{W}}_i\right)$ and rewrite the

optimization problem as

$$\max_{\tilde{\mathbf{W}}_k,\mathbf{R}_N} \frac{\rho}{|\mathbf{J}|_{UB}}|\mathbf{J}| + \frac{1-\rho}{\mathrm{SR}_{UB}} \min_{k,m,n} \left[R_{C_k}\left(\tilde{\mathbf{W}}_k, \mathbf{R}_N\right) - \log\left(1 + \frac{|\alpha_m|^2 \mathbf{a}^H(\vartheta_{m,n}) \sum_{k=1}^{K} \tilde{\mathbf{W}}_k \mathbf{a}(\vartheta_{m,n})}{|\alpha_m|^2 \mathbf{a}^H(\vartheta_{m,n}) \mathbf{R}_N \mathbf{a}(\vartheta_{m,n}) + \sigma_R^2} \right) \right]^+,$$

$$\vartheta_{m,n} \in \mathrm{card}(\Omega_m), \forall\, m \tag{5.33a}$$

$$\text{s.t. (5.32b), (5.32c), (5.32c) and (5.32e).} \tag{5.33b}$$

According to [213], the weighted optimization problem can be recast as (5.34) by introducing the scalar b.

$$\max_{\tilde{\mathbf{W}}_k,\mathbf{R}_N} \min_{k} \left(\frac{\rho}{|\mathbf{J}|_{UB}}|\mathbf{J}| + \frac{1-\rho}{2^{SR_{UB}}} \frac{\Sigma_k + \mathrm{tr}\left(\tilde{\mathbf{H}}_k \mathbf{R}_N\right) + 1}{b\left(\Sigma_k - \mathrm{tr}\left(\tilde{\mathbf{H}}_k \tilde{\mathbf{W}}_k\right) + \mathrm{tr}\left(\tilde{\mathbf{H}}_k \mathbf{R}_N\right) + 1\right)} \right) \tag{5.34a}$$

$$\text{s.t.} \quad \frac{|\alpha_m|^2 \mathbf{a}^H(\vartheta_{m,n}) \sum_{k=1}^{K} \tilde{\mathbf{W}}_k \mathbf{a}(\vartheta_{m,n})}{|\alpha_m|^2 \mathbf{a}^H(\vartheta_{m,n}) \mathbf{R}_N \mathbf{a}(\vartheta_{m,n}) + 1} \leq b - 1, \forall\, \vartheta_{m,n} \in \mathrm{card}(\Omega_m), \forall\, m \tag{5.34b}$$

$$\text{(5.32b), (5.32c), (5.32c) and (5.32e).} \tag{5.34c}$$

It is noted that the min operator only applies to the second term of the objective function of problem (5.34). According to the Fractional Programming (FP) algorithm [297], the optimization problem can be further reformulated by replacing the fraction term with the coefficient z, which is given as

$$\max_{\tilde{\mathbf{W}}_k,\mathbf{R}_N,\mathbf{y},z} \frac{\rho}{|\mathbf{J}|_{UB}}|\mathbf{J}| + \frac{1-\rho}{2^{SR_{UB}}} z \tag{5.35a}$$

$$\text{s.t.} \quad 2y_k \sqrt{\Sigma_k + \mathrm{tr}\left(\tilde{\mathbf{H}}_k \mathbf{R}_N\right) + 1} - y_k^2 \left(b\left(\Sigma_k - \mathrm{tr}\left(\tilde{\mathbf{H}}_k \tilde{\mathbf{W}}_k\right) + \mathrm{tr}\left(\tilde{\mathbf{H}}_k \mathbf{R}_N\right) + 1\right)\right) \geq z, \forall\, k \tag{5.35b}$$

$$\text{(5.34b), (5.32b), (5.32c), (5.32d), and (5.32e),} \tag{5.35c}$$

where $\mathbf{y}$ denotes a collection of variables $\mathbf{y} = \{y_1, \ldots, y_K\}$. Referring to [213], let $c = \frac{1}{b}$, where $c \in \left[\left(\min_k\ 1 + P_0 \|\mathbf{h}_k\|^2 \right)^{-1}, 1 \right]$. Thus, problem (5.35) can be rewritten as

follows by replacing b with c

$$\max_{\tilde{\mathbf{W}}_k,\mathbf{R}_N,\mathbf{y},z} \ \frac{\rho}{|\mathbf{J}|_{UB}}|\mathbf{J}| + \frac{1-\rho}{2^{SR_{UB}}}z \tag{5.36a}$$

$$\text{s.t.} \quad 2cy_k\sqrt{\Sigma_k + \text{tr}\left(\tilde{\mathbf{H}}_k\mathbf{R}_N\right)+1} - y_k^2\left(\Sigma_k - \text{tr}\left(\tilde{\mathbf{H}}_k\tilde{\mathbf{W}}_k\right) + \text{tr}\left(\tilde{\mathbf{H}}_k\mathbf{R}_N\right)+1\right) \geq cz, \forall\, k \tag{5.36b}$$

$$c|\alpha_m|^2\mathbf{a}^H(\vartheta_{m,n})\sum_{k=1}^{K}\tilde{\mathbf{W}}_k\mathbf{a}(\vartheta_{m,n}) \leq (1-c)\left(|\alpha_m|^2\mathbf{a}^H(\vartheta_{m,n})\mathbf{R}_N\mathbf{a}(\vartheta_{m,n})+1\right),$$

$$\forall\, \vartheta_{m,n} \in \text{card}(\Omega_m), \forall\, m \tag{5.36c}$$

$$\text{(5.32b), (5.32c), (5.32d) and (5.32e).} \tag{5.36d}$$

where the optimal y_k can be found in the following closed form

$$y_k = \frac{c\sqrt{\Sigma_k + \text{tr}\left(\tilde{\mathbf{H}}_k\mathbf{R}_N\right)+1}}{\Sigma_k - \text{tr}\left(\tilde{\mathbf{H}}_k\tilde{\mathbf{W}}_k\right) + \text{tr}\left(\tilde{\mathbf{H}}_k\mathbf{R}_N\right)+1}. \tag{5.37}$$

Note that problem (5.36) can be efficiently solved by the cvx toolbox [310, 334]. Given the interval of c, the optimal variables. $\tilde{\mathbf{W}}_k^\star, \mathbf{R}_N^\star, z^\star$ can be consequently obtained by performing a one-dimensional line search over c, such as uniform sampling or the golden search [335]. To this end, the optimal CRB* and SR* can be accordingly calculated.

To further generalize the problem above and simplify the objective function, we equivalently consider the determinant minimization problem of $\mathbf{P}^H\mathbf{J}^{-1}\mathbf{P}$ by introducing the matrix $\mathbf{P}$, where $\mathbf{P}$ associates with activated Eves with the dimension of $\mathbf{P}$ is $3K\times 3$. For example, when the CRB minimization is only associated with the first Eve, the first, the $(M+1)$-th, and the $(2M+1)$-th rows are the first, second, and third rows of the identity matrix $\mathbf{I}_{3\times 3}$, respectively [323]. Then, by noting that the inequality $\boldsymbol{\Upsilon}^{-1} \geq \mathbf{P}^H\mathbf{J}^{-1}\mathbf{P}$ is equivalent to $\boldsymbol{\Upsilon} \geq \boldsymbol{\Upsilon}\mathbf{P}^H\mathbf{J}^{-1}\mathbf{P}\boldsymbol{\Upsilon}$, and based on the

Schur-complement condition, problem (5.32) can be recast as

$$\begin{aligned} &\max_{\tilde{\mathbf{W}}_k,\mathbf{R}_N,z,\boldsymbol{\Upsilon}} \frac{\rho}{|\mathbf{J}|_{UB}}|\boldsymbol{\Upsilon}| + \frac{1-\rho}{2^{SR_{UB}}}z \\ &\text{s.t.} \quad \begin{bmatrix} \boldsymbol{\Upsilon} & \boldsymbol{\Upsilon}\mathbf{P}^H \\ \mathbf{P}\boldsymbol{\Upsilon} & \mathbf{J} \end{bmatrix} \succeq \mathbf{0} \\ &\quad (5.36b), (5.36c) \text{ and } (5.36d). \end{aligned} \tag{5.38}$$

Similarly, the determinant maximization problem above is convex and readily solvable. For clarity, the above procedure has been summarized in Algorithm 5.1.

5.7 Numerical Results

In this section, we provide the numerical results to evaluate the effectiveness of the proposed sensing-aided secure ISAC system design. We assume that both the ISAC BS and the radar receiver are equipped with uniform linear arrays (ULAs) with the same number of elements with half-wavelength spacing between adjacent antennas. In the following simulations, the number of transmit antennas and receive antennas is set as $N_t = N_r = 10$ serving $K = 3$ CUs, the frame length is set as $L = 64$, the noise variance of the communication system is $\sigma_C^2 = 0$ dBm.

Resultant beampatterns of the proposed sensing-aided ISAC security technique are shown in Fig. 5.4 and Fig. 5.5, which demonstrate the single-Eve (located at $\vartheta_{1,0} = -25°$) scenario and multi-Eve scenario (located at $\vartheta_{1,0} = -25°, \vartheta_{2,0} = 15°$), respectively. Note that the Rician factor is set as $v_k = 0.1$ for generating a Rician channel with a weak LoS component, aiming to alleviate the impact on the radar beamppattern caused by the channel correlation, and α is set as $\alpha = 0.05$. To verify the efficiency of the proposed approach, the received SNR of the echo signal is set as SNR=-22 dB, which is defined as SNR = $\frac{|\beta|^2 LP_0}{\sigma_R^2}$. The ISAC BS first transmits an omnidirectional beampattern for Eve estimation, with the aid of the CAML technique, which is denoted by green dashed lines in Fig. 5.4 and Fig. 5.5. It is referred to as the first iteration and the CRB can be accordingly calculated. Then, to ensure that Eves stay within the angle range of main lobes, we design a beampattern with a

wide main beam with a beamwidth determined by the CRB obtained from the last iteration, which has been elaborated in Section 5.6. By updating the CRB iteratively, the main lobes get narrow and point to the directions of Eves, as illustrated by the rest of the lines in Fig. 5.4 and Fig. 5.5. In the simulations, we repeat the weighted optimization problem until the CRB and the secrecy rate both convergence to a local optimum. The beampatterns also indicate that the main beam gain grows with the main lobe width getting narrow. Besides, Fig. 5.5 shows that the power towards Eves of interest gets lower compared with the single-Eve scenario, while it still outperforms the omnidirectional beampattern design.

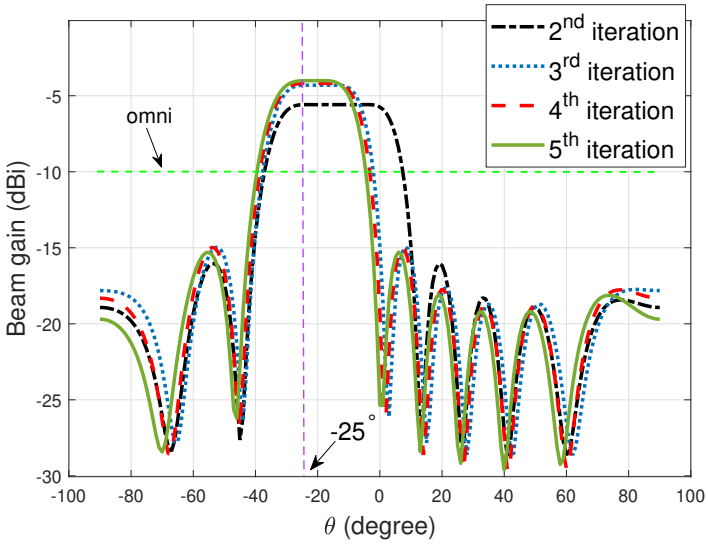

Figure 5.4: Beampatterns for the scenario of single Eve angle estimation, where the main beam width narrows over each iteration, $\vartheta_{1,0} = -25°, I = 3, K = 1, P_0 = 35$dBm, SNR=-22dB.

Fig. 5.6 illustrates the convergence of the CRB and the secrecy rate of the proposed algorithm. The benchmark in Fig. 5.6 (c) is generated following the AN design techniques in Section 5.3, where the covariance of AWGN received by Eves is set as $\sigma_0^2 = 0$ dBm. It is noted that the performance of metrics converges after five iterations when SNR=-22 dB, while the convergence requires less iterations at higher SNR. Additionally, the secrecy rate obtained by the proposed algorithm converges to 7.5 bit/s/Hz and 7.8 bit/s/Hz when SNR=-22 dB and SNR=-15 dB, which outperforms the isotropical AN methods.

In Fig. 5.7, we investigate the secrecy rate versus the main beam width with

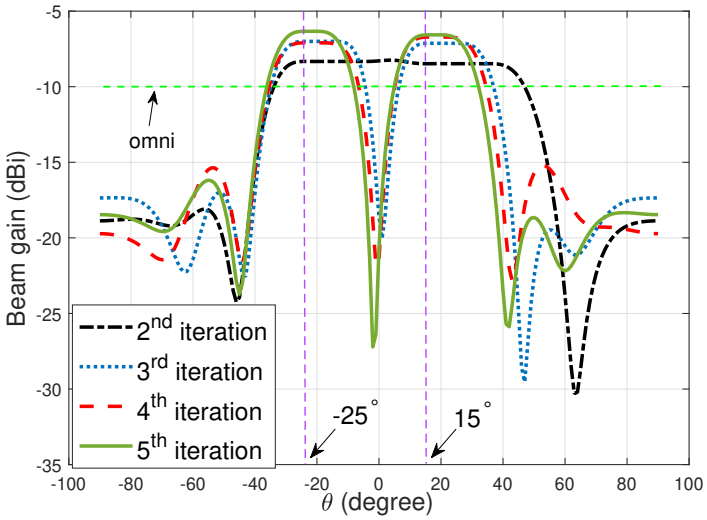

Figure 5.5: Beampatterns for the scenario of two Eves to be estimated, illustrating the circumstance when the main lobes overlap at the first iteration, $\vartheta_{1,0} = -25°, \vartheta_{2,0} = 15°, I = 3, K = 2, P_0 = 35$dBm, SNR=-22dB.

different power budget P_0, and the benchmarks are given in dashed lines and dotted lines which are obtained by the AN design techniques with knowledge of $\mathbf{G}_m$ and with no information of Eves' channels as given in Section 5.3, respectively. Generally, the secrecy rate gets higher with the increase of the power budget and it is obvious that the proposed algorithm outperforms benchmark methods. It is worthwhile to stress that the proposed weighted optimization (5.32) is implemented with no information of Eves. Note that the secrecy rate increases first and then decreases with the expansion of Eve's location uncertainty. The initial increase is because the gain of the beam towards the target/Eve of interest decreases with the growth of the main beam width, resulting in the deterioration of the eavesdropping SNR_m^{E}. With respect to the expression in (5.16), the secrecy rate improves when SNR_m^{E} reduces. However, the power budget constraint becomes tight when the main beam keeps being expanded. This indicates that more power is allocated to the Eve estimation, thus, the secrecy rate decreases. Additionally, when the main beam is wider, the transmission needs to secure the data over a wider range of angles, which is reflected in an SR expression with high channel uncertainty. Particularly, when the power budget is low, for example, $P_0 = 25$ dBm, we note that the secrecy rate monotonically decreases with the growth of $\Delta\theta$, while the weighted optimization

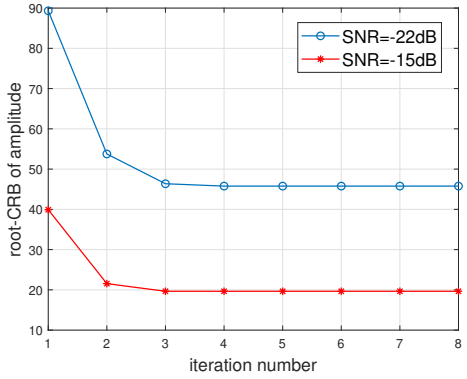

(a)

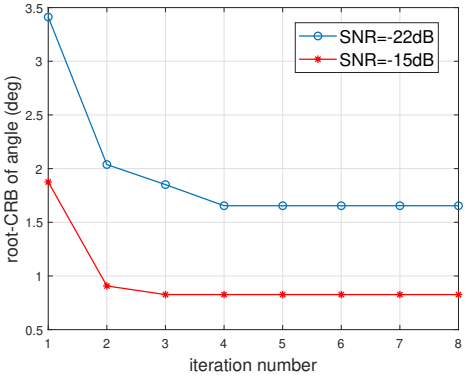

(b)

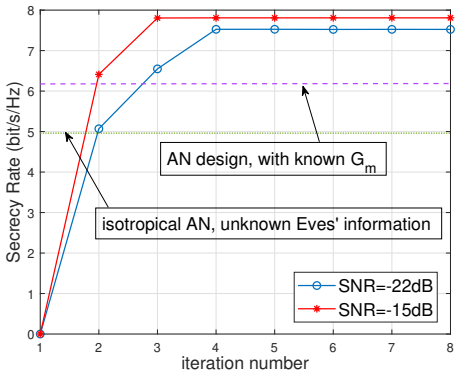

(c)

Figure 5.6: Convergence with iterations when SNR=-15dB and SNR= 22dB. $I = 3, K = 1, P_0 =$ 35dBm. (a) Convergence of root-CRB of amplitude estimation; (b) Convergence of root-CRB of angle estimation; (c) Convergence of the secrecy rate.

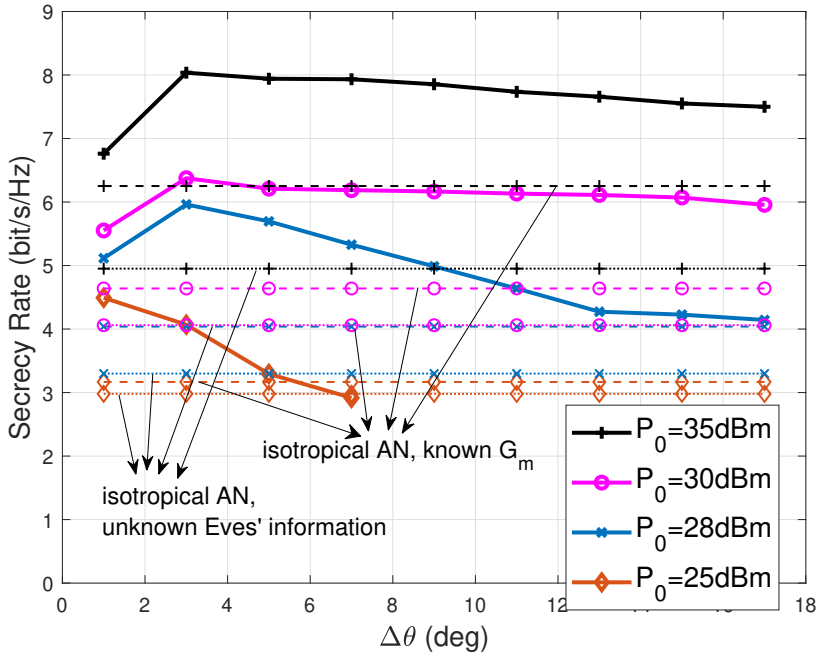

Figure 5.7: The secrecy rate analysis versus Eve's location uncertainty with various power budgets, where the AN design techniques with no information of Eves' channels and with known $\mathbf{G}_k$ are denoted by dotted lines and dashed lines, respectively. $\vartheta_{1,0} = -25°, I = 3, K = 1$, SNR=-15dB.

problem is infeasible due to the power budget limit when the $\Delta\theta$ is larger than 5 degree.

Moreover, it is illustrated in Fig. 5.8 that the secrecy rate decreases with the growth of CU number, given different power budgets P_0. Note that a higher power budget achieves better security performance. Particularly, the secrecy rate cannot be ensured if the ISAC system serves more than 5 CUs when $P_0 = 25$ dBm. In Fig. 5.9, we consider the performance tradeoff between the target/Eve estimation and communication data security with different power budgets by varying the weighting factor ρ. We note that higher P_0 results in a better performance of the estimation metric, i.e., root-CRB of the amplitude and the angle. Additionally, with the increase of secrecy rate, the CRB grows as well, which demonstrates the deterioration of Eve's angle estimation accuracy.

Furthermore, we consider a scenario including one CU and one Eve for exploiting impacts on security and sensing metrics resulting from the angle difference between the CU and the Eve. In this case, the Rician channel model with a strong

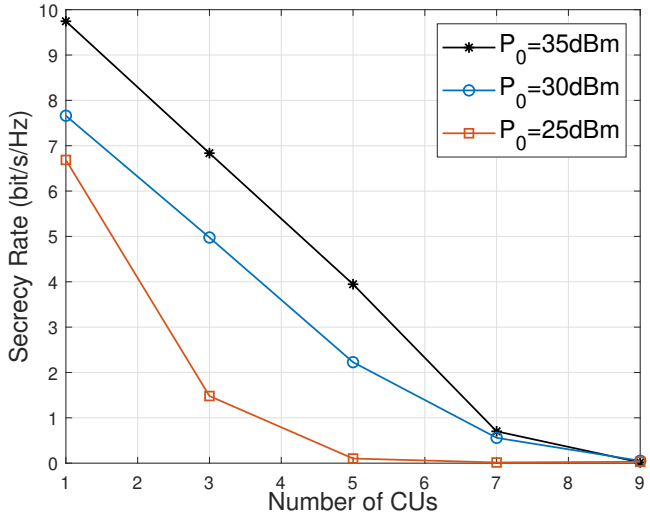

Figure 5.8: The secrecy rate analysis versus the number of CUs, with various power budgets. $K = 1, \text{SNR}=\text{-}15\text{dB}$.

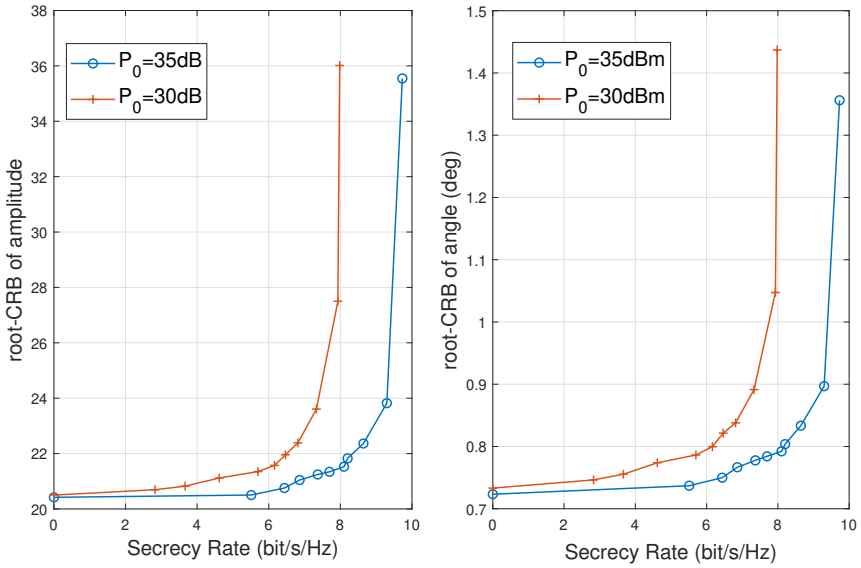

(a) (b)

Figure 5.9: Tradeoff between the CRB and the secrecy rate with different power budget. $\vartheta_{1,0} = -25°, I = 3, K = 1, \text{SNR}=\text{-}15\text{dB}$.

LoS component is deployed, i.e., $v_k = 7$ in (5.2), and the CU is assumed to locate at $-20°$. Resultant beampatterns are shown in Fig. 5.10 when the Eve is at $-20°$ as well. It is demonstrated that the main beam width converges after four iterations and the generated angle root-CRB at the second iteration is lower than the case of a weak Rician channel, which is validated in Fig. 5.11. Fig. 5.11 illustrates the analysis of the secrecy rate and the root-CRB of the angle with various angle differences. Generally speaking, with the expansion of the uncertain angular interval $\Delta\theta$, both of the metrics are deteriorated. The secrecy rate decreases when the Eve and the CU directions get closer, while the performance of the CRB improves since the tradeoff is revealed in Fig. 5.9.

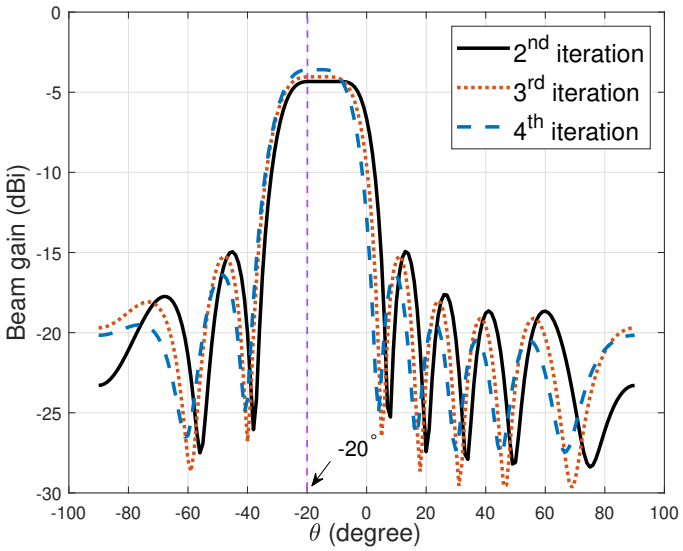

Figure 5.10: Beampatterns for the scenario when the CU and the Eve both locate at $-20°$, narrowing with each iteration until convergence. $I = 1, K = 1$, SNR=-22dB, $P_0 = 35$dBm.

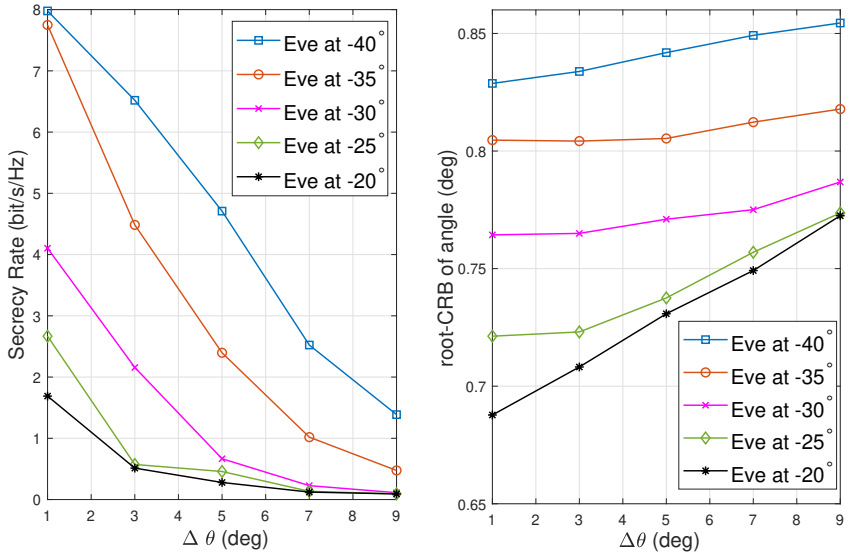

(a) (b)

Figure 5.11: Secrecy rate and root-CRB of angle performances versus uncertain angular interval of the target/Eve, with various angle differences between the Eve and the CU, where the CU locates at $-20°$. $I = 1, K = 1$, SNR=-15dB, $P_0 = 35$dBm.

5.8 Conclusion

In this chapter, we have considered the sensing-aided secure ISAC systems, where the dual-functional BS emitted waveforms to estimate the amplitudes and the directions of potential eavesdroppers and send confidential communication data to CUs simultaneously. The proposed design has promoted the cooperation between sensing and communication rather than conventionally individual functionalities. The weighted optimization problem has been designed to optimize the normalized CRB and secrecy rate while constraining the system power budget. Our numerical results have demonstrated that the secrecy rate was enhanced with the decreasing CRB in both single and multi-Eve scenarios.

Chapter 6

Conclusions and Future Work

This Dissertation focuses on the optimization designs for ensuring the PLS in ISAC systems. In this Thesis, a general overview of ISAC systems, some fundamental concepts and state-of-the-art works are provided in Chapter 2. Then in Chapter 3, Chapter 4, and Chapter 5, we demonstrate the secure DFRC system designs, including secrecy rate improvement with the assistance of AN, direct amplitude and phase designs of each symbol at receivers by applying the CI technique, and secure communication data transmission assisted by sensing functionality. Next, we summarize the conclusions and contributions of each chapter in detail.

Chapter 3: AN-aided PLS in ISAC systems. Considering the increasingly deeper integration between radar and communication, the objective of Chapter 3 is to guarantee communication data security for ISAC systems. The beamformer and the AN are jointly designed to maximize the SNR at the target, while ensuring the QoS of CUs. The following specific remarks can be derived from the results of this chapter:

- In ISAC systems, the proposed AN-aided PLS technique effectively prevents the communication data from being intercepted by the target, i.e., potential eavesdropper, which is illustrated by the analysis of the secrecy rate. Taking the robustness of the communication channel estimation into account, the secrecy rate increases first with the growth of the CSI error bound since more power is allocated to achieve the QoS requirement for communication. However, it deteriorates the secrecy performance when the CSI error bound keeps

increasing. This is for the reason that the transmission rate of communications decreases with the growth of the CSI error bound, which has been demonstrated in the analysis of secrecy rate versus imperfectly known instantaneous CSI.

- The scenario then extends to considering the target direction robustness, the generated beampattern is designed to be with a wide main beam covering all possible angles of the target. In this way, it is predictable that the main beam power gets lower with the expansion of the target angular interval uncertainty with a fixed power budget. Furthermore, what we found interesting is that the secrecy rate increases with the expansion of target location uncertainty. This is because the main beam power decrease when the angle estimation error increases, which raises the data rate difference between the Eves and LUs.

- **Future Work:** As per above, it is noted that the performance of the secrecy rate is dramatically impacted by the robustness of both the radar and communication channels. To design a system adjustable for practical implementations, it would be critical to address the flexibility of the power allocation. That is, a dynamic power allocation design is induced for our future work, which allows this secure ISAC system to be flexible to achieve desired performance tradeoff between the radar and communication functionalities dynamically. This design would be an appealing approach to further improve the energy efficiency for secure ISAC systems. To achieve this, a weighted factor $\rho \in [0, 1]$ can be applied as an extra variable designing the ratio of the achievable rate of communication and radar. To start with, the AN can be assumed to fall into the null space of the communication channel, then we optimize the weighted factor with an extra constraint of energy efficient threshold. Then, this problem can be expanded to design the AN via the optimization problem jointly. The main obstacle of this work would be the efficient solver of the complicated problem and should be deeply investigated.

Chapter 4: Secure ISAC Systems Deploying the CI Technique. The objective

of chapter 4 is to propose an SLP technique, i.e., deploying DM to exploit CI, aiming to constrain symbols received by CUs falling into the constructive region and the symbols received by the target falling into the destructive region. To this end, the SER at CUs can be guaranteed while deteriorating the decoding capability of the target. The conclusions and contributions of this chapter are summarized as follows:

- The proposed CI/DI technique can well ensure communication data security in the ISAC system, even in the context of mmWave frequency, which implies the correlation between the CUs' channels and the target's channel. Comparing the AN-aided approach, it reduces the redundant power consumption caused by the AN and improves the flexibility benefiting from the SLP. In the CI-only case, the SER analysis demonstrates that the channel correlation degrades the SER at the target, which deteriorates the data security compared with the scenario of uncorrelated main and wiretap channels. To tackle this issue, deployment of the DI approach obviously improved the SER at the target/Eve, which is close to 1 when the angle difference is getting larger.

- The proposed waveform design optimization problem outperforms the DFRC precoder design in [5] since the amplitudes and the phases of symbols are directly designed at the receiver side which gains more flexibility and achieves lower sidelobe power at the expense of RF chains' number. Moreover, the FP solver we employed in this work outperforms the SQ algorithm given in [308]. Considering the robustness of the target location, the main beam of the generated beampattern covers possible angles and the main beam power is accordingly decreased.

- **Future Work:** The CI technique can be classified as the digital PLS, which enables a true implementation of mathematical algorithms with maximum flexibility. However, since each antenna element has its own dedicated RF chain as well as individual DACs and ADCs, it is achieved at the expense of a large number of RF chains. On the other hand, analog beamforming is an efficient approach to reducing RF chains, but at the expense of spectral

efficiency. To balance the benefits of both, the hybrid SLP technique is appealing for our future work. To achieve this, the optimization problem can be designed in the presence of limited RF chains under the transmit power constraint and the low-resolution PSs' constraint. The energy efficiency will be accordingly improved thanks to the reduced RF chains and the finite-precision PSs. Herein, the joint design problem may be difficult to solve and will be studied in depth. This problem also implies an existing tradeoff between the number of RF chains and the resolution of the PSs, which can be further explored in this study as an extension of future work.

Chapter 5: Sensing-assisted PLS in ISAC Systems. Studies in Chapter 3 and Chapter 4 are designed in a single-target scenario, and each radar and communication works in an individual functionality. This motivates the studies in Chapter 5, where we present a sensing-assisted approach for the ISAC system. The proposed approach can be summarized in two steps: 1) estimating angles of targets by emitting an omnidirectional waveform; 2) designing a weighted optimization problem to iteratively optimize the secrecy and the CRB by updating the main beam width, which is calculated by the optimal CRB from the last iteration. The main contributions of the chapter can be highlighted in the following list:

- The proposed sensing-aided PLS algorithm is promising in the research field of secure ISAC systems, which is initially designed to obtain the information of the Eves' channels, i.e., the well-known limitation of conventional PLS studies, with the assistance of sensing functionality. It is found that the secrecy rate and the CRB can mutually benefit each other for a given weighted factor ρ. This is because the secrecy rate decreases with the expansion of the uncertain target angular interval when the power constraint is tight. Hence, in our designs, the secrecy rate increases as Eve's estimation improves until the angular interval of the estimation error $\Delta\theta$ is less than 3 degrees. Moreover, the given beampatterns in numerical results verify that the proposed algorithm enables not only single-target/Eve but also multi-target/Eve sensing.

- In the mmWave frequency band, the channel correlation between the radar and

communication systems is further considered. Herewith, the Rician channel model with a strong LoS component is deployed, where the Rician factor $\upsilon_k = 7$, and both the CU and the target are assumed to locate at $-20°$. With this channel setup, the generated angle root-CRB at the second iteration is lower than in the case of deploying the weak Rician channel. Additionally, the secrecy rate decreases when the Eve and the CU directions get closer, while the performance of the CRB improves.

- **Future Work:** Existing literature regarding secure ISAC systems mainly focuses on a dual-functional BS emitting a waveform for both sensing and communication functionalities. The communication transmission is protected by related PLS approaches, while both the radar and communication systems still work individually. The study in Chapter 5 is a promising design of a sensing-assisted PLS approach for ISAC systems, which is aided by inserting AN at the transmitter. However, the redundant power consumption caused by the AN has been indicated in many works. As a future work, it is particularly interesting to deploy the DM technique instead of the added AN in order to improve energy efficiency and reduce power consumption. To be specific, the optimization problem is designed to minimize the CRB with the constraint of power budget and the CI technique by optimizing the emitted waveform at a symbol level. Moreover, this study may further motivate the research of hybrid structures for balancing the benefits of analog and digital SLP.

To finally summarize, the Thesis has presented several approaches to ensuring communication data security in ISAC systems. The author hopes that the given results and observations within this Thesis can be with the help of practical implementation and motivate further work in the field of secure ISAC systems in the future 5G-and-beyond wireless communication networks.

Bibliography

[1] Yuan Ding and Vincent Fusco. Vector representation of directional modulation transmitters. In *The 8th European conference on antennas and propagation (EuCAP 2014)*, pages 367–371. IEEE, 2014.

[2] Christos Masouros and Gan Zheng. Exploiting known interference as green signal power for downlink beamforming optimization. *IEEE Transactions on Signal processing*, 63(14):3628–3640, 2015.

[3] Fan Liu, Le Zheng, Yuanhao Cui, Christos Masouros, Athina P Petropulu, Hugh Griffiths, and Yonina C Eldar. Seventy years of radar and communications: The road from separation to integration. *arXiv preprint arXiv:2210.00446*, 2022.

[4] Kevin Sherwood Ryland. *Software-Defined Radio Implementation of Two Physical Layer Security Techniques*. PhD thesis, Virginia Tech, 2018.

[5] Li Chen, Fan Liu, Jun Liu, and Christos Masouros. Composite signalling for DFRC: Dedicated probing signal or not? *arXiv preprint arXiv:2009.03528*, 2020.

[6] Xiaohu You, Cheng-Xiang Wang, Jie Huang, Xiqi Gao, Zaichen Zhang, Mao Wang, Yongming Huang, Chuan Zhang, Yanxiang Jiang, Jiaheng Wang, et al. Towards 6G wireless communication networks: Vision, enabling technologies, and new paradigm shifts. *Science China Information Sciences*, 64(1):1–74, 2021.

[7] Zhiyong Feng, Zixi Fang, Zhiqing Wei, Xu Chen, Zhi Quan, and Danna Ji. Joint radar and communication: A survey. *China Communications*, 17(1):1–27, 2020.

[8] Le Zheng, Marco Lops, Yonina C. Eldar, and Xiaodong Wang. Radar and communication coexistence: An overview: A review of recent methods. *IEEE Signal Processing Magazine*, 36(5):85–99, 2019.

[9] Fan Liu, Yuanhao Cui, Christos Masouros, Jie Xu, Tony Xiao Han, Yonina C Eldar, and Stefano Buzzi. Integrated sensing and communications: Towards dual-functional wireless networks for 6G and beyond. *IEEE Journal on Selected Areas in Communications*, 2022.

[10] Yuanhao Cui, Fan Liu, Xiaojun Jing, and Junsheng Mu. Integrating sensing and communications for ubiquitous IoT: Applications, trends, and challenges. *IEEE Network*, 35(5):158–167, 2021.

[11] Reem Melki, Hassan N Noura, Mohammad M Mansour, and Ali Chehab. A survey on OFDM physical layer security. *Physical Communication*, 32:1–30, 2019.

[12] Li Sun and Qinghe Du. Physical layer security with its applications in 5G networks: A review. *China communications*, 14(12):1–14, 2017.

[13] Wei-Cheng Liao, Tsung-Hui Chang, Wing-Kin Ma, and Chong-Yung Chi. QoS-based transmit beamforming in the presence of eavesdroppers: An optimized artificial-noise-aided approach. *IEEE Transactions on Signal Processing*, 59(3):1202–1216, 2011.

[14] Satashu Goel and Rohit Negi. Guaranteeing secrecy using artificial noise. *IEEE transactions on wireless communications*, 7(6):2180–2189, 2008.

[15] Rohit Negi and Satashu Goel. Secret communication using artificial noise. In *IEEE Vehicular Technology Conference*, volume 62, page 1906. Citeseer, 2005.

[16] Zhongxiang Wei, Christos Masouros, and Fan Liu. Secure directional modulation with Few-Bit phase shifters: Optimal and Iterative-Closed-Form designs. *IEEE Transactions on Communications*, 2020.

[17] Shihao Yan, Nan Yang, Giovanni Geraci, Robert Malaney, and Jinhong Yuan. Optimization of code rates in SISOME wiretap channels. *IEEE Transactions on Wireless Communications*, 14(11):6377–6388, 2015.

[18] Elie J Baghdady. Directional signal modulation by means of switched spaced antennas. *IEEE Transactions on Communications*, 38(4):399–403, 1990.

[19] Feng Shu, Tong Shen, Ling Xu, Yaolu Qin, Siming Wan, Shi Jin, Xiaohu You, and Jiangzhou Wang. Directional modulation: A physical-layer security solution to B5G and future wireless networks. *IEEE Network*, 34(2):210–216, 2019.

[20] Christos Masouros, Mathini Sellathurai, and Tharmalingam Ratnarajah. Vector perturbation based on symbol scaling for limited feedback MISO downlinks. *IEEE Transactions on Signal Processing*, 62(3):562–571, 2014.

[21] Fan Liu, Christos Masouros, Ang Li, Tharmalingam Ratnarajah, and Jianming Zhou. MIMO radar and cellular coexistence: A power-efficient approach enabled by interference exploitation. *IEEE Transactions on Signal Processing*, 66(14):3681–3695, 2018.

[22] Muhammad RA Khandaker, Christos Masouros, Kai-Kit Wong, and Stelios Timotheou. Secure SWIPT by exploiting constructive interference and artificial noise. *IEEE Transactions on Communications*, 67(2):1326–1340, 2018.

[23] Wikipedia. Precoding — Wikipedia, the free encyclopedia. `http://en.wikipedia.org/w/index.php?title=Precoding&oldid=1076998739`, 2022. [Online; accessed 16-November-2022].

[24] Mai Vu and Arogyaswami Paulraj. MIMO wireless linear precoding. *IEEE Signal Processing Magazine*, 24(5):86–105, 2007.

[25] Claude E Shannon. Channels with side information at the transmitter. *IBM journal of Research and Development*, 2(4):289–293, 1958.

[26] Giuseppe Caire and Shlomo Shamai. On the capacity of some channels with channel state information. *IEEE Transactions on Information Theory*, 45(6):2007–2019, 1999.

[27] Mikael Skoglund and George Jongren. On the capacity of a multiple-antenna communication link with channel side information. *IEEE Journal on Selected Areas in Communications*, 21(3):395–405, 2003.

[28] Guangxu Zhu, Caijun Zhong, Himal A Suraweera, Zhaoyang Zhang, Chau Yuen, and Rui Yin. Ergodic capacity comparison of different relay precoding schemes in dual-hop AF systems with co-channel interference. *IEEE Transactions on Communications*, 62(7):2314–2328, 2014.

[29] Liutong Du, Lihua Li, Hien Quoc Ngo, Trang C Mai, and Michail Matthaiou. Cell-free massive mimo: Joint maximum-ratio and zero-forcing precoder with power control. *IEEE Transactions on Communications*, 69(6):3741–3756, 2021.

[30] Nusrat Fatema, Guang Hua, Yong Xiang, Dezhong Peng, and Iynkaran Natgunanathan. Massive MIMO linear precoding: A survey. *IEEE systems journal*, 12(4):3920–3931, 2017.

[31] Mahmood Mazrouei-Sebdani, Witold A Krzymień, and Jordan Melzer. Massive MIMO with nonlinear precoding: large-system analysis. *IEEE Transactions on Vehicular Technology*, 65(4):2815–2820, 2015.

[32] Mahmoud A Albreem, Alaa H Al Habbash, Ammar M Abu-Hudrouss, and Salama S Ikki. Overview of precoding techniques for massive MIMO. *IEEE Access*, 9:60764–60801, 2021.

[33] Ang Li, Danilo Spano, Jevgenij Krivochiza, Stavros Domouchtsidis, Christos G Tsinos, Christos Masouros, Symeon Chatzinotas, Yonghui Li, Branka Vucetic, and Björn Ottersten. A tutorial on interference exploitation via symbol-level precoding: overview, state-of-the-art and future directions. *IEEE Communications Surveys & Tutorials*, 22(2):796–839, 2020.

[34] Xianghao Yu, Juei-Chin Shen, Jun Zhang, and Khaled B Letaief. Alternating minimization algorithms for hybrid precoding in millimeter wave MIMO systems. *IEEE Journal of Selected Topics in Signal Processing*, 10(3):485–500, 2016.

[35] Shiwen He, Yongming Huang, Luxi Yang, and Björn Ottersten. Coordinated multicell multiuser precoding for maximizing weighted sum energy efficiency. *IEEE Transactions on Signal Processing*, 62(3):741–751, 2013.

[36] Long Zhao, Kan Zheng, Hang Long, Hui Zhao, and Wenbo Wang. Performance analysis for downlink massive multiple-input multiple-output system with channel state information delay under maximum ratio transmission precoding. *IET Communications*, 8(3):390–398, 2014.

[37] J Zhang, Y Wu, M Xu, and J Wang. Linear transmitter precoding design for downlink of multiuser MIMO systems. *Electronics Letters*, 41(14):811–813, 2005.

[38] Ahmed Hesham Mehana and Aria Nosratinia. Diversity of MIMO linear precoding. *IEEE Transactions on Information Theory*, 60(2):1019–1038, 2013.

[39] Ami Wiesel, Yonina C Eldar, and Shlomo Shamai. Zero-forcing precoding and generalized inverses. *IEEE Transactions on Signal Processing*, 56(9):4409–4418, 2008.

[40] Harsh Tataria, Peter J Smith, Larry J Greenstein, and Pawel A Dmochowski. Zero-forcing precoding performance in multiuser MIMO systems with hetero-

geneous ricean fading. *IEEE Wireless Communications Letters*, 6(1):74–77, 2016.

[41] Yanki Aslan, Antoine Roederer, Nelson JG Fonseca, Piero Angeletti, and Alexander Yarovoy. Orthogonal versus zero-forced beamforming in multi-beam antenna systems: review and challenges for future wireless networks. *IEEE Journal of Microwaves*, 2021.

[42] Michael Joham, Wolfgang Utschick, and Josef A Nossek. Linear transmit processing in MIMO communications systems. *IEEE Transactions on signal Processing*, 53(8):2700–2712, 2005.

[43] Jakob Hoydis, Stephan Ten Brink, and Mérouane Debbah. Massive MIMO in the UL/DL of cellular networks: How many antennas do we need? *IEEE Journal on selected Areas in Communications*, 31(2):160–171, 2013.

[44] Long D Nguyen, Hoang Duong Tuan, Trung Q Duong, and H Vincent Poor. Multi-user regularized zero-forcing beamforming. *IEEE Transactions on Signal Processing*, 67(11):2839–2853, 2019.

[45] David A Schmidt, Michael Joham, and Wolfgang Utschick. Minimum mean square error vector precoding. *European Transactions on Telecommunications*, 19(3):219–231, 2008.

[46] Arafat Omar, Seeme Fatima, and Md Mushtaq Arman. A comparative simulation of mobile wimax physical layer performance for Zero-Force (ZF) and minimum mean square error (mmse) channel equalizers. *International Journal of Physical Sciences*, 5(16):2503–2515, 2010.

[47] Daniel L Colon, Fernando H Gregorio, and Juan Cousseau. Linear precoding in multi-user massive mimo systems with imperfect channel state information. In *2015 XVI Workshop on Information Processing and Control (RPIC)*, pages 1–6. IEEE, 2015.

[48] Ruoheng Liu, Tie Liu, H Vincent Poor, and Shlomo Shamai. MIMO gaussian broadcast channels with confidential and common messages. In *2010 IEEE International Symposium on Information Theory*, pages 2578–2582. IEEE, 2010.

[49] Lei Zhang, Yunlong Cai, Benoit Champagne, and Minjian Zhao. Tomlinson-Harashima precoding design in MIMO wiretap channels based on the MMSE criterion. In *2015 IEEE International Conference on Communication Workshop (ICCW)*, pages 470–474. IEEE, 2015.

[50] Rui Zhang, Chin Choy Chai, and Ying-Chang Liang. Joint beamforming and power control for multiantenna relay broadcast channel with QoS constraints. *IEEE Transactions on Signal Processing*, 57(2):726–737, 2008.

[51] Xun Zou, Mehdi Ganji, and Hamid Jafarkhani. Cooperative asynchronous non-orthogonal multiple access with power minimization under qos constraints. *IEEE Transactions on Wireless Communications*, 19(3):1503–1518, 2019.

[52] Eleftherios Karipidis, Nicholas D Sidiropoulos, and Zhi-Quan Luo. Quality of service and max-min fair transmit beamforming to multiple cochannel multicast groups. *IEEE Transactions on Signal Processing*, 56(3):1268–1279, 2008.

[53] Trinh Van Chien, Emil Björnson, and Erik G Larsson. Joint power allocation and user association optimization for massive MIMO systems. *IEEE Transactions on Wireless Communications*, 15(9):6384–6399, 2016.

[54] Wei Yu and Tian Lan. Transmitter optimization for the multi-antenna downlink with per-antenna power constraints. *IEEE Transactions on signal processing*, 55(6):2646–2660, 2007.

[55] Dimitrios Christopoulos, Symeon Chatzinotas, and Björn Ottersten. Weighted fair multicast multigroup beamforming under per-antenna power constraints. *IEEE Transactions on Signal Processing*, 62(19):5132–5142, 2014.

[56] Maha Alodeh, Danilo Spano, Ashkan Kalantari, Christos G Tsinos, Dimitrios Christopoulos, Symeon Chatzinotas, and Björn Ottersten. Symbol-level and multicast precoding for multiuser multiantenna downlink: A state-of-the-art, classification, and challenges. *IEEE Communications Surveys & Tutorials*, 20(3):1733–1757, 2018.

[57] Ashkan Kalantari, Mojtaba Soltanalian, Sina Maleki, Symeon Chatzinotas, and Björn Ottersten. Directional modulation via symbol-level precoding: A way to enhance security. *IEEE Journal of Selected Topics in Signal Processing*, 10(8):1478–1493, 2016.

[58] Lai-U Choi and Ross D Murch. A transmit preprocessing technique for multiuser MIMO systems using a decomposition approach. *IEEE Transactions on Wireless Communications*, 3(1):20–24, 2004.

[59] Ashkan Kalantari, Mojtaba Soltanalian, Sina Maleki, Symeon Chatzinotas, and Björn Ottersten. Secure M-PSK communication via directional modulation. In *2016 IEEE International Conference on Acoustics, Speech and Signal Processing (ICASSP)*, pages 3481–3485. IEEE, 2016.

[60] Arthur H Chang, Aydin Babakhani, and Ali Hajimiri. Near-field direct antenna modulation (NFDAM) transmitter at 2.4 ghz. In *2009 IEEE Antennas and Propagation Society International Symposium*, pages 1–4. IEEE, 2009.

[61] Javad Lavaei, Aydin Babakhani, Ali Hajimiri, and John C Doyle. A study of near-field direct antenna modulation systems using convex optimization. In *Proceedings of the 2010 American Control Conference*, pages 1065–1072. IEEE, 2010.

[62] Aydin Babakhani, David B Rutledge, and Ali Hajimiri. A near-field modulation technique using antenna reflector switching. In *2008 IEEE International Solid-State Circuits Conference-Digest of Technical Papers*, pages 188–605. IEEE, 2008.

[63] Aydin Babakhani, David B Rutledge, and Ali Hajimiri. Transmitter architectures based on near-field direct antenna modulation. *IEEE Journal of Solid-State Circuits*, 43(12):2674–2692, 2008.

[64] Michael P Daly and Jennifer T Bernhard. Beamsteering in pattern reconfigurable arrays using directional modulation. *IEEE Transactions on Antennas and Propagation*, 58(7):2259–2265, 2010.

[65] Quanjiang Zhu, Shiwen Yang, Ruilin Yao, and Zaiping Nie. Directional modulation based on 4-D antenna arrays. *IEEE Transactions on Antennas and Propagation*, 62(2):621–628, 2013.

[66] Tao Hong, Mao-Zhong Song, and Yu Liu. RF directional modulation technique using a switched antenna array for physical layer secure communication applications. *Progress In Electromagnetics Research*, 116:363–379, 2011.

[67] Veljko Stankovic and Martin Haardt. Generalized design of multi-user MIMO precoding matrices. *IEEE Transactions on Wireless Communications*, 7(3):953–961, 2008.

[68] Thanh V Pham, Hoa Le-Minh, and Anh T Pham. Multi-user visible light communication broadcast channels with zero-forcing precoding. *IEEE Transactions on Communications*, 65(6):2509–2521, 2017.

[69] Hang Yuan, Jianping An, Nan Yang, Kai Yang, and Trung Q Duong. Low complexity hybrid precoding for multiuser millimeter wave systems over frequency selective channels. *IEEE Transactions on Vehicular Technology*, 68(1):983–987, 2018.

[70] Christos Masouros. Correlation rotation linear precoding for MIMO broadcast communications. *IEEE Transactions on Signal Processing*, 59(1):252–262, 2010.

[71] Christos Masouros, Tharmalingam Ratnarajah, Mathini Sellathurai, Constantinos B Papadias, and Anil K Shukla. Known interference in the cellular

downlink: A performance limiting factor or a source of green signal power? *IEEE Communications Magazine*, 51(10):162–171, 2013.

[72] Shahram Yousefi and Amir K Khandani. Generalized tangential sphere bound on the ML decoding error probability of linear binary block codes in awgn interference. *IEEE transactions on information theory*, 50(11):2810–2815, 2004.

[73] Monirosharieh Vameghestahbanati, Ian D Marsland, Ramy H Gohary, and Halim Yanikomeroglu. Multidimensional constellations for uplink SCMA systems—a comparative study. *IEEE Communications Surveys & Tutorials*, 21(3):2169–2194, 2019.

[74] Yudong Zhang, Shuihua Wang, and Genlin Ji. A comprehensive survey on particle swarm optimization algorithm and its applications. *Mathematical problems in engineering*, 2015, 2015.

[75] Alireza Haqiqatnejad, Farbod Kayhan, and Björn Ottersten. Symbol-level precoding design based on distance preserving constructive interference regions. *IEEE Transactions on Signal Processing*, 66(22):5817–5832, 2018.

[76] Alireza Haqiqatnejad, Farbod Kayhan, and Björn Ottersten. Constructive interference for generic constellations. *IEEE Signal Processing Letters*, 25(4):586–590, 2018.

[77] Stelios Timotheou, Gan Zheng, Christos Masouros, and Ioannis Krikidis. Exploiting constructive interference for simultaneous wireless information and power transfer in multiuser downlink systems. *IEEE Journal on Selected Areas in Communications*, 34(5):1772–1784, 2016.

[78] Maha Alodeh, Symeon Chatzinotas, and Björn Ottersten. Constructive multiuser interference in symbol level precoding for the miso downlink channel. *IEEE Transactions on Signal processing*, 63(9):2239–2252, 2015.

[79] Doyle Kwon, Hyeon Su Kang, and Duk Kyung Kim. Robust interference exploitation-based precoding scheme with quantized CSIT. *IEEE Communications Letters*, 20(4):780–783, 2016.

[80] Ganapati Hegde, Christos Masouros, and Marius Pesavento. Interference exploitation-based hybrid precoding with robustness against phase errors. *IEEE Transactions on Wireless Communications*, 18(7):3683–3696, 2019.

[81] Doyle Kwon, Woon-Young Yeo, and Duk Kyung Kim. A new precoding scheme for constructive superposition of interfering signals in multiuser MIMO systems. *IEEE Communications Letters*, 18(11):2047–2050, 2014.

[82] S Morteza Razavi and Tharmalingam Ratnarajah. Adaptively regularized phase alignment precoding for multiuser multiantenna downlink. *IEEE Transactions on Vehicular Technology*, 64(10):4863–4869, 2014.

[83] Guangyang Zhang, Chao Shen, Bo Ai, and Zhangdui Zhong. Robust symbol-level precoding and passive beamforming for IRS-aided communications. *IEEE Transactions on Wireless Communications*, 2022.

[84] Danilo Spano, Maha Alodeh, Symeon Chatzinotas, and Björn Ottersten. PAPR minimization through spatio-temporal symbol-level precoding for the non-linear multi-user MISO channel. In *2018 IEEE International Conference on Acoustics, Speech and Signal Processing (ICASSP)*, pages 3599–3603. IEEE, 2018.

[85] Per Zetterberg and Björn Ottersten. The spectrum efficiency of a base station antenna array system for spatially selective transmission. *IEEE Transactions on Vehicular Technology*, 44(3):651–660, 1995.

[86] Eleftherios Karipidis, Nicholas D Sidiropoulos, and Zhi-Quan Luo. Transmit beamforming to multiple co-channel multicast groups. In *1st IEEE International Workshop on Computational Advances in Multi-Sensor Adaptive Processing, 2005.*, pages 109–112. IEEE, 2005.

[87] Eleftherios Karipidis, Nicholas D Sidiropoulos, and Zhi-Quan Luo. Far-field multicast beamforming for uniform linear antenna arrays. *IEEE Transactions on Signal Processing*, 55(10):4916–4927, 2007.

[88] Dimitrios Christopoulos, Symeon Chatzinotas, and Björn Ottersten. Multicast multigroup beamforming under per-antenna power constraints. In *2014 IEEE International Conference on Communications (ICC)*, pages 4704–4710. IEEE, 2014.

[89] Yan Gao and Martin Schubert. Group-oriented beamforming for multi-stream multicasting based on quality-of-service requirements. In *1st IEEE International Workshop on Computational Advances in Multi-Sensor Adaptive Processing, 2005.*, pages 193–196. IEEE, 2005.

[90] Yuri CB Silva and Anja Klein. Linear transmit beamforming techniques for the multigroup multicast scenario. *IEEE Transactions on Vehicular Technology*, 58(8):4353–4367, 2009.

[91] Mats Bengtsson and Björn Ottersten. Optimum and suboptimum transmit beamforming. In *Handbook of antennas in wireless communications*, pages 18–1. CRC press, 2018.

[92] Mirette Sadek, Alireza Tarighat, and Ali H Sayed. A leakage-based precoding scheme for downlink multi-user MIMO channels. *IEEE transactions on Wireless Communications*, 6(5):1711–1721, 2007.

[93] Quentin H Spencer, A Lee Swindlehurst, and Martin Haardt. Zero-forcing methods for downlink spatial multiplexing in multiuser MIMO channels. *IEEE transactions on signal processing*, 52(2):461–471, 2004.

[94] Peng Cheng, Meixia Tao, and Wenjun Zhang. A new slnr-based linear precoding for downlink multi-user multi-stream mimo systems. *IEEE communications letters*, 14(11):1008–1010, 2010.

[95] Piya Patcharamaneepakorn, Simon Armour, and Angela Doufexi. On the equivalence between SLNR and MMSE precoding schemes with single-antenna receivers. *IEEE Communications Letters*, 16(7):1034–1037, 2012.

[96] Nikos D Sidiropoulos, Timothy N Davidson, and Zhi-Quan Luo. Transmit beamforming for physical-layer multicasting. *IEEE transactions on signal processing*, 54(6):2239–2251, 2006.

[97] Oskari Tervo, Le-Nam Tran, and Markku Juntti. Optimal energy-efficient transmit beamforming for multi-user miso downlink. *IEEE Transactions on Signal Processing*, 63(20):5574–5588, 2015.

[98] Christos G Tsinos, Sina Maleki, Symeon Chatzinotas, and Björn Ottersten. On the energy-efficiency of hybrid analog–digital transceivers for single-and multi-carrier large antenna array systems. *IEEE Journal on Selected Areas in Communications*, 35(9):1980–1995, 2017.

[99] Dimitrios Christopoulos, Symeon Chatzinotas, and Björn Ottersten. Multicast multigroup beamforming for per-antenna power constrained large-scale arrays. In *2015 IEEE 16th International Workshop on Signal Processing Advances in Wireless Communications (SPAWC)*, pages 271–275. IEEE, 2015.

[100] Hamdi Joudeh and Bruno Clerckx. A rate-splitting strategy for max-min fair multigroup multicasting. In *2016 IEEE 17th International Workshop on Signal Processing Advances in Wireless Communications (SPAWC)*, pages 1–5. IEEE, 2016.

[101] Holger Boche and Martin Schubert. Resource allocation in multiantenna systems-achieving max-min fairness by optimizing a sum of inverse sir. *IEEE Transactions on Signal Processing*, 54(6):1990–1997, 2006.

[102] Man-Chung Yue, Sissi Xiaoxiao Wu, and Anthony Man-Cho So. A robust design for MISO physical-layer multicasting over line-of-sight channels. *IEEE Signal Processing Letters*, 23(7):939–943, 2016.

[103] Ka L Law, Imran Wajid, and Marius Pesavento. Robust downlink beamforming in multi-group multicasting using trace bounds on the covariance mismatches. In *2012 IEEE International Conference on Acoustics, Speech and Signal Processing (ICASSP)*, pages 3229–3232. IEEE, 2012.

[104] Binyue Liu, Long Shi, and Xiang-Gen Xia. Robust rank-two multicast beamforming under a unified CSI uncertainty model. *IEEE Signal Processing Letters*, 23(10):1419–1423, 2016.

[105] Jing Huang and A Lee Swindlehurst. Robust secure transmission in MISO channels based on worst-case optimization. *IEEE Transactions on Signal Processing*, 60(4):1696–1707, 2011.

[106] Hong Shen, Wei Xu, A Lee Swindlehurst, and Chunming Zhao. Transmitter optimization for per-antenna power constrained multi-antenna downlinks: An SLNR maximization methodology. *IEEE Transactions on Signal Processing*, 64(10):2712–2725, 2016.

[107] Michael Botros Shenouda and Timothy N Davidson. Nonlinear and linear broadcasting with QoS requirements: Tractable approaches for bounded channel uncertainties. *IEEE Transactions on Signal Processing*, 57(5):1936–1947, 2009.

[108] Dhananjaya Ponukumati, Feifei Gao, and Mathias Bode. Robust multicell downlink beamforming based on second-order statistics of channel state information. In *2011 IEEE Global Telecommunications Conference-GLOBECOM 2011*, pages 1–5. IEEE, 2011.

[109] Gan Zheng, Shaodan Ma, Kai-Kit Wong, and Tung-Sang Ng. Robust beamforming in the miso downlink with quadratic channel estimation and optimal training. *IEEE Transactions on Wireless communications*, 8(3):1067–1072, 2009.

[110] Wei Wu, Su Wu, and Baoyun Wang. Robust multi-objective beamforming design for power efficient and secure communication in MU-MISO networks. *IEEE Access*, 5:13277–13285, 2017.

[111] Niranjay Ravindran and Nihar Jindal. Limited feedback-based block diagonalization for the MIMO broadcast channel. *IEEE Journal on Selected Areas in Communications*, 26(8):1473–1482, 2008.

[112] Wing-Kin Ma, Jiaxian Pan, Anthony Man-Cho So, and Tsung-Hui Chang. Unraveling the rank-one solution mystery of robust MISO downlink transmit optimization: A verifiable sufficient condition via a new duality result. *IEEE Transactions on Signal Processing*, 65(7):1909–1924, 2017.

[113] Zhengmin Kong, Shaoshi Yang, Die Wang, and Lajos Hanzo. Robust beamforming and jamming for enhancing the physical layer security of full duplex radios. *IEEE Transactions on Information Forensics and Security*, 14(12):3151–3159, 2019.

[114] Imran Wajid, Yonina C Eldar, and Alex Gershman. Robust downlink beamforming using covariance channel state information. In *2009 IEEE International Conference on Acoustics, Speech and Signal Processing*, pages 2285–2288. IEEE, 2009.

[115] Fan Liu, Christos Masouros, Ang Li, and Tharmalingam Ratnarajah. Robust MIMO beamforming for cellular and radar coexistence. *IEEE Wireless Communications Letters*, 6(3):374–377, 2017.

[116] Hui Ma, Julian Cheng, Xianfu Wang, and Piming Ma. Robust MISO beamforming with cooperative jamming for secure transmission from perspectives of QoS and secrecy rate. *IEEE Transactions on Communications*, 66(2):767–780, 2017.

[117] Nihar Jindal and Zhi-Quan Luo. Capacity limits of multiple antenna multicast. In *2006 IEEE International Symposium on Information Theory*, pages 1841–1845. IEEE, 2006.

[118] Giuseppe Caire and Shlomo Shamai. On the achievable throughput of a multiantenna gaussian broadcast channel. *IEEE Transactions on Information Theory*, 49(7):1691–1706, 2003.

[119] Wei-Cheng Liao, Tsung-Hui Chang, Wing-Kin Ma, and Chong-Yung Chi. QoS-based transmit beamforming in the presence of eavesdroppers: An optimized artificial-noise-aided approach. *IEEE Transactions on Signal Processing*, 59(3):1202–1216, 2010.

[120] Ashkan Kalantari, Gan Zheng, Zhen Gao, Zhu Han, and Björn Ottersten. Secrecy analysis on network coding in bidirectional multibeam satellite communications. *IEEE Transactions on Information Forensics and Security*, 10(9):1862–1874, 2015.

[121] Kang An, Min Lin, Jian Ouyang, and Wei-Ping Zhu. Secure transmission in cognitive satellite terrestrial networks. *IEEE Journal on Selected Areas in Communications*, 34(11):3025–3037, 2016.

[122] Haiyang Zhang, Chunguo Li, Yongming Huang, and Luxi Yang. Secure beamforming for SWIPT in multiuser MISO broadcast channel with confidential messages. *IEEE Communications Letters*, 19(8):1347–1350, 2015.

[123] Wei Zhang, Jian Chen, Yonghong Kuo, and Yuchen Zhou. Artificial-noise-aided optimal beamforming in layered physical layer security. *IEEE Communications Letters*, 23(1):72–75, 2018.

[124] Wei Wang, Kah Chan Teh, and Kwok Hung Li. Artificial noise aided physical layer security in multi-antenna small-cell networks. *IEEE Transactions on Information Forensics and Security*, 12(6):1470–1482, 2017.

[125] Hui-Ming Wang, Jiale Bai, and Limeng Dong. Intelligent reflecting surfaces assisted secure transmission without eavesdropper's CSI. *IEEE Signal Processing Letters*, 27:1300–1304, 2020.

[126] Christos G Tsinos, Sina Maleki, Symeon Chatzinotas, and Bjorn Ottersten. Hybrid analog-digital transceiver designs for cognitive radio millimiter wave systems. In *2016 50th Asilomar Conference on Signals, Systems and Computers*, pages 1785–1789. IEEE, 2016.

[127] Yahia R Ramadan, Hlaing Minn, and Ahmed S Ibrahim. Hybrid analog–digital precoding design for secrecy mmwave MISO-OFDM systems. *IEEE Transactions on Communications*, 65(11):5009–5026, 2017.

[128] Tadilo Endeshaw Bogale, Long Bao Le, Afshin Haghighat, and Luc Vandendorpe. On the number of RF chains and phase shifters, and scheduling design with hybrid analog–digital beamforming. *IEEE Transactions on Wireless Communications*, 15(5):3311–3326, 2016.

[129] Ahmed Alkhateeb and Robert W Heath. Frequency selective hybrid precoding for limited feedback millimeter wave systems. *IEEE Transactions on Communications*, 64(5):1801–1818, 2016.

[130] Meysam Sadeghi, Luca Sanguinetti, and Chau Yuen. Hybrid precoding for multi-group physical layer multicasting. In *European Wireless 2018; 24th European Wireless Conference*, pages 1–6. VDE, 2018.

[131] Maha Alodeh, Symeon Chatzinotas, and Björn Ottersten. Symbol-level multiuser MISO precoding for multi-level adaptive modulation. *IEEE Transactions on Wireless Communications*, 16(8):5511–5524, 2017.

[132] Maha Alodeh, Symeon Chatzinotas, and Björn Ottersten. A multicast approach for constructive interference precoding in MISO downlink channel. In *2014 IEEE International Symposium on Information Theory*, pages 2534–2538. IEEE, 2014.

[133] Maha Alodeh, Symeon Chatzinotas, and Björn Ottersten. Energy efficient symbol-level precoding in multiuser MISO channels. In *2015 IEEE 16th International Workshop on Signal Processing Advances in Wireless Communications (SPAWC)*, pages 36–40. IEEE, 2015.

[134] Maha Alodeh, Symeon Chatzinotas, and Björn Ottersten. Symbol based precoding in the downlink of cognitive MISO channel. In *International Conference on Cognitive Radio Oriented Wireless Networks*, pages 370–380. Springer, 2015.

[135] Maha Alodeh, Symeon Chatzinotas, and Björn Ottersten. Energy-efficient symbol-level precoding in multiuser MISO based on relaxed detection region. *IEEE transactions on Wireless Communications*, 15(5):3755–3767, 2016.

[136] Danilo Spano, Maha Alodeh, Symeon Chatzinotas, and Björn Ottersten. Symbol-level precoding for the nonlinear multiuser MISO downlink channel. *IEEE Transactions on Signal Processing*, 66(5):1331–1345, 2017.

[137] Muhammad RA Khandaker, Christos Masouros, and Kai-Kit Wong. Constructive interference based secure precoding: A new dimension in physical layer security. *IEEE Transactions on Information Forensics and Security*, 13(9):2256–2268, 2018.

[138] Abderrahmane Mayouche, Danilo Spano, Christos G Tsinos, Symeon Chatzinotas, and Björn Ottersten. Learning-assisted eavesdropping and symbol-level precoding countermeasures for downlink MU-MISO systems. *IEEE Open Journal of the Communications Society*, 1:535–549, 2020.

[139] Rang Liu, Ming Li, Qian Liu, and A Lee Swindlehurst. Secure symbol-level precoding in MU-MISO wiretap systems. *IEEE Transactions on Information Forensics and Security*, 15:3359–3373, 2020.

[140] Zhongxiang Wei, Christos Masouros, Fan Liu, Symeon Chatzinotas, and Bjorn Ottersten. Energy-and cost-efficient physical layer security in the era of IoT: The role of interference. *IEEE Communications Magazine*, 58(4):81–87, 2020.

[141] Wen-Qin Wang and Zhi Zheng. Hybrid MIMO and phased-array directional modulation for physical layer security in mmWave wireless communications. *IEEE journal on selected areas in communications*, 36(7):1383–1396, 2018.

[142] Reem Melki, Hassan N Noura, Mohammad M Mansour, and Ali Chehab. Physical layer security schemes for MIMO systems: an overview. *Wireless networks*, 26(3):2089–2111, 2020.

[143] Saif Khan Mohammed and Erik G Larsson. Per-antenna constant envelope precoding for large multi-user MIMO systems. *IEEE Transactions on Communications*, 61(3):1059–1071, 2013.

[144] Pierluigi Vito Amadori and Christos Masouros. Constant envelope precoding by interference exploitation in phase shift keying-modulated multiuser transmission. *IEEE Transactions on Wireless Communications*, 16(1):538–550, 2016.

[145] Jianjun Zhang, Yongming Huang, Jiaheng Wang, Björn Ottersten, and Luxi Yang. Per-antenna constant envelope precoding and antenna subset selection: A geometric approach. *IEEE Transactions on Signal Processing*, 64(23):6089–6104, 2016.

[146] Shuowen Zhang, Rui Zhang, and Teng Joon Lim. MISO multicasting with constant envelope precoding. *IEEE Wireless Communications Letters*, 5(6):588–591, 2016.

[147] Christos G Tsinos, Stavros Domouchtsidis, Symeon Chatzinotas, and Björn Ottersten. Symbol level precoding with low resolution DACs for constant envelope OFDM MU-MIMO systems. *IEEE Access*, 8:12856–12866, 2020.

[148] Ang Li, Christos Masouros, A Lee Swindlehurst, and Wei Yu. 1-bit massive MIMO transmission: Embracing interference with symbol-level precoding. *IEEE Communications Magazine*, 59(5):121–127, 2021.

[149] Saif Khan Mohammed and Erik G Larsson. Constant-envelope multi-user precoding for frequency-selective massive MIMO systems. *IEEE Wireless Communications Letters*, 2(5):547–550, 2013.

[150] Mingjie Shao, Qiang Li, Wing-Kin Ma, and Anthony Man-Cho So. A framework for one-bit and constant-envelope precoding over multiuser massive MISO channels. *IEEE Transactions on Signal Processing*, 67(20):5309–5324, 2019.

[151] Christos Masouros and Emad Alsusa. Dynamic linear precoding for the exploitation of known interference in MIMO broadcast systems. *IEEE Transactions on Wireless Communications*, 8(3):1396–1404, 2009.

[152] Faheem A Khan, Christos Masouros, and Tharmalingam Ratnarajah. Interference-driven linear precoding in multiuser MISO downlink cognitive radio network. *IEEE Transactions on Vehicular Technology*, 61(6):2531–2543, 2012.

[153] Christos Masouros and Tharmalingam Ratnarajah. Interference as a source of green signal power in cognitive relay assisted co-existing MIMO wireless transmissions. *IEEE Transactions on Communications*, 60(2):525–536, 2011.

[154] Christos Masouros, Mathini Sellathurai, and Tharmalingam Ratnarajah. Interference optimization for transmit power reduction in Tomlinson-Harashima precoded MIMO downlinks. *IEEE transactions on signal processing*, 60(5):2470–2481, 2012.

[155] Maha Alodeh, Danilo Spano, Symeon Chatzinotas, and Björn Ottersten. Peak power minimization in symbol-level precoding for cognitive MISO downlink channels. In *2016 IEEE International Conference on Digital Signal Processing (DSP)*, pages 240–244. IEEE, 2016.

[156] Alireza Haqiqatnejad, Farbod Kayhan, and Björn Ottersten. Robust SINR-constrained symbol-level multiuser precoding with imperfect channel knowledge. *IEEE Transactions on Signal Processing*, 68:1837–1852, 2020.

[157] Xin Yuan, Zhiyong Feng, Andrew Zhang, Wei Ni, Ren Ping Liu, Zhiqing Wei, and Changqiao Xu. Spatio-Temporal power optimization for MIMO

joint communication and radio sensing systems with training overhead. *IEEE Transactions on Vehicular Technology*, 2020.

[158] Jiaojiao Xiong, Haoran Yin, Jiajun Zhu, and Yanqun Tang. An overview of waveform design for integrated sensing and communication. In *2022 IEEE/CIC International Conference on Communications in China (ICCC)*, pages 991–996. IEEE, 2022.

[159] Fan Liu, Longfei Zhou, Christos Masouros, Ang Li, Wu Luo, and Athina Petropulu. Toward dual-functional radar-communication systems: Optimal waveform design. *IEEE Transactions on Signal Processing*, 66(16):4264–4279, 2018.

[160] Petre Stoica, Jian Li, and Yao Xie. On probing signal design for MIMO radar. *IEEE Transactions on Signal Processing*, 55(8):4151–4161, 2007.

[161] Jian Li and Petre Stoica. MIMO radar with colocated antennas. *IEEE Signal Processing Magazine*, 24(5):106–114, 2007.

[162] Rathapon Saruthirathanaworakun, Jon M Peha, and Luis M Correia. Opportunistic primary-secondary spectrum sharing with a rotating radar. In *2012 International Conference on Computing, Networking and Communications (ICNC)*, pages 1025–1030. IEEE, 2012.

[163] HT Hayvaci and B Tavli. Spectrum sharing in radar and wireless communication systems: A review. In *2014 International Conference on Electromagnetics in Advanced Applications (ICEAA)*, pages 810–813. IEEE, 2014.

[164] Nil Garcia, Alessio Fascista, Angelo Coluccia, Henk Wymeersch, Canan Aydogdu, Rico Mendrzik, and Gonzalo Seco-Granados. Cramér-rao bound analysis of radars for extended vehicular targets with known and unknown shape. *IEEE Transactions on Signal Processing*, 70:3280–3295, 2022.

[165] Fan Liu, Ya-Feng Liu, Ang Li, Christos Masouros, and Yonina C Eldar. Cramér-rao bound optimization for joint radar-communication beamforming. *IEEE Transactions on Signal Processing*, 70:240–253, 2021.

[166] J Andrew Zhang, Fan Liu, Christos Masouros, Robert W Heath, Zhiyong Feng, Le Zheng, and Athina Petropulu. An overview of signal processing techniques for joint communication and radar sensing. *IEEE Journal of Selected Topics in Signal Processing*, 2021.

[167] Christian Sturm and Werner Wiesbeck. Waveform design and signal processing aspects for fusion of wireless communications and radar sensing. *Proceedings of the IEEE*, 99(7):1236–1259, 2011.

[168] Christian Sturm and Werner Wiesbeck. Joint integration of digital beamforming radar with communication. In *2009 IET International Radar Conference*, pages 1–4. IET, 2009.

[169] H Zeng, LIF JI LX, et al. 16QAM-LFM waveform design for integrated radar and communication. *Journal on Communications*, 41(3):182–189, 2020.

[170] Christian Sturm, Thomas Zwick, and Werner Wiesbeck. An OFDM system concept for joint radar and communications operations. In *VTC Spring 2009-IEEE 69th Vehicular Technology Conference*, pages 1–5. IEEE, 2009.

[171] Xuanxuan Tian and Zhaohui Song. On radar and communication integrated system using OFDM signal. In *2017 IEEE Radar Conference (RadarConf)*, pages 0318–0323. IEEE, 2017.

[172] Salil Sharma, Maarit Melvasalo, and Visa Koivunen. Multicarrier DS-CDMA waveforms for joint radar-communication system. In *2020 IEEE Radar Conference (RadarConf20)*, pages 1–6. IEEE, 2020.

[173] Anum Ali, Nuria Gonzalez-Prelcic, Robert W Heath, and Amitava Ghosh. Leveraging sensing at the infrastructure for mmwave communication. *IEEE Communications Magazine*, 58(7):84–89, 2020.

[174] Preeti Kumari, Junil Choi, Nuria González-Prelcic, and Robert W Heath. IEEE 802.11 ad-based radar: An approach to joint vehicular communication-radar system. *IEEE Transactions on Vehicular Technology*, 67(4):3012–3027, 2017.

[175] Preeti Kumari, Sergiy A Vorobyov, and Robert W Heath. Adaptive virtual waveform design for millimeter-wave joint communication–radar. *IEEE Transactions on Signal Processing*, 68:715–730, 2019.

[176] Gaurav Duggal, Shelly Vishwakarma, Kumar Vijay Mishra, and Shobha Sundar Ram. Doppler-resilient 802.11 ad-based ultrashort range automotive joint radar-communications system. *IEEE Transactions on Aerospace and Electronic Systems*, 56(5):4035–4048, 2020.

[177] Emanuele Grossi, Marco Lops, Luca Venturino, and Alessio Zappone. Opportunistic radar in IEEE 802.11 ad networks. *IEEE Transactions on Signal Processing*, 66(9):2441–2454, 2018.

[178] Andrew Zhang, Md Lushanur Rahman, Xiaojing Huang, Yingjie Jay Guo, Shanzhi Chen, and Robert W Heath. Perceptive mobile networks: Cellular networks with radio vision via joint communication and radar sensing. *IEEE Vehicular Technology Magazine*, 16(2):20–30, 2020.

[179] Md Lushanur Rahman, J Andrew Zhang, Xiaojing Huang, Y Jay Guo, and Robert W Heath. Framework for a perceptive mobile network using joint communication and radar sensing. *IEEE Transactions on Aerospace and Electronic Systems*, 56(3):1926–1941, 2019.

[180] Lei Xie, SH Song, Yonina C Eldar, and Khaled B Letaief. Collaborative sensing in perceptive mobile networks: Opportunities and challenges. *arXiv preprint arXiv:2205.15805*, 2022.

[181] Lei Xie, Peilan Wang, SH Song, and Khaled B Letaief. Perceptive mobile network with distributed target monitoring terminals: Leaking communication energy for sensing. *IEEE Transactions on Wireless Communications*, 2022.

[182] Aboulnasr Hassanien, Moeness G Amin, Yimin D Zhang, and Fauzia Ahmad. Signaling strategies for dual-function radar communications: An overview. *IEEE Aerospace and Electronic Systems Magazine*, 31(10):36–45, 2016.

[183] Aboulnasr Hassanien, Moeness G Amin, Yimin D Zhang, and Fauzia Ahmad. Dual-function radar-communications: Information embedding using sidelobe control and waveform diversity. *IEEE Transactions on Signal Processing*, 64(8):2168–2181, 2015.

[184] Shannon D Blunt and Padmaja Yantham. Waveform design for radar-embedded communications. In *2007 International Waveform Diversity and Design Conference*, pages 214–218. IEEE, 2007.

[185] Ammar Ahmed, Yimin D Zhang, and Yujie Gu. Dual-function radar-communications using qam-based sidelobe modulation. *Digital Signal Processing*, 82:166–174, 2018.

[186] Alex R Chiriyath, Bryan Paul, and Daniel W Bliss. Radar-communications convergence: Coexistence, cooperation, and co-design. *IEEE Transactions on Cognitive Communications and Networking*, 3(1):1–12, 2017.

[187] Aboulnasr Hassanien, Moeness G Amin, Elias Aboutanios, and Braham Himed. Dual-function radar communication systems: A solution to the spectrum congestion problem. *IEEE Signal Processing Magazine*, 36(5):115–126, 2019.

[188] Carl W Rossler, Emre Ertin, and Randolph L Moses. A software defined radar system for joint communication and sensing. In *2011 IEEE RadarCon (RADAR)*, pages 1050–1055. IEEE, 2011.

[189] Michael Nowak, Michael Wicks, Zhiping Zhang, and Zhiqiang Wu. Co-designed radar-communication using linear frequency modulation waveform. *IEEE Aerospace and Electronic Systems Magazine*, 31(10):28–35, 2016.

[190] George N Saddik, Rahul S Singh, and Elliott R Brown. Ultra-wideband multifunctional communications/radar system. *IEEE Transactions on Microwave Theory and Techniques*, 55(7):1431–1437, 2007.

[191] Wen-Qin Wang, Hing Cheung So, and Alfonso Farina. An overview on time/frequency modulated array processing. *IEEE Journal of Selected Topics in Signal Processing*, 11(2):228–246, 2016.

[192] Elie BouDaher, Aboulnasr Hassanien, Elias Aboutanios, and Moeness G Amin. Towards a dual-function MIMO radar-communication system. In *2016 IEEE Radar Conference (RadarConf)*, pages 1–6. IEEE, 2016.

[193] Tianyao Huang, Nir Shlezinger, Xingyu Xu, Yimin Liu, and Yonina C Eldar. MAJoRCom: A dual-function radar communication system using index modulation. *IEEE transactions on signal processing*, 68:3423–3438, 2020.

[194] Kai Wu, J Andrew Zhang, Xiaojing Huang, Y Jay Guo, and Robert W Heath. Waveform design and accurate channel estimation for frequency-hopping MIMO radar-based communications. *IEEE Transactions on Communications*, 69(2):1244–1258, 2020.

[195] William Baxter, Elias Aboutanios, and Aboulnasr Hassanien. Dual-function MIMO radar-communications via frequency-hopping code selection. In *2018 52nd Asilomar Conference on Signals, Systems, and Computers*, pages 1126–1130. IEEE, 2018.

[196] Yabin Gu, Linrang Zhang, Yu Zhou, and Qiuyue Zhang. Embedding communication symbols into radar waveform with orthogonal FM scheme. *IEEE Sensors Journal*, 18(21):8709–8719, 2018.

[197] Le Zheng, Marco Lops, Yonina C Eldar, and Xiaodong Wang. Radar and communication coexistence: An overview: A review of recent methods. *IEEE Signal Processing Magazine*, 36(5):85–99, 2019.

[198] Domenico Gaglione, Carmine Clemente, Christos V Ilioudis, Adriano Rosario Persico, Ian K Proudler, and John J Soraghan. Fractional fourier based waveform for a joint radar-communication system. In *2016 IEEE Radar Conference (RadarConf)*, pages 1–6. IEEE, 2016.

[199] Momin Jamil, Hans-Jurgen Zepernick, and Mats I Pettersson. On integrated radar and communication systems using oppermann sequences. In *MILCOM 2008-2008 IEEE Military Communications Conference*, pages 1–6. IEEE, 2008.

[200] Dingyou Ma, Nir Shlezinger, Tianyao Huang, Yimin Liu, and Yonina C Eldar. Joint radar-communication strategies for autonomous vehicles: Combining two key automotive technologies. *IEEE signal processing magazine*, 37(4):85–97, 2020.

[201] Aaron D Wyner. The wire-tap channel. *Bell system technical journal*, 54(8):1355–1387, 1975.

[202] Imre Csiszár and Janos Korner. Broadcast channels with confidential messages. *IEEE transactions on information theory*, 24(3):339–348, 1978.

[203] Xiaoming Chen, Derrick Wing Kwan Ng, Wolfgang H Gerstacker, and Hsiao-Hwa Chen. A survey on multiple-antenna techniques for physical layer security. *Ieee communications surveys & tutorials*, 19(2):1027–1053, 2016.

[204] Weiping Shi, Xinyi Jiang, Jinsong Hu, Abdeldime Mohamed Salih Abdelgader, Yin Teng, Yang Wang, Hangjia He, Rongen Dong, Feng Shu, and Jiangzhou Wang. Physical layer security techniques for data transmission for future wireless networks. *Security and Safety*, 1:2022007, 2022.

[205] Yang Cao, Nan Zhao, Yunfei Chen, Minglu Jin, Zhiguo Ding, Yonghui Li, and F Richard Yu. Secure transmission via beamforming optimization for NOMA networks. *IEEE Wireless Communications*, 27(1):193–199, 2019.

[206] Abraham Sanenga, Galefang Allycan Mapunda, Tshepiso Merapelo Ludo Jacob, Leatile Marata, Bokamoso Basutli, and Joseph Monamati Chuma. An overview of key technologies in physical layer security. *Entropy*, 22(11):1261, 2020.

[207] Leonardo Jimenez Rodriguez, Nghi H Tran, Trung Q Duong, Tho Le-Ngoc, Maged Elkashlan, and Sachin Shetty. Physical layer security in wireless cooperative relay networks: State of the art and beyond. *IEEE Communications Magazine*, 53(12):32–39, 2015.

[208] Poonam Yadav, Sandeep Kumar, and Rajesh Kumar. A comprehensive survey of physical layer security over fading channels: Classifications, applications, and challenges. *Transactions on Emerging Telecommunications Technologies*, 32(9):e4270, 2021.

[209] Qiang Li, Ye Yang, Wing-Kin Ma, Meilu Lin, Jianhua Ge, and Jingran Lin. Robust cooperative beamforming and artificial noise design for physical-layer secrecy in AF multi-antenna multi-relay networks. *IEEE Transactions on Signal Processing*, 63(1):206–220, 2014.

[210] Chenxi Liu, Nan Yang, Robert Malaney, and Jinhong Yuan. Artificial-noise-aided transmission in multi-antenna relay wiretap channels with spatially random eavesdroppers. *IEEE Transactions on Wireless Communications*, 15(11):7444–7456, 2016.

[211] Xiaoming Chen, Caijun Zhong, Chau Yuen, and Hsiao-Hwa Chen. Multi-antenna relay aided wireless physical layer security. *IEEE Communications Magazine*, 53(12):40–46, 2015.

[212] Pin-Hsun Lin, Szu-Hsiang Lai, Shih-Chun Lin, and Hsuan-Jung Su. On secrecy rate of the generalized artificial-noise assisted secure beamforming for wiretap channels. *IEEE Journal on Selected Areas in Communications*, 31(9):1728–1740, 2013.

[213] Qiang Li and Wing-Kin Ma. Spatially selective artificial-noise aided transmit optimization for MISO multi-eves secrecy rate maximization. *IEEE Transactions on Signal Processing*, 61(10):2704–2717, 2013.

[214] Tong-Xing Zheng and Hui-Ming Wang. Optimal power allocation for artificial noise under imperfect CSI against spatially random eavesdroppers. *IEEE Transactions on Vehicular Technology*, 65(10):8812–8817, 2015.

[215] Minyan Pei, Jibo Wei, Kai-Kit Wong, and Xin Wang. Masked beamforming for multiuser MIMO wiretap channels with imperfect CSI. *IEEE Transactions on Wireless Communications*, 11(2):544–549, 2011.

[216] Amitav Mukherjee and A Lee Swindlehurst. Robust beamforming for security in MIMO wiretap channels with imperfect CSI. *IEEE Transactions on Signal Processing*, 59(1):351–361, 2010.

[217] Yanqun Tang, Jun Xiong, Dongtang Ma, and Xiaoying Zhang. Robust artificial noise aided transmit design for MISO wiretap channels with channel uncertainty. *IEEE communications letters*, 17(11):2096–2099, 2013.

[218] Maoxin Tian, Xiaobin Huang, Qi Zhang, and Jiayin Qin. Robust an-aided secure transmission scheme in MISO channels with simultaneous wireless information and power transfer. *IEEE Signal Processing Letters*, 22(6):723–727, 2014.

[219] Bo Wang, Pengcheng Mu, and Zongze Li. Secrecy rate maximization with artificial-noise-aided beamforming for MISO wiretap channels under secrecy outage constraint. *IEEE Communications Letters*, 19(1):18–21, 2014.

[220] Yang Lu, Ke Xiong, Pingyi Fan, Zhangdui Zhong, and Khaled Ben Letaief. Coordinated beamforming with artificial noise for secure SWIPT under nonlinear EH model: Centralized and distributed designs. *IEEE Journal on Selected Areas in Communications*, 36(7):1544–1563, 2018.

[221] Jehad M Hamamreh and Huseyin Arslan. Joint PHY/MAC layer security design using ARQ with MRC and null-space independent PAPR-aware artificial noise in SISO systems. *IEEE Transactions on Wireless Communications*, 17(9):6190–6204, 2018.

[222] Shih-Chun Lin, Tsung-Hui Chang, Ya-Lan Liang, Y-W Peter Hong, and Chong-Yung Chi. On the impact of quantized channel feedback in guaranteeing secrecy with artificial noise: The noise leakage problem. *IEEE Transactions on Wireless Communications*, 10(3):901–915, 2011.

[223] Shuiyin Liu, Yi Hong, and Emanuele Viterbo. Practical secrecy using artificial noise. *IEEE Communications Letters*, 17(7):1483–1486, 2013.

[224] Wei-Cheng Liao, Tsung-Hui Chang, Wing-Kin Ma, and Chong-Yung Chi. Joint transmit beamforming and artificial noise design for qos discrimination inwireless downlink. In *2010 IEEE International Conference on Acoustics, Speech and Signal Processing*, pages 2562–2565. IEEE, 2010.

[225] Tao Xie, Jiang Zhu, and Yang Li. Artificial-noise-aided zero-forcing synthesis approach for secure multi-beam directional modulation. *IEEE Communications Letters*, 22(2):276–279, 2017.

[226] Ta-Yuan Liu, Pin-Hsun Lin, Shih-Chun Lin, Y-W Peter Hong, and Eduard Axel Jorswieck. To avoid or not to avoid CSI leakage in physical layer secret communication systems. *IEEE Communications Magazine*, 53(12):19–25, 2015.

[227] Xi Zhang, Matthew R McKay, Xiangyun Zhou, and Robert W Heath. Artificial-noise-aided secure multi-antenna transmission with limited feedback. *IEEE Transactions on Wireless Communications*, 14(5):2742–2754, 2015.

[228] Yunchuan Yang, Wenbo Wang, Hui Zhao, and Long Zhao. Transmitter beamforming and artificial noise with delayed feedback: Secrecy rate and

power allocation. *Journal of Communications and Networks*, 14(4):374–384, 2012.

[229] Tao Hong, Mao-Zhong Song, and Yu Liu. Dual-beam directional modulation technique for physical-layer secure communication. *IEEE Antennas and Wireless Propagation Letters*, 10:1417–1420, 2011.

[230] Michael P Daly and Jennifer T Bernhard. Directional modulation technique for phased arrays. *IEEE Transactions on Antennas and Propagation*, 57(9):2633–2640, 2009.

[231] Yuan Ding and Vincent F Fusco. MIMO-inspired synthesis of directional modulation systems. *IEEE Antennas and Wireless Propagation Letters*, 15:580–584, 2015.

[232] Yuan Ding and Vincent Fusco. Orthogonal vector approach for synthesis of multi-beam directional modulation transmitters. *IEEE Antennas and Wireless Propagation Letters*, 14:1330–1333, 2015.

[233] Mohammed Hafez and Hüseyin Arslan. On directional modulation: An analysis of transmission scheme with multiple directions. In *2015 IEEE International Conference on Communication Workshop (ICCW)*, pages 459–463. IEEE, 2015.

[234] Yuan Ding and Vincent F Fusco. Constraining directional modulation transmitter radiation patterns. *IET Microwaves, Antennas & Propagation*, 8(15):1408–1415, 2014.

[235] Jinsong Hu, Feng Shu, and Jun Li. Robust synthesis method for secure directional modulation with imperfect direction angle. *IEEE Communications Letters*, 20(6):1084–1087, 2016.

[236] Yuan Ding and Vincent F Fusco. Directional modulation far-field pattern separation synthesis approach. *IET Microwaves, Antennas & Propagation*, 9(1):41–48, 2015.

[237] Yuan Ding and Vincent Fusco. Directional modulation-enhanced retrodirective array. *Electronics Letters*, 51(1):118–120, 2015.

[238] Yuan Ding and Vincent F Fusco. A vector approach for the analysis and synthesis of directional modulation transmitters. *IEEE Transactions on Antennas and Propagation*, 62(1):361–370, 2013.

[239] Muhammad RA Khandaker, Christos Masouros, and Kai-Kit Wong. Constructive interference based secure precoding. In *2017 IEEE International Symposium on Information Theory (ISIT)*, pages 2875–2879. IEEE, 2017.

[240] Feng Shu, Xiaomin Wu, Jinsong Hu, Jun Li, Riqing Chen, and Jiangzhou Wang. Secure and precise wireless transmission for random-subcarrier-selection-based directional modulation transmit antenna array. *IEEE Journal on Selected Areas in Communications*, 36(4):890–904, 2018.

[241] Hui-Ming Wang and Xiang-Gen Xia. Enhancing wireless secrecy via cooperation: Signal design and optimization. *IEEE Communications Magazine*, 53(12):47–53, 2015.

[242] Yi-Sheng Shiu, Shih Yu Chang, Hsiao-Chun Wu, Scott C-H Huang, and Hsiao-Hwa Chen. Physical layer security in wireless networks: A tutorial. *IEEE wireless Communications*, 18(2):66–74, 2011.

[243] Bin Li, Zesong Fei, Yan Zhang, and Mohsen Guizani. Secure UAV communication networks over 5G. *IEEE Wireless Communications*, 26(5):114–120, 2019.

[244] Bin Li, Zesong Fei, Caiqiu Zhou, and Yan Zhang. Physical-layer security in space information networks: A survey. *IEEE Internet of things journal*, 7(1):33–52, 2019.

[245] Muharrem Tuncay Gençoğlu. Importance of cryptography in information security. *IOSR J. Comput. Eng*, 21(1):65–68, 2019.

[246] Xiaowei Wang, Meixia Tao, Jianhua Mo, and Youyun Xu. Power and subcarrier allocation for physical-layer security in OFDMA-based broadband wireless networks. *IEEE Transactions on Information Forensics and Security*, 6(3):693–702, 2011.

[247] Cheol Jeong and Il-Min Kim. Optimal power allocation for secure multicarrier relay systems. *IEEE Transactions on Signal Processing*, 59(11):5428–5442, 2011.

[248] Tiejun Lv, Hui Gao, and Shaoshi Yang. Secrecy transmit beamforming for heterogeneous networks. *IEEE Journal on Selected Areas in Communications*, 33(6):1154–1170, 2015.

[249] Jiangyuan Li, Athina P Petropulu, and Steven Weber. On cooperative relaying schemes for wireless physical layer security. *IEEE transactions on signal processing*, 59(10):4985–4997, 2011.

[250] Yulong Zou, Xianbin Wang, and Weiming Shen. Optimal relay selection for physical-layer security in cooperative wireless networks. *IEEE journal on selected areas in communications*, 31(10):2099–2111, 2013.

[251] Lun Dong, Zhu Han, Athina P Petropulu, and H Vincent Poor. Improving wireless physical layer security via cooperating relays. *IEEE transactions on signal processing*, 58(3):1875–1888, 2009.

[252] Ye Yang, Qiang Li, Wing-Kin Ma, Jianhua Ge, and PC Ching. Cooperative secure beamforming for AF relay networks with multiple eavesdroppers. *IEEE Signal Processing Letters*, 20(1):35–38, 2012.

[253] Jiangyuan Li, Athina P Petropulu, and H Vincent Poor. Cooperative transmission for relay networks based on second-order statistics of channel state information. *IEEE Transactions on Signal Processing*, 59(3):1280–1291, 2010.

[254] Andrea Goldsmith, Syed Ali Jafar, Nihar Jindal, and Sriram Vishwanath. Capacity limits of MIMO channels. *IEEE Journal on selected areas in Communications*, 21(5):684–702, 2003.

[255] Derrick Wing Kwan Ng, Ernest S Lo, and Robert Schober. Robust beamforming for secure communication in systems with wireless information and power transfer. *IEEE Transactions on Wireless Communications*, 13(8):4599–4615, 2014.

[256] Chao Wang and Hui-Ming Wang. Robust joint beamforming and jamming for secure AF networks: Low-complexity design. *IEEE Transactions on Vehicular Technology*, 64(5):2192–2198, 2014.

[257] Jiang Lei, Zhu Han, María Ángeles Vázquez-Castro, and Are Hjorungnes. Secure satellite communication systems design with individual secrecy rate constraints. *IEEE Transactions on Information Forensics and Security*, 6(3):661–671, 2011.

[258] Hui-Ming Wang, Miao Luo, Xiang-Gen Xia, and Qinye Yin. Joint cooperative beamforming and jamming to secure AF relay systems with individual power constraint and no eavesdropper's CSI. *IEEE Signal Processing Letters*, 20(1):39–42, 2012.

[259] Yi Zhang, Hui-Ming Wang, Qian Yang, and Zhiguo Ding. Secrecy sum rate maximization in non-orthogonal multiple access. *IEEE Communications Letters*, 20(5):930–933, 2016.

[260] Yuzhen Huang, Fawaz S Al-Qahtani, Trung Q Duong, and Jinlong Wang. Secure transmission in mimo wiretap channels using general-order transmit antenna selection with outdated csi. *IEEE Transactions on Communications*, 63(8):2959–2971, 2015.

[261] Tong-Xing Zheng, Hui-Ming Wang, and Hao Deng. Improving anti-eavesdropping ability without eavesdropper's csi: A practical secure transmis-

sion design perspective. *IEEE Wireless Communications Letters*, 7(6):946–949, 2018.

[262] Hongliang He, Pinyi Ren, Qinghe Du, and Hai Lin. Joint feedback and artificial noise design for secure communications over fading channels without eavesdropper's CSI. *IEEE Transactions on Vehicular Technology*, 66(12):11414–11418, 2017.

[263] Y-W Peter Hong, Pang-Chang Lan, and C-C Jay Kuo. Enhancing physical-layer secrecy in multiantenna wireless systems: An overview of signal processing approaches. *IEEE Signal Processing Magazine*, 30(5):29–40, 2013.

[264] Bin Li, Meiying Zhang, Yue Rong, and Zhu Han. Artificial noise-aided secure relay communication with unknown channel knowledge of eavesdropper. *IEEE Transactions on Wireless Communications*, 20(5):3168–3179, 2021.

[265] Nabil Romero-Zurita, Mounir Ghogho, and Des McLernon. Outage probability based power distribution between data and artificial noise for physical layer security. *IEEE Signal Processing Letters*, 19(2):71–74, 2011.

[266] Samuel Kotz and Norman L Johnson. *Breakthroughs in Statistics: Foundations and basic theory*. Springer Science & Business Media, 2012.

[267] Petre Stoica and Thomas L Marzetta. Parameter estimation problems with singular information matrices. *IEEE Transactions on Signal Processing*, 49(1):87–90, 2001.

[268] Merrill Ivan Skolnik. Introduction to radar systems. *New York*, 1980.

[269] John Mulcahy-Stanislawczyk. Properties of ambiguity functions. 2014.

[270] Simon Kingsley and Shaun Quegan. *Understanding radar systems*, volume 2. SciTech Publishing, 1999.

[271] An Liu, Zhe Huang, Min Li, Yubo Wan, Wenrui Li, Tony Xiao Han, Chenchen Liu, Rui Du, Danny Kai Pin Tan, Jianmin Lu, et al. A survey on fundamental

limits of integrated sensing and communication. *IEEE Communications Surveys & Tutorials*, 24(2):994–1034, 2022.

[272] Claude E Shannon. Communication in the presence of noise. *Proceedings of the IRE*, 37(1):10–21, 1949.

[273] Peter Swerling. Probability of detection for fluctuating targets. *IRE Transactions on Information theory*, 6(2):269–308, 1960.

[274] Praveen Kumar Gopala, Lifeng Lai, and Hesham El Gamal. On the secrecy capacity of fading channels. *IEEE Transactions on Information Theory*, 54(10):4687–4698, 2008.

[275] Matthieu Bloch and Joao Barros. *Physical-layer security: from information theory to security engineering*. Cambridge University Press, 2011.

[276] Biao He, Xiangyun Zhou, and A Lee Swindlehurst. On secrecy metrics for physical layer security over quasi-static fading channels. *IEEE Transactions on Wireless Communications*, 15(10):6913–6924, 2016.

[277] Ertuğrul Güvenkaya, Jehad M Hamamreh, and Hüseyin Arslan. On physical-layer concepts and metrics in secure signal transmission. *Physical Communication*, 25:14–25, 2017.

[278] Bo Li and Athina P Petropulu. Joint transmit designs for coexistence of MIMO wireless communications and sparse sensing radars in clutter. *IEEE Transactions on Aerospace and Electronic Systems*, 53(6):2846–2864, 2017.

[279] Pradeep Reddy Vaka, Sudeep Bhattarai, and Jung-Min Park. Location privacy of non-stationary incumbent systems in spectrum sharing. In *2016 IEEE Global Communications Conference (GLOBECOM)*, pages 1–6. IEEE, 2016.

[280] Anastasios Dimas, Bo Li, Matthew Clark, Konstantinos Psounis, and Athina Petropulu. Spectrum sharing between radar and communication systems: Can the privacy of the radar be preserved? In *2017 51st Asilomar Conference on Signals, Systems, and Computers*, pages 1285–1289. IEEE, 2017.

[281] Anastasios Deligiannis, Abdullahi Daniyan, Sangarapillai Lambotharan, and Jonathon A Chambers. Secrecy rate optimizations for MIMO communication radar. *IEEE Transactions on Aerospace and Electronic Systems*, 54(5):2481–2492, 2018.

[282] Batu K Chalise and Moeness G Amin. Performance tradeoff in a unified system of communications and passive radar: A secrecy capacity approach. *Digital Signal Processing*, 82:282–293, 2018.

[283] K. Shen and W. Yu. Fractional programming for communication systems-Part I: Power control and beamforming. *IEEE Transactions on Signal Processing*, 66(10):2616–2630, May 2018.

[284] F. Liu, C. Masouros, A. Li, H. Sun, and L. Hanzo. MU-MIMO communications with MIMO radar: From co-existence to joint transmission. *IEEE Transactions on Wireless Communications*, 17(4):2755–2770, April 2018.

[285] Emre Telatar. Capacity of multi-antenna Gaussian channels. *European transactions on telecommunications*, 10(6):585–595, 1999.

[286] Muhammad Fainan Hanif, Le-Nam Tran, Markku Juntti, and Savo Glisic. On linear precoding strategies for secrecy rate maximization in multiuser multiantenna wireless networks. *IEEE transactions on signal processing*, 62(14):3536–3551, 2014.

[287] F. Wang, X. Wang, and Y. Zhu. Transmit beamforming for multiuser downlink with per-antenna power constraints. In *2014 IEEE International Conference on Communications (ICC)*, pages 4692–4697, June 2014.

[288] Alok Aggarwal and Teresa H Meng. Minimizing the peak-to-average power ratio of ofdm signals via convex optimization. In *GLOBECOM'03. IEEE Global Telecommunications Conference (IEEE Cat. No. 03CH37489)*, volume 4, pages 2385–2389. IEEE, 2003.

[289] Fan Liu, Christos Masouros, Pierluigi Vito Amadori, and Huafei Sun. An efficient manifold algorithm for constructive interference based constant envelope precoding. *IEEE Signal Processing Letters*, 24(10):1542–1546, 2017.

[290] Fan Liu, Christos Masouros, Athina Petropulu, Hugh Griffiths, and Lajos Hanzo. Joint radar and communication design: Applications, state-of-the-art, and the road ahead. *arXiv preprint arXiv:1906.00789*, 2019.

[291] D. R. Fuhrmann and G. San Antonio. Transmit beamforming for MIMO radar systems using signal cross-correlation. *IEEE Transactions on Aerospace and Electronic Systems*, 44(1):171–186, January 2008.

[292] Werner Dinkelbach. On nonlinear fractional programming. *Management science*, 13(7):492–498, 1967.

[293] Zhi-Quan Luo, Wing-Kin Ma, Anthony Man-Cho So, Yinyu Ye, and Shuzhong Zhang. Semidefinite relaxation of quadratic optimization problems. *IEEE Signal Processing Magazine*, 27(3):20–34, 2010.

[294] Kun-Yu Wang, Anthony Man-Cho So, Tsung-Hui Chang, Wing-Kin Ma, and Chong-Yung Chi. Outage constrained robust transmit optimization for multiuser MISO downlinks: Tractable approximations by conic optimization. *IEEE Transactions on Signal Processing*, 62(21):5690–5705, 2014.

[295] Miguel Sousa Lobo, Lieven Vandenberghe, Stephen Boyd, and Hervé Lebret. Applications of second-order cone programming. *Linear algebra and its applications*, 284(1-3):193–228, 1998.

[296] J. Li and P. Stoica. MIMO radar with colocated antennas. *IEEE Signal Processing Magazine*, 24(5):106–114, Sep. 2007.

[297] Kaiming Shen and Wei Yu. Fractional programming for communication systems part I: Power control and beamforming. *IEEE Transactions on Signal Processing*, 66(10):2616–2630, 2018.

[298] Stephen Boyd and Lieven Vandenberghe. *Convex optimization*. Cambridge university press, 2004.

[299] Ka L Law, Imran Wajid, and Marius Pesavento. Optimal downlink beamforming for statistical CSI with robustness to estimation errors. *Signal Processing*, 131:472–482, 2017.

[300] Michael Grant, Stephen Boyd, and Yinyu Ye. Cvx: Matlab software for disciplined convex programming, 2008.

[301] Ang Li, Christos Masouros, Xuewen Liao, Yonghui Li, and Branka Vucetic. Multiplexing more data streams in the MU-MISO downlink by interference exploitation precoding. In *2020 IEEE Wireless Communications and Networking Conference (WCNC)*, pages 1–6. IEEE, 2020.

[302] Shuowen Zhang, Rui Zhang, and Teng Joon Lim. Constant envelope precoding for MIMO systems. *IEEE Transactions on Communications*, 66(1):149–162, 2017.

[303] Mohammad Kazemi, Hassan Aghaeinia, and Tolga M Duman. Discrete-phase constant envelope precoding for massive MIMO systems. *IEEE Transactions on Communications*, 65(5):2011–2021, 2017.

[304] Lou Zhao, Giovanni Geraci, Tao Yang, Derrick Wing Kwan Ng, and Jinhong Yuan. A tone-based AoA estimation and multiuser precoding for millimeter wave massive MIMO. *IEEE Transactions on Communications*, 65(12):5209–5225, 2017.

[305] Xiaoling Hu, Caijun Zhong, Xiaoming Chen, Weiqiang Xu, and Zhaoyang Zhang. Cluster grouping and power control for angle-domain MmWave MIMO NOMA systems. *IEEE Journal of Selected Topics in Signal Processing*, 13(5):1167–1180, 2019.

[306] Qian Xu, Pinyi Ren, and A Lee Swindlehurst. Rethinking secure precoding via interference exploitation: A smart eavesdropper perspective. *IEEE Transactions on Information Forensics and Security*, 16:585–600, 2020.

[307] Shafi Bashar, Zhi Ding, and Chengshan Xiao. On secrecy rate analysis of MIMO wiretap channels driven by finite-alphabet input. *IEEE Transactions on Communications*, 60(12):3816–3825, 2012.

[308] O. Aldayel, V. Monga, and M. Rangaswamy. Successive QCQP refinement for MIMO radar waveform design under practical constraints. *IEEE Transactions on Signal Processing*, 64(14):3760–3774, 2016.

[309] Guolong Cui, Hongbin Li, and Muralidhar Rangaswamy. MIMO radar waveform design with constant modulus and similarity constraints. *IEEE Transactions on signal processing*, 62(2):343–353, 2013.

[310] Michael Grant and Stephen Boyd. CVX: Matlab software for disciplined convex programming, version 2.1, 2014.

[311] Aharon Ben-Tal and Arkadi Nemirovski. *Lectures on modern convex optimization: analysis, algorithms, and engineering applications*. SIAM, 2001.

[312] Lieven Vandenberghe and Stephen Boyd. Semidefinite programming. *SIAM review*, 38(1):49–95, 1996.

[313] Jaehyun Park and Stephen Boyd. General heuristics for nonconvex quadratically constrained quadratic programming. *arXiv preprint arXiv:1703.07870*, 2017.

[314] Yurii Nesterov and Arkadii Nemirovskii. *Interior-point polynomial algorithms in convex programming*. SIAM, 1994.

[315] Yong Cheng, Marius Pesavento, and Anne Philipp. Joint network optimization and downlink beamforming for CoMP transmissions using mixed integer conic programming. *IEEE Transactions on Signal Processing*, 61(16):3972–3987, 2013.

[316] Derrick Wing Kwan Ng, Yongpeng Wu, and Robert Schober. Power efficient resource allocation for full-duplex radio distributed antenna networks. *IEEE Transactions on Wireless Communications*, 15(4):2896–2911, 2016.

[317] Ang Li, Christos Masouros, Fan Liu, and A Lee Swindlehurst. Massive MIMO 1-bit DAC transmission: A low-complexity symbol scaling approach. *IEEE Transactions on Wireless Communications*, 17(11):7559–7575, 2018.

[318] Amine Mezghani, Rafik Ghiat, and Josef A Nossek. Transmit processing with low resolution D/A-converters. In *2009 16th IEEE International Conference on Electronics, Circuits and Systems-(ICECS 2009)*, pages 683–686. IEEE, 2009.

[319] Hela Jedda, Amine Mezghani, A Lee Swindlehurst, and Josef A Nossek. Quantized constant envelope precoding with PSK and QAM signaling. *IEEE Transactions on Wireless Communications*, 17(12):8022–8034, 2018.

[320] Steven M Kay. *Fundamentals of statistical signal processing: estimation theory*. Prentice-Hall, Inc., 1993.

[321] Nanchi Su, Fan Liu, Zhongxiang Wei, Ya-Feng Liu, and Christos Masouros. Secure dual-functional radar-communication transmission: Exploiting interference for resilience against target eavesdropping. *IEEE Transactions on Wireless Communications*, 2022.

[322] Fan Liu, Ya-Feng Liu, Ang Li, Christos Masouros, and Yonina C. Eldar. Cramér-Rao bound optimization for joint Radar-Communication beamforming. *IEEE Transactions on Signal Processing*, pages 1–1, 2021.

[323] Jian Li, Luzhou Xu, Petre Stoica, Keith W Forsythe, and Daniel W Bliss. Range compression and waveform optimization for MIMO radar: a Cramér-Rao bound based study. *IEEE Transactions on Signal Processing*, 56(1):218–232, 2007.

[324] Muhammad Fainan Hanif, Le-Nam Tran, Markku Juntti, and Savo Glisic. On linear precoding strategies for secrecy rate maximization in multiuser multiantenna wireless networks. *IEEE Transactions on Signal Processing*, 62(14):3536–3551, 2014.

[325] Nanchi Su, Fan Liu, and Christos Masouros. Secure Radar-Communication systems with malicious targets: Integrating radar, communications and jamming functionalities. *IEEE Transactions on Wireless Communications*, 2020.

[326] Babak Hassibi and Thomas L Marzetta. Multiple-antennas and isotropically random unitary inputs: The received signal density in closed form. *IEEE Transactions on Information Theory*, 48(6):1473–1484, 2002.

[327] Bing Fang, Zuping Qian, Wei Shao, and Wei Zhong. Precoding and artificial noise design for cognitive MIMOME wiretap channels. *IEEE Transactions on Vehicular Technology*, 65(8):6753–6758, 2015.

[328] Zheng Chu, Hong Xing, Martin Johnston, and Stéphane Le Goff. Secrecy rate optimizations for a MISO secrecy channel with multiple multiantenna eavesdroppers. *IEEE Transactions on Wireless Communications*, 15(1):283–297, 2015.

[329] Andreas Jakobsson and Petre Stoica. Combining capon and apes for estimation of spectral lines. *Circuits, Systems and Signal Processing*, 19(2):159–169, 2000.

[330] Luzhou Xu, Jian Li, and Petre Stoica. Target detection and parameter estimation for MIMO radar systems. *IEEE Transactions on Aerospace and Electronic Systems*, 44(3):927–939, 2008.

[331] Jian Li, P. Stoica, and Zhisong Wang. On robust capon beamforming and diagonal loading. *IEEE Transactions on Signal Processing*, 51(7):1702–1715, 2003.

[332] Varun Chandola, Arindam Banerjee, and Vipin Kumar. Anomaly detection: A survey. *ACM computing surveys (CSUR)*, 41(3):1–58, 2009.

[333] P Tichavsky. Posterior Cramér-Rao bound for adaptive harmonic retrieval. *IEEE Transactions on Signal Processing*, 43(5):1299–1302, 1995.

[334] Shao-Po Wu, Lieven Vandenberghe, and Stephen Boyd. Software for determinant maximization problems—user's guild, 1996.

[335] Dimitri P Bertsekas. Nonlinear programming. *Journal of the Operational Research Society*, 48(3):334–334, 1997.